การกำเนิดชุดหินอัคนีบาดาลซับซ้อนในบริเวณวังน้ำเขียว จังหวัดนครราชสีมา

นายอลงกต ฝั้นกา

วิทยานิพนธ์นี้เป็นส่วนหนึ่งของการศึกษาตามหลักสูตรปริญญาวิทยาศาสตรดุษฎีบัณฑิต
สาขาวิชาธรณีวิทยา ภาควิชาธรณีวิทยา
คณะวิทยาศาสตร์ จุฬาลงกรณ์มหาวิทยาลัย
ปีการศึกษา 2559

PETROGENESIS OF PLUTONIC COMPLEX IN WANG NAM KHIAO AREA, CHANGWAT NAKHON RATCHASIMA

Mr. Alongkot Fanka

A Dissertation Submitted in Partial Fulfillment of the Requirements
for the Degree of Doctor of Philosophy Program in Geology
Department of Geology
Faculty of Science
Chulalongkorn University
Academic Year 2016

Thesis Title	
By	Mr. Alongkot Fanka
Field of Study	Geology
Thesis Advisor	Associate Professor Chakkaphan Sutthirat, Ph.D.

Accepted by the Faculty of Science, Chulalongkorn University in Partial Fulfillment of the Requirements for the Doctoral Degree

.....Dean of the Faculty of Science
(No data found)

THESIS COMMITTEE

.....Chairman
(Professor Montri Choowong, Ph.D.)

.....Thesis Advisor
(Associate Professor Chakkaphan Sutthirat, Ph.D.)

.....Examiner
(Associate Professor Pitsanupong Kanjanapayont, Dr.rer.nat.)

.....Examiner
(Sakonvan Chawchai, Ph.D.)

.....External Examiner
(Prayath Nantasin, Ph.D.)

.....External Examiner
(Somboon Khositanont, Ph.D.)

อลงกต ฝั้นกา : การกำเนิดชุดหินอัคนีบาดาลซับซ้อนในบริเวณวังน้ำเขียว จังหวัดนครราชสีมา (PETROGENESIS OF PLUTONIC COMPLEX IN WANG NAM KHIAO AREA, CHANGWAT NAKHON RATCHASIMA) อ.ที่ปรึกษาวิทยานิพนธ์หลัก: รศ. ดร. จักรพันธ์ สุทธิรัตน์, 138 หน้า.

บริเวณอำเภอวังน้ำเขียว จังหวัดนครราชสีมา พบชุดหินอัคนีบาดาลซับซ้อนที่ประกอบด้วยหินหลากหลายชนิดสามารถแบ่งเป็น 2 กลุ่ม คือ กลุ่มหินอัคนีบาดาลสีเข้มถึงสีเข้มจัด ได่แก่ หินฮอร์นเบลนไดต์ หินฮอร์นเบลนแกบโบรและหินฮอร์นเบลนแกบโบรเนื้อละเอียด และกลุ่มหินแกรนิต ได้แก่ หินไบโอไทต์แกรนิตยุคคาร์บอนิเฟอรัส หินฮอร์นเบลนแกรนิตยุคเพอร์เมียนตอนปลายและหินไบโอไทต์ฮอร์นเบลนแกรนิตยุคไทรแอสสิก จากการศึกษาศิลาวรรณนาเคมีแร่และธรณีเคมีบ่งชี้ว่าหินอัคนีบาดาลทั้งหมดจัดอยู่ในกลุ่ม I-type granite ซึ่งเกิดจากการตกผลึกลำดับส่วนจากหินหนืดชนิดแคลก์อัลคาไลน์ จากการศึกษาธรณีเคมีพบว่าหินอัคนีเหล่านี้มีองค์ประกอบ LILE (เช่น Ba, K, Sr) สูง และ HFSE (เช่น Nb, Ta, Zr) ต่ำ ประกอบกับผลการศึกษาเคมีแร่ของแร่ไคลโนไพรอกซีน ฮอร์นเบลนด์ และไบโอไทต์ บ่งชี้ว่าหินอัคนีเหล่านี้เกิดบริเวณแนวภูเขาไฟจากการชนกันของแผ่นเปลือกโลก การศึกษาอุณหพลศาสตร์บ่งชี้ว่าหินอัคนีบาดาลสีเข้มถึงสีเข้มจัดตกผลึกที่อุณหภูมิ 670-1,000 ^{o}ซ และความดัน 5.3-9.8 กิโลบาร์ ที่ชั้นเปลือกโลกตอนล่าง ประมาณ 28-30 กม. ส่วนหินแกรนิตตกผลึกที่อุณหภูมิ 600-820 ^{o}ซ และความดัน 2.0-5.8 กิโลบาร์ บริเวณชั้นเปลือกโลกตอนกลางถึงตอนบน ประมาณ 10-15 กม. ผลการหาอายุโดยวิธี U-Pb จากแร่เซอร์คอนพบว่าหินอัคนีบาดาลสีเข้มถึงสีเข้มจัดมีอายุ 257 ล้านปี ส่วนหินแกรนิตมีอายุแตกต่างกัน คือ หินไบโอไทต์แกรนิตยุคคาร์บอนิเฟอรัสมีอายุ 314.6 ถึง 284.9 ล้านปี หินฮอร์นเบลนแกรนิตยุคเพอร์เมียนตอนปลายมีอายุ 253.4 ล้านปี และหินไบโอไทต์ฮอร์นเบลนแกรนิตยุคไทรแอสสิกมีอายุ 237 ล้านปี ซึ่งสามารถบ่งบอกอายุของการเกิดกระบวนการทางแมกมาที่สัมพันธ์กับการชนกันของแผ่นเปลือกโลกในช่วงเวลาต่างๆได้อย่างชัดเจน

ภาควิชา ธรณีวิทยา ลายมือชื่อนิสิต .....

สาขาวิชา ธรณีวิทยา ลายมือชื่อ อ.ที่ปรึกษาหลัก .....

ปีการศึกษา 2559

5672900623 : MAJOR GEOLOGY
KEYWORDS: ARC MAGMATISM, ZIRCON U-PB GEOCHRONOLOGY, GEOTHERMOBAROMETRY, HORNBLENDITE, GRANITE

ALONGKOT FANKA: PETROGENESIS OF PLUTONIC COMPLEX IN WANG NAM KHIAO AREA, CHANGWAT NAKHON RATCHASIMA. ADVISOR: ASSOC. PROF. CHAKKAPHAN SUTTHIRAT, Ph.D., 138 pp.

Plutonic complex with a variety of rock has been discovered in Wang Nam Khiao Area, Changwat Nakhon Ratchasima. These rocks can be classified, based on petrographic features as mafic-ultramafic rocks (i.e., hornblendite, hornblende gabbro, and hornblende microgabbro) and granitic rocks (i.e., biotite granite, hornblende granite, and biotite-hornblende granite). Mineral chemistry and whole-rock geochemistry indicate that these mafic-ultramafic rocks and granitic rocks, significantly I-type granite, appear to have been formed by crystallization from the hydrous calc-alkaline magma. Both of the mafic-ultramafic and granitic rocks show similar enrichment of LILE (e.g. Ba, K, Sr) and depletion of HFSE (e.g. Nb, Ta, Zr). Moreover, mineral chemistries of particular minerals (e.g., clinopyroxene, hornblende and biotite) indicate arc-related subduction forming the continental arc. Amphibole-plagioclase thermometry and Al in hornblende barometry are selected appropriately to estimate PT conditions of crystallization. The mafic-ultramafic rocks yield 5.3-9.8 kbar and 670-1,000 ºC whereas the granitic rocks are estimated at 2.0-5.8 kbar and 600 - 820 ºC. Therefore, the mafic-ultramafic rocks appear to be stored and crystallized at 28-31 km depth of the lower crust while the granitic rocks may have intruded into the middle to upper crust at about 10-15 km depth. Zircon U-Pb age dating yields 257 Ma of mafic-ultramafic rocks, 314.6 Ma and 284.9 Ma of Carboniferous biotite granite, 253.4 Ma of Late Permian hornblende granite, and 237.8 Ma of Triassic biotite-hornblende granite. These data introduce the genetic model of multiple arc-related magmatism in association with Palaeo-Tethys subduction beneath the Indochina Terrane during Late Carboniferous/Early Permian, Late Permian, and Middle Triassic.

Department: Geology
Field of Study: Geology
Academic Year: 2016

Student's Signature .....
Advisor's Signature .....

ACKNOWLEDGEMENTS

The author would like to express deeply gratitude to Associate Professor Dr. Chakkaphan Sutthirat, Department of Geology, Faculty of Science, Chulalongkorn University, for his valuable support and suggestion to make this research well achieved. I would like to deliver my special thanks to Assistant Professor Veerote Daorerk, Department of Geology, Faculty of Science, Chulalongkorn University, for his support in field investigation and discussions. The special thank is given to Professor Dr. Toshiaki Tsunogae and his research group, and Professor Dr. Ken-ichiro Hisada, Graduate School of Life and Environmental Science, University of Tsukuba, Japan for valuable suggestion and the wonderful experiences in Japan during the exchange program. In addition, Dr. Yukiyasu Tsutsumi, Department of Geology and Paleontology, National Museum of Nature and Science, Japan, who kindly supported the geochronological study, is greatly appreciated. My grateful thank is also extended to Associate Professor Dr. Punya Charusiri, Dr. Sakonvan Chawchai, Dr. Ladda Tangwattananukul, Dr. Kantapon Suraprasit for their valuable discussions and suggestions, Dr. Ekgachai Jeratthitikul, Mr. Kittitat Wisittikoson, Mr. Sutheekarn Suksanguan, Mr. Irapot Saengrayab, Ms. Pattaraporn Tejo, Ms. Sasithorn Chornkrathok, Ms. Chutimon Promsuk for their helps during the field investigations, Ms. Sopit Poompuang, Ms. Jiraprapa Neampan, Mr. Prajin Thongprachum for laboratory assistances, Ms. Thitiphan Assawincharoenkij, Ms. Parisa Nimnate, Mr. Peerasit Surakiatchai for the wonderful experiences and memories during my Ph.D. study, all staffs and students of the Department of Geology, Faculty of Science, Chulalongkorn University for their helps. I would also like to extend my deepest thanks to the Human Resources Development in Science Project (Science Achievement Scholarship of Thailand, SAST), Graduate School of Chulalongkorn University, and Department of Geology, Faculty of Science, Chulalongkorn University for kind supports.

Finally, I wish to thanks my family for their supports and encouragements.

CONTENTS

Page

LIST OF TABLES

LIST OF FIGURES

CHAPTER 1
INTRODUCTION

1.1 General statement

Thailand comprises two main tectonic terranes namely Sibumasu (Sone and Metcalfe, 2008) or Shan-Thai (Bunopas, 1981; Charusiri et al., 2002) Terrane in the west and Indochina Terrane in the east (Bunopas, 1981; Charusiri et al., 2002; Sone and Metcalfe, 2008) (Fig. 1.1) together with other two terranes inbetween: Loei Fold Belt (Bunopas, 1981) to the east and Sukhothai Terrane (Sone and Metcalfe, 2008) or Sukhothai Fold Belt (Bunopas, 1981) to the west. According to the geological structure and rock formation (Bunopas, 1981; Sone and Metcalfe, 2008), in the northern part of Thailand, the Loei Fold Belt (LFB) and Sukhothai Terrane (ST) are clearly separated by Nan suture (Bunopas, 1981; Zaw et al., 2014), whereas these terranes are undistinguished in the central part of the country in which the Sukhothai Terrane (ST) disappears. In the eastern part of Thailand, the Loei Fold Belt is bounded by Sra Keao Suture and Chanthaburi Terrane (CT) (Fig. 1.1). The CT is correlated with Sukhothai Terrane (Sone and Metcalfe, 2008; Sone et al., 2012). Both Loei Fold Belt and Sukhothai Terrane-Chanthaburi Terrane were reported the arc magmatism history, particularly in the north (e.g. Nan Suture, Sukhothai, Loei and Phetchabun) and the east (e.g. Sra Keao Suture) of Thailand (Fig. 1.1). These magmatic processes are results of collision between Indochina and Sibumasu together with their Palaeo-Tethys (Sone and Metcalfe, 2008; Metcalfe, 2011b, a, 2013) during Late Carboniferous to Late Triassic (Bunopas, 1981; Charusiri, 1989; Barr et al., 1990; Singharajwarapan and Berry, 2000; Charusiri et al., 2002; Barr et al., 2006; Sone and Metcalfe, 2008; Boonsoong et al., 2011; Kamvong et al., 2014; Salam et al., 2014; Zaw et al., 2014).

In the middle Thailand, Wang Nam Khiao area, Nakhon Ratchasima (Fig. 1.1) is situated in a complex conjunction of tectonic terranes, close to the southwestern edge of Khorat Plateau. This area has been reported exposures of variety of plutonic complex; plutonic rocks, felsic–to mafic–ultramafic plutonic rocks (Putthaphiban et al., 1981a, b, 1989a, b; Jiratitipat, 2010; Nonsung, 2010; Booncharoen, 2011; Hunyek, 2012); however, no detailed study of petrogenesis and geochronology has been

examined. Such varieties of magmatic rocks bear significance in understanding the tectonic setting and magmatic event of this region.

Therefore, petrological and geochemical details as well as zircon U- Pb geochronology of plutonic complex in Wang Nam Khiao area, Nakhon Ratchasima are also focused in this study. The results of petrology, geochemistry, and geochronology provide the insights into the petrogenesis and emplacement ages of these plutonic rocks.

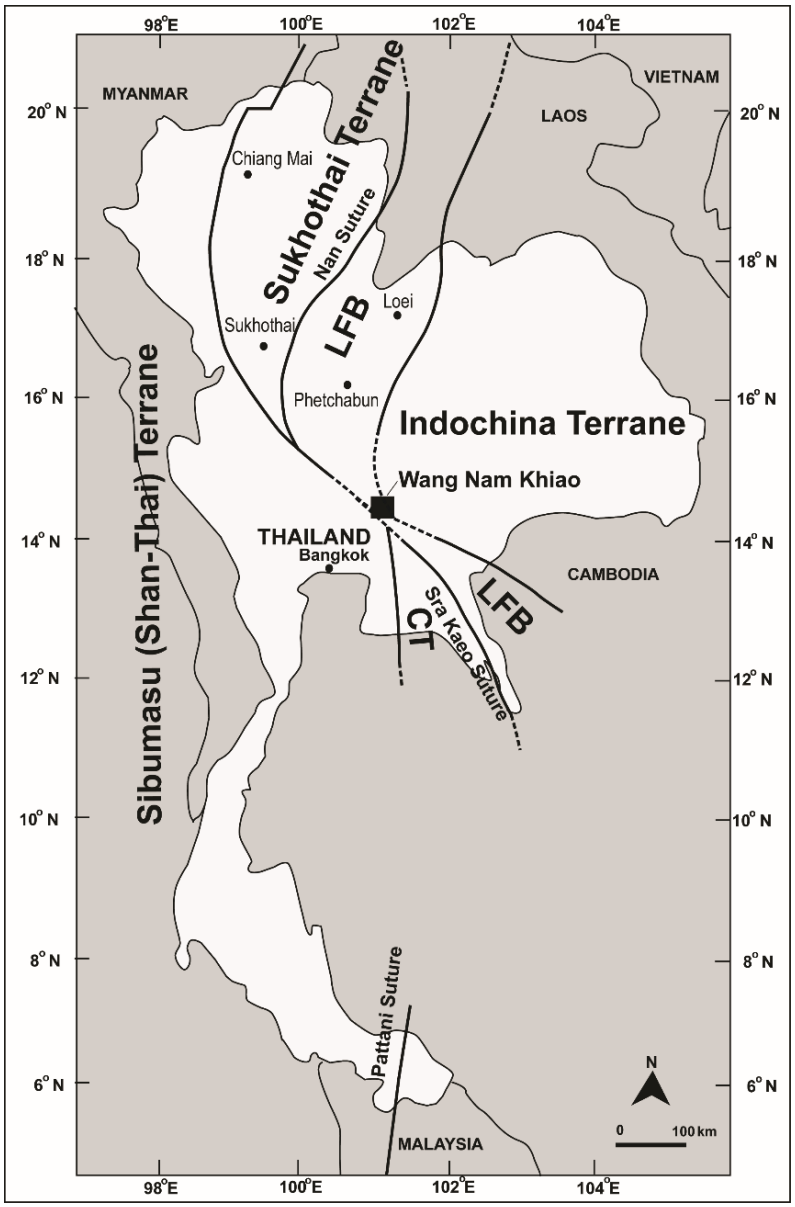

Figure 1.1 The simplified map of Thailand showing main tectonic terranes including Indochina Terrane, Sibumasu (Shan-Thai) Terrane, Loei Fold Belt (LFB), Sukhothai Terrane (ST), and Chanthaburi Terrane (CT) (Modified afterCharusiri et al. (2002);

Sone and Metcalfe (2008); Sone et al. (2012); Metcalfe (2013); Zaw et al. (2014)). The location of study area, Wang Nam Khiao area, Nakhon Ratchasima is shown in the black square.

1.2 Objective

The overall aim of this study is to obtain the petrogenesis, crystallization P-T condition, and tectonic model of plutonic complex in Wang Nam Khiao area, Changwat Nakhon Ratchasima.

1.3 Methodology

The methods of this study are summarized in flow chart (Fig. 1.2) and details of each method are also explained below.

1.3.1 Literature reviews

Previous researches on the geology, tectonic setting, geochronology, and methodology related to this study are synthesized to understand the background and design research plan. The comprehensive review from this step together with results of this study was used to support the interpretation and discussion in this thesis.

1.3.2 Field investigation and sample collection

The general geology and accessibility of the study area were summarized in Chapter 2. The field investigation and sample collection were subsequently carried out. Occurrences and relationship of the plutonic rocks in the study area were then investigated. The exposure of mafic-ultramafic plutonic rocks and granitic rocks was focused in the field mapping (Fig. 2.3).

1.3.3 Petrography

Representative of all plutonic rocks, more than 50 samples, collected from the study area were prepared for the polished thin sections (c. 30 μm). The rock slab

samples that slab surface was stick with the glass slide using petropoxy were also polished using grinding powders 400, 800, 1500, and 3000, respectively. Finally, diamond pastes 6 µm, 3 µm, and 1 µm were used for the last step of polishing. These polished-thin sections were prepared at the Graduate School of Life and Environmental Sciences, University of Tsukuba, Japan. Petrographic descriptions, mineral assemblages, textures, were determined using a NIKON polarizing binocular microscope. In addition, the representative samples were selected for investigations of whole-rock geochemistry and geochronology.

1.3.4 Mineral chemistry

The polished thin sections are used for the chemical analyses. These polished thin sections were carbon coated prior to mineral elementals analysis using an Electron Probe Micro Analyzer (EPMA, model JEOL JXA8530F) at the Chemical Analysis Division of the Research Facility Center for Science and Technology, the University of Tsukuba. Focused beam (3µm) with operating conditions were set up at an accelerating voltage of 15.0 kV with 20 nA sample current for hornblende and biotite and at 15.0 kV with 10 nA sample current for feldspar and opaque minerals. The analytical results were then undertaken automatic ZAF correction supplied by JEOL. The Fe^{2+} and Fe^{3+} ratios of hornblende, clinopyroxene and biotite were recalculated using the equation of Droop (1987). Representative analyses of hornblende, plagioclase and pyroxene in mafic-ultramafic plutonic rocks are presented in Tables 3.1 to 3.3 where those of hornblende, feldspar and biotite in granitic rocks are presented in Tables 4.1 to 4.3.

1.3.5 Whole−rock geochemistry

Whole-rocks major and minor elements of mafic-ultramafic rocks and granitic rocks were obtained by X-ray Fluorescence (XRF), Bruker Model AXS S4 PIONEER, based at Department of Geology, Faculty of Science, Chulalongkorn University. Nine major oxides (i.e., SiO_2, TiO_2, FeO_{total}, MnO, MgO, CaO, Na_2O, K_2O and P_2O_5) were measured and calibrated with rock standards provided by Geological Survey of Japan (GSJ) and United States Geological Survey (USGS). Moreover, loss on ignition (LOI) was also measured prior XRF analysis.

Trace and rare earth elements were measured by an Inductively Coupled Plasma-Mass Spectrometry (ICP-MS), model iCAP Q based at the Scientific and Technological Research Equipment Centre, Chulalongkorn University. The rock powder samples were digested by the hydrofluoric acid and nitric acid, as suggested by Shapiro (1975). Detection limits range from 0.0001 ppm to 0.01% for trace elements. The results of whole-rock geochemistry study are presented in Tables 3.4 and 4.4 for the mafic-ultramafic plutonic rocks and granitic rocks, respectively.

1.3.6 Zircon U–Pb geochronology

The U-Pb geochronology study was dated using the zircon grains extracted from mafic-ultramafic rocks (e.g., hornblende gabbro sample no. 2WK6) (Table 3.5) and granitic rocks (Carboniferous biotite granite: sample no. WKG1, Late Permian hornblende granite sample no. 2WK4, and Triassic biotite-hornblende granite sample no. 2WK15) (Tables 4.5 to 4.7). The detailed analytical procedures for zircon analyses were followed by Tsutsumi et al. (2012). Firstly, the rock samples were crushed using iron-mortar and sieved to less than 0.2 mm. Dust was removed by water washing and then dried in a hot plate. The magnetic separation technique, heavy liquid (Tetrabromoethane) and finally hand picking under binocular microscope were then used to separate the zircon grains. The selected zircons were mounted in the resin with the zircon standard FC1 ($^{206}Pb/^{238}U$=0.1859, Paces and Miller (1993)) and NIST SRM 610 standard glass. Internal structure of zircon was investigated using the Cathodoluminescence (CL) images from scanning electron microprobe analyses. The U-Th-Pb isotopes were analyzed by a LA-ICP-MS (Inductively Coupled Plasma-Mass Spectrometer, Agilent 7700x, with ESI NWR213 Laser Ablation system) based at the National Museum of Nature and Science, Japan. The operating condition was designed using Nd-YAG laser with a 213 nm wavelength and 5 ns pulse together with a 25-micro spot size and 4-5 J/cm^2 laser power. Instead of Argon gas, Helium gas was used as carrier to enhance a higher transport efficiency of ablated materials (Eggins et al., 1998; Tsutsumi et al., 2012). The common Pb correlation for concordia diagrams and each age determination using the ^{208}Pb and ^{207}Pb (Williams, 1998) were pprocessed, on the basis of the proposed model for common Pb compositions by Stacey and Kramers

(1975). The calculation of the upper and lower intercepts in the Concordia diagram was studied by Isoplot 4.15/ Ex software (Ludwig, 2008).

1.3.7 Discussion and conclusion

The results of field investigation, petrography, mineral chemistry, whole-rock geochemistry and zircon U-Pb geochronology obtained from this study are reported in chapters 3 and 4, respectively. The results were interpreted and discussed on aspects of intrusion depth, magma genesis, age of rocks formation, and tectonic model. Finally, conclusions on specific aspects are stated in chapter 5.

1.3.8 Research publication and report writing

The results of this study were divided into 2 main parts, based on rock groups (i.e., mafic-ultramafic plutonic rocks and granitic rocks). Therefore, the manuscripts submitted to international journals were also prepared and entitled as:

1) Petrochemistry and mineral chemistry of Late Permian hornblendite and hornblende gabbro from the Wang Nam Khiao area, Nakhon Ratchasima, Thailand: Indication of Palaeo-Tethyan subduction

2) Petrology and zircon U-Pb geochronology of granitic rocks in the Wang Nam Khiao area, Nakhon Ratchasima, Thailand: Petrogenesis and tectonic implications

Both manuscripts were submitted to Journal of Asian Earth Sciences. The first manuscript has been already published in volume 130, pages 239-255 since November 2016. Currently, the second one is under reviewing process and expected to be published in 2017.

Regarding to the thesis report, it is arranged into 5 chapters including: 1) Introduction; 2) Geologic Setting; 3) mafic-ultramafic plutonic rocks; 4) granitic rocks; 5) conclusion. Overall background, objective, study area, and methodology is explained herein this chapter (Chapter 1). General geologic setting, tectonic framework, lithology and magmatism and sample collections are reported in chapter 2. Subsequently, chapters 3 and 4 are the main results and discussion of this study. Mafic-ultramafic plutonic rocks are described in chapter 3 whereas details of granitic rocks are reported

in chapter 4 which both chapters are conformed to the manuscripts mentioned above. Finally, conclusions of this study are present in chapter 5.

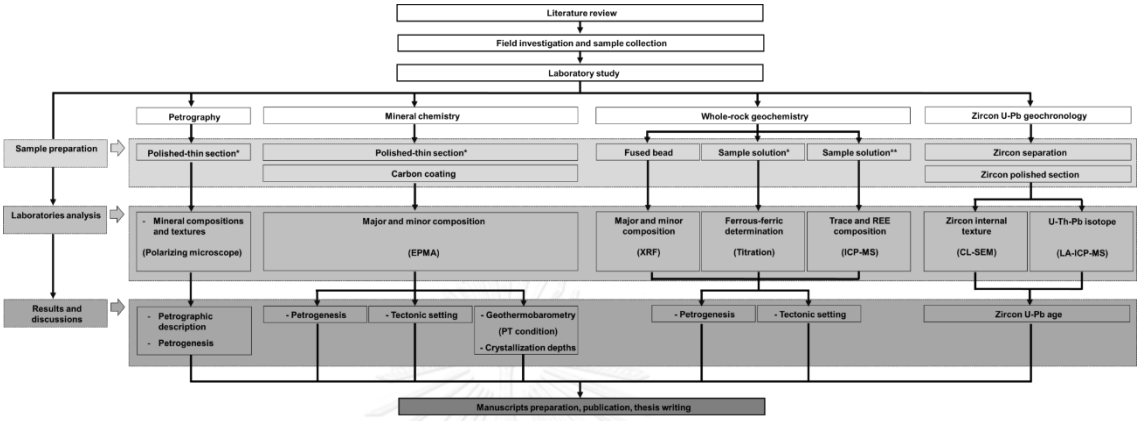

Figure 1.2 Summary of research methodology under this study, consisting of 5 main steps: literature review; field investigation and sample collection; laboratory study; results and discussion; manuscripts preparation, publication, thesis writing.

CHAPTER 2
GEOLOGIC SETTING

2.1 Tectonic framework

The main tectonic terranes in Thailand (Fig. 2.1) can be distinguished into Indochina and Shan-Thai (or Sibumadu of Sone and Metcalfe (2008)) Terranes to the east and west, respectively. They were purposed by Bunopas (1981); Bunopas and Vella (1992); Charusiri et al. (2002). Both terranes cover from north to south of the country; moreover, they also extended to the mainland of Southeast Asia (Fig. 2.1). Both microcontinents are separated by Sukhothai Fold Belt (Sukhothai Terrane; Sone and Metcalfe (2008)) and Loei Fold Belt (Loei-Petchabun Fold Belt; Burrett et al. (2014)). The tectonic units are explained below.

2.1.1 Indochina Terrane

Indochina terrane, a large tectonic terrane in SE Asia and eastern Thailand, has been bounded by the Ailaoshan - Song Ma Suture (Bunopas, 1981; Bunopas and Vella, 1992; Metcalfe, 2013; Zaw et al., 2014) to the northeast with the Truong Son Fold Belt (Kamvong et al., 2014; Zaw et al., 2014) in the eastern margin which is separated from the South China Terrane. In the west of this terrane, it is bounded by the Jinhong, Nan – Uttaradit, Sra Keao Suture (Bunopas, 1981; Bunopas and Vella, 1992; Metcalfe, 2013) with defined the Loei Fold Belt (Bunopas, 1981; Zaw et al., 2014) along the western margin of Indochina Terrane. The Indochina terrane is dominated by Palaeozoic marine volcanic rocks, Early Permian-Triassic granitoids, volcanic rocks (Carter and Clift, 2008; Lepvrier et al., 2008; Lepvrier et al., 2011; Zaw et al., 2014), and thick Mesozoic sedimentary rocks (Brown, 1951; Piyasin, 1985; Racey et al., 1994; Booth and Sattayarak, 2011).

2.1.2 Shan-Thai Terrane (Sibumasu Terrane)

Shan-Thai Terrane (Bunopas, 1981; Charusiri et al., 2002; Ferrari et al., 2008) or Sibumasu Terrane (Sone and Metcalfe, 2008; Metcalfe, 2013) (Fig. 2.1) is bordered by the Sakaing Fault – Mokok Metamorphic Belt to the west in Myanmar and Sukhothai Fold Belts (Bunopas, 1981; Bunopas and Vella, 1992) including Inthanon terrane

(Ferrari et al., 2008; Sone and Metcalfe, 2008; Zaw et al., 2014) to the east in Thailand extending southwards to the Malay Peninsula in which is bounded by the Pattani (Bentong Raub) Suture Zone to the east (Bunopas, 1981; Charusiri et al., 2002; Ferrari et al., 2008; Searle et al., 2012; Metcalfe, 2013). The Shan-Thai Terrane is dominated by the Paleozoic sedimentary rocks (Javanaphet, 1969; Bunopas, 1981; Raksaskulwong and Wongwanich, 1994), Mesozoic sedimentary rocks (Raksaskulwong and Wongwanich, 1994), and Triassic granitoids (Cobbing et al., 1986; Cobbing et al., 1992; Nakapadungrat and Putthapiban, 1992; Charusiri et al., 1993; Searle et al., 2012; Ng et al., 2015a; Ng et al., 2015b).

2.1.3 Loei Fold Belt

Loei Fold Belt (Fig. 2.1) (Bunopas, 1981) is located along the western edge of Indochina Terrane from northern Laos – Loei – Petchabun – Sra Keao in Thailand and run into the western Cambodia (Zaw et al., 2014) which is bounded by the Jinghong – Nan – Sra Keao Suture to the west (Bunopas, 1981; Zaw et al., 2014). This Loei Fold Belt is equivalent to the Nakhon Thai Terrane of Charusiri et al. (2002). The Loei Fold Belt is composed of the multiple arc-magmatic events which generated the different volcanic rocks (Jungyusuk and Khositanont, 1992; Intasopa, 1993; Intasopa and Dunn, 1994; Panjasawatwong et al., 2006; Khositanont et al., 2008; Barr and Charusiri, 2011; Boonsoong et al., 2011; Kamvong et al., 2014; Salam et al., 2014; Qian et al., 2015) and plutonic rocks (Cobbing et al., 1986; Cobbing et al., 1992; Nakapadungrat and Putthapiban, 1992; Charusiri et al., 1993; Khositanont et al., 2008; Morley et al., 2011; Salam et al., 2014; Zaw et al., 2014).

2.1.4 Sukhothai Terrane-Chanthaburi Terrane

Sukhothai Terrane (Sone and Metcalfe, 2008) or Sukhothai Fold Belt (Bunopas, 1981) (Fig. 2.1) is separated from Loei Fold Belt by the Jinghong – Nan – Uttaradit – Sra Kaeo Suture. This terrane is located in the north of Thailand and regionally continues to the Chanthaburi Terrane (Sone and Metcalfe, 2008; Sone et al., 2012) in eastern Thailand, to southwestern Cambodia (Sone et al., 2012). This terrane is interpreted to link with the East Malaya Fold Belt (Metcalfe, 2013) to the south in the Malaysia and the Lincang Terrane to the north in Yunnan (Zaw et al., 2014). The Sukhothai Terrane is dominated by the deep water volcanic clastic rocks inter-bedded

with volcanic rocks (Barr et al., 2006), volcanic rocks (Srichan et al., 2009), deformed shallow-marine sedimentary rocks (Burrett et al., 2014) and I- or S-type granitoids (Cobbing et al., 1986; Cobbing et al., 1992; Nakapadungrat and Putthapiban, 1992; Charusiri et al., 1993).

2.2 Background geology

Wang Nam Khiao area, Nakhon Ratchasima, northeastern Thailand is considered to be a part of the Loei Fold Belt (Fig. 2.1) (Bunopas, 1981; Zaw et al., 2007; Kamvong et al., 2014; Zaw et al., 2014; Fanka et al., 2016) or Loei-Petchabun Fold Belt (Burrett et al., 2014) in the east of the Nan – Sra Kaeo suture (Zaw et al., 2007; Sone and Metcalfe, 2008; Metcalfe, 2011b, a, 2013; Zaw et al., 2014) which is located between the Sibumasu (Shan-Thai) Terrane and Indochina Terrane (Charusiri et al., 2002) (Fig. 2.1) and associated with the close Sukhothai Terrane (ST) – Chathaburi Terrane (CT) (Sone and Metcalfe, 2008; Metcalfe, 2011b, a; Sone et al., 2012; Metcalfe, 2013).

In Loei Fold Belt, the magmatic rocks have been reported for both volcanic rocks (Jungyusuk and Khositanont, 1992; Intasopa, 1993; Intasopa and Dunn, 1994; Panjasawatwong et al., 2006; Khositanont et al., 2008; Barr and Charusiri, 2011; Boonsoong et al., 2011; Kromkhun et al., 2013; Kamvong et al., 2014; Salam et al., 2014; Vivatpinyo et al., 2014; Qian et al., 2015) and plutonic rocks (Cobbing et al., 1986; Cobbing et al., 1992; Nakapadungrat and Putthapiban, 1992; Charusiri et al., 1993; Khositanont et al., 2008; Morley et al., 2011; Salam et al., 2014; Zaw et al., 2014) (Fig. 2.1).

In term of plutonic rocks in the LFB, there are widespread exposures of mafic – ultramafic rocks (Putthaphiban et al., 1981a, b, 1989a, b; Fanka et al., 2016) to granitic rocks (Nakapadungrat and Putthapiban, 1992; Charusiri et al., 1993; Kromkhun et al., 2013; Salam et al., 2014; Zaw et al., 2014) grouped as both I-type granitoids (Kamvong et al., 2014; Salam et al., 2014; Zaw et al., 2014) and S-type granitoids (Sone and Metcalfe, 2008; Morley et al., 2011) belonging to the Eastern Granite Belt of Thailand (Cobbing et al., 1986; Cobbing et al., 1992; Nakapadungrat and Putthapiban, 1992;

Charusiri et al., 1993; Searle et al., 2012). These rocks are characterized significantly by the calc-alkaline affinities (Khositanont et al., 2008; Kromkhun et al., 2013; Kamvong et al., 2014; Salam et al., 2014). They were interpreted as the arc-magmatic events related to the Carboniferous to Triassic Indochina subduction (Nakapadungrat and Putthapiban, 1992; Charusiri et al., 1993; Intasopa, 1993; Searle et al., 2012; Salam et al., 2014; Ng et al., 2015a; Ng et al., 2015b), and related to the reported arc-related volcanism in the LFB during Early Silurian to Late Cenozoic (Bunopas, 1981; Intasopa and Dunn, 1994; Panjasawatwong et al., 2006; Khositanont et al., 2008; Boonsoong et al., 2011; Zaw et al., 2014).

In the Wang Nam Khiao area, a variety of plutonic rocks have been reported (Putthaphiban et al., 1981b, a, 1989b, a; Nonsung, 2010; Booncharoen, 2011) ranging in compositions from mafic-ultramafic plutonic rocks (e.g., hornblendite, hornblende gabbro) (Putthaphiban et al., 1981a, b, 1989a, b; Jiratitipat, 2010; Hunyek, 2012; Fanka et al., 2016) to granitic rocks (Putthaphiban et al., 1981a, b, 1989a, b; Jiratitipat, 2010; Nonsung, 2010; Booncharoen, 2011). They are however referred to the Eastern Granite Belts of Thailand located in LFB (Putthaphiban et al., 1981a, b, 1989a, b; Nakapadungrat and Putthapiban, 1992; Charusiri et al., 1993) (Fig. 2.1). The mafic-ultramafic plutonic rocks were reported as the magmatism of Late Permian arc-related subduction of Palaeo-Tethys beneath Indochina (Fanka et al., 2016). In addition, the granitic rocks in the Wang Nam Khiao area were interpreted as I-type granites formed by magmatism of arc-related subduction and continental collision (Nonsung, 2010; Booncharoen, 2011) based on the mineral composition and petrography study.

These plutonic rocks were associated with the Permo-Triassic volcanic rocks, particularly rhyolite and andesite (Putthaphiban et al., 1981a, b, 1989a, b) which may be comparable to volcanism of LFB (Jungyusuk and Khositanont, 1992; Intasopa, 1993; Intasopa and Dunn, 1994; Panjasawatwong et al., 2006; Khositanont et al., 2008; Barr and Charusiri, 2011; Boonsoong et al., 2011; Kromkhun et al., 2013; Kamvong et al., 2014; Salam et al., 2014; Vivatpinyo et al., 2014; Qian et al., 2015). The magmatic rocks in the Wang Nam Khiao area are covered by the Mesozoic Khorat Group (Putthaphiban et al., 1981a, b; Piyasin, 1985; Putthaphiban et al., 1989a, b) (Fig. 2.3).

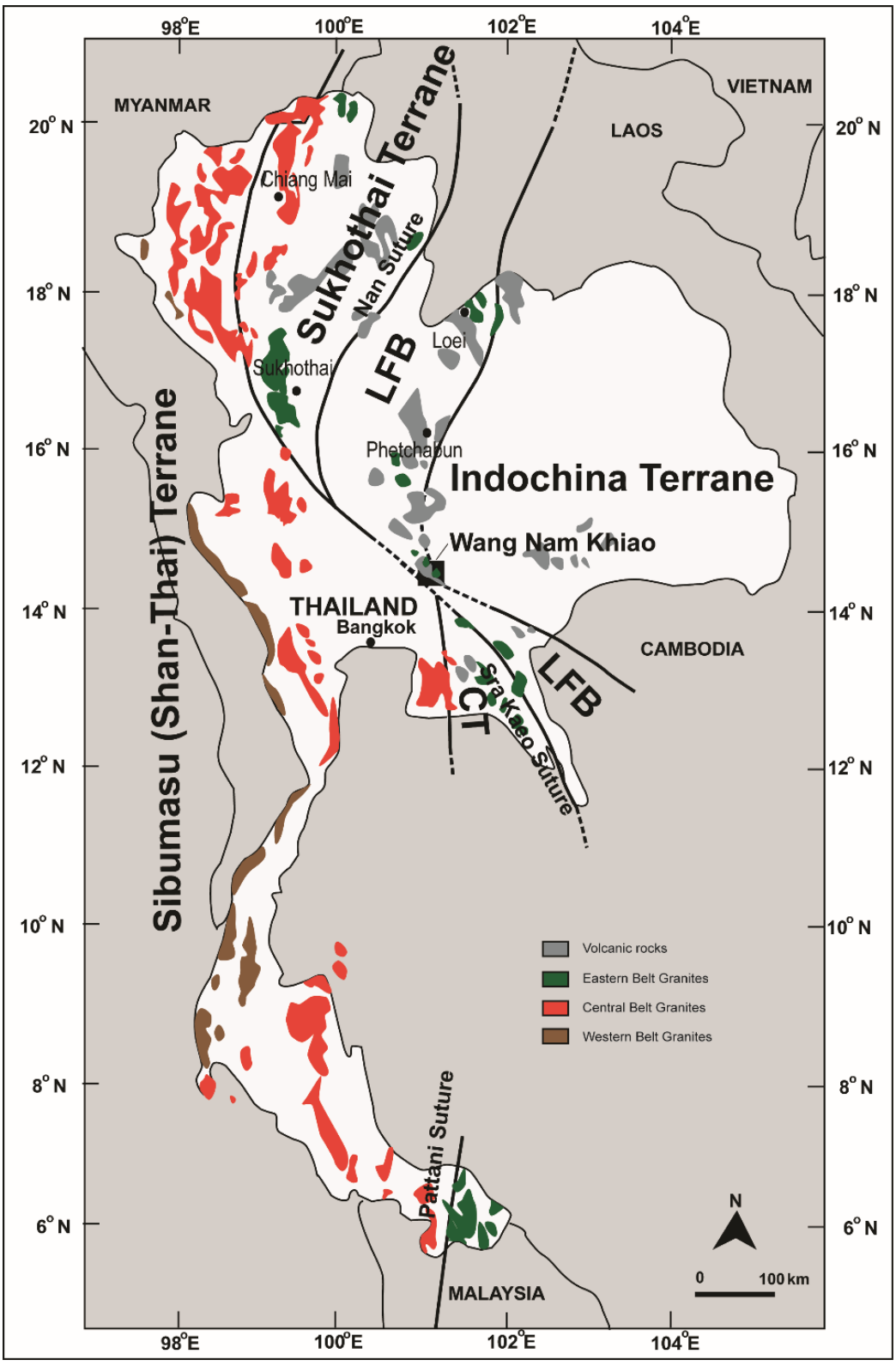

Figure 2. 1 The distribution of the igneous rocks, both plutonic and volcanic rocks, within the main tectonic terranes of Thailand (Modified after Charusiri et al. (2002);

Sone and Metcalfe (2008); Sone et al. (2012); Metcalfe (2013); Zaw et al. (2014)). The distributions of granitic rocks are modified from Nakapadungrat and Putthapiban (1992); Charusiri et al. (1993), and volcanic rocks are modified from Jungyusuk and Khositanont (1992); Panjasawatwong et al. (2006); Barr and Charusiri (2011).

According to structural geology, the well-known N-S and NE-SW lineaments were purposed in the northern and central Thailand (Tapponnier et al., 1986; Morley et al., 2013). The Wang Nam Khiao area is located nearby the WNW–ESE to NW-SE trending Khao Yai Fault zone (Ridd and Morley, 2011; Morley et al., 2013) extending to the south (Fig. 2.2) which is similar trend to the NW-SE trending Cenozoic strike-slip Mae Ping Fault or Wang Chao Fault (Tapponnier et al., 1986; Morley, 2007; Ridd and Morley, 2011; Ueno and Charoentitirat, 2011; Ridd, 2012; Morley et al., 2013).

In term of microstructural geology of the Wang Nam Khiao area, carried out by Na Lampang (2015), show ENE-WSW, ESE-WNW, and NE-SW directions for the granitic rocks, volcanic rocks, and Permian sedimentary rocks, NW-SE direction for the clastic sedimentary Khorat Group which are interpreted as the results of Indosinian Orogeny during the Late Permian to Late Triassic (Booth and Sattayarak, 2011).

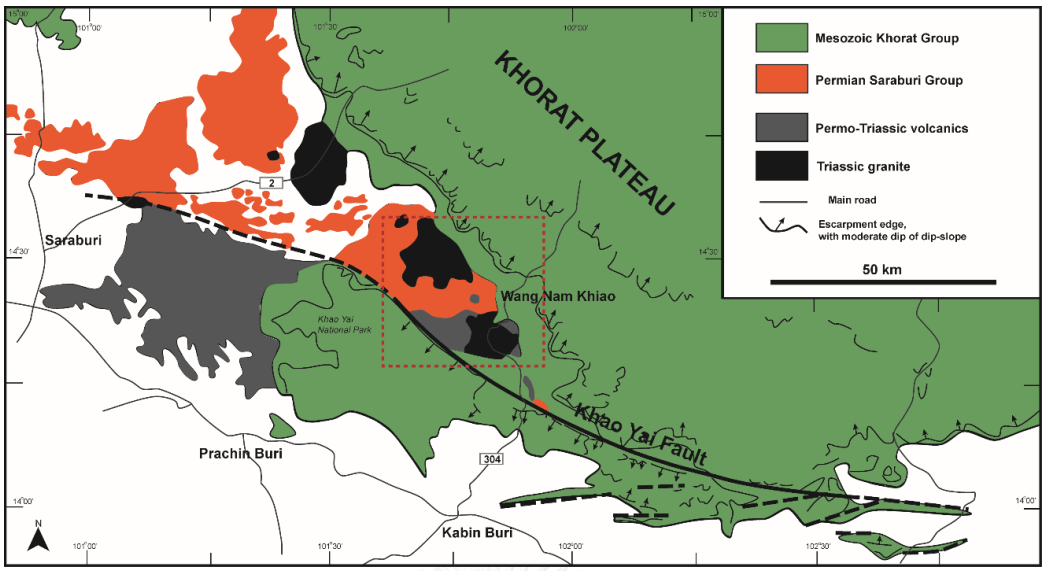

Figure 2.2 Simplified geologic map with the lineaments of the southern border of the Khorat Plateau including Wang Nam Khiao area (red dashed block) and the interpreted Khao Yai Fault (thick solid black line) (Modified after Ridd and Morley (2011)).

2.3 Sample collection

The study area, Wang Nam Khiao Plutonic Complex, is located in Amphoe Wang Nam Khiao, Changwat Nakhon Ratchasima, and some parts of Amphoe Na Di, Changwat Prachin Buri which cover the plutonic exposures varying in composition from mafic-ultramafic rocks to granitic rocks which should be defined as plutonic complex (Fig. 2.3). The study area covers approximately 1,120 square kilometers between the latitude 14° 15' – 14° 33' N and longitude 101° 37' - 101° 55' E.

This study area is about 200 kilometers northeast of Bangkok (Fig. 2.3). The highway no. 304 can be used to access the southern plutonic bodies and the highway number 2082 (crossing with highway number 304) is the main road to access the northern plutonic bodies (Fig. 2.3). Natural exposures and artificial quarries are main outcrops exposed in the general rolling topography (Fig. 2.4).

Fifty-two sample locations (Table 2.1) were representatively observed and collected the rock samples within this study area. There are 16 samples of mafic-ultramafic plutonic rocks and 36 samples of granitic rocks. Mafic-ultramafic plutonic

samples consist of 10 hornblendites, 5 hornblende gabbros and 1 hornblende microgabbro. For the granitic samples, 10 biotite granites, 18 hornblende granites, and 8 biotite-hornblende granites were collected to be representatives.

Details of the field investigation will be reported in chapters 3 and 4 together with laboratory results.

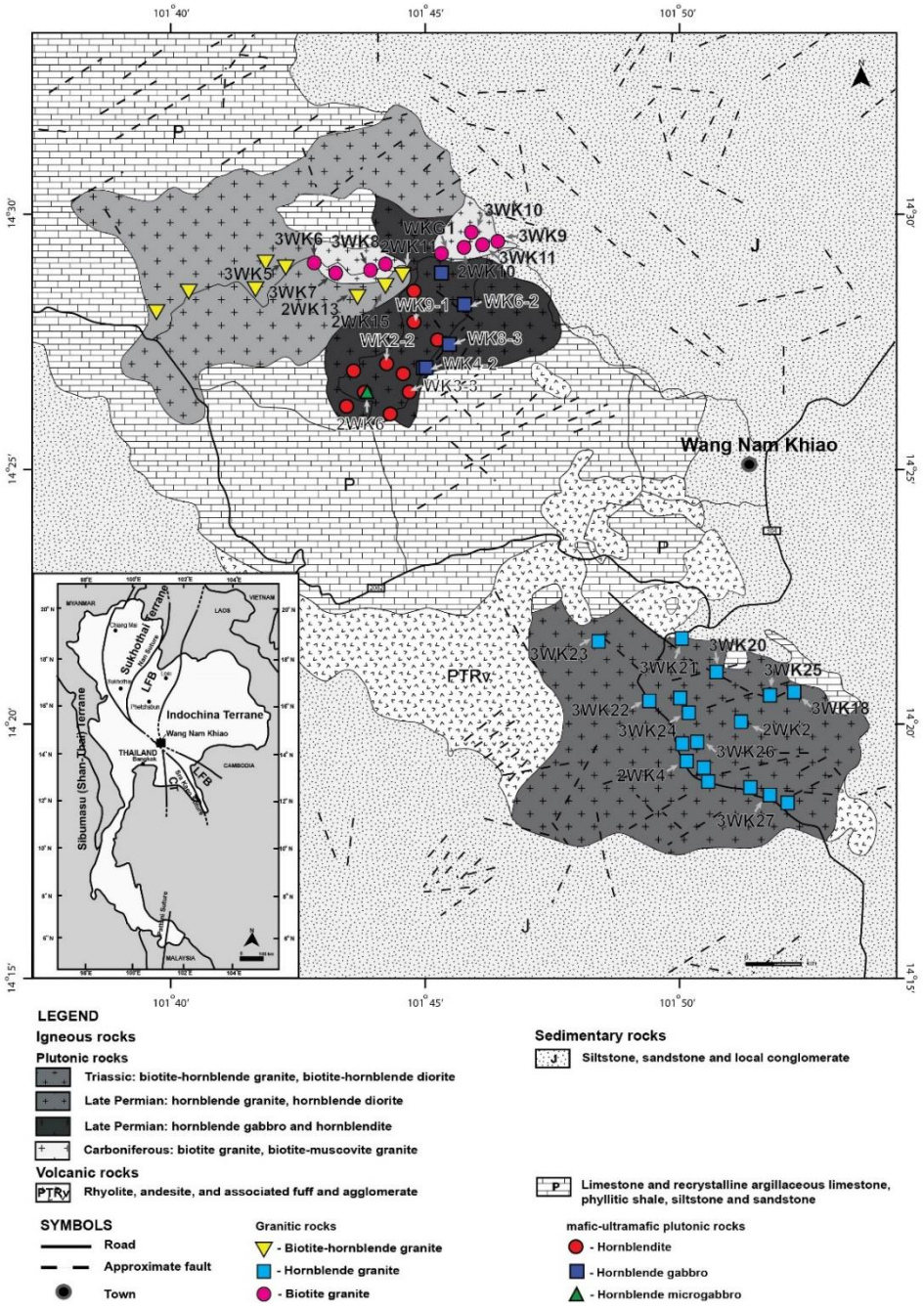

Figure 2.3 The geological map of the study area, Wang Nam Khiao area, Nakhon Ratchasima, northeastern Thailand (modified after Putthaphiban et al. (1981a, 1981b, 1989a, 1989b)) showing sample locations as summarized in Table 2.1.

Figure 2.4 The exposures of rocks in the study area: (a, b) natural outcrops; (c, d) artificial quarry in the (e) rolling land.

Table 2.1 Sample locations of the plutonic rocks in the study area.

Sample location		Sample no.	Rock type	Rock unit
Easting	Northing			
795612	1597861	WK1	hornblendite	mafic-ultramafic rocks
795124	1599851	WK2	hornblendite	
795463	1599628	WK3	hornblendite	
794995	1601513	WK9	hornblendite	
795523	1597763	WK10	hornblendite & marble	
794699	1598593	2WK5	hornblendite	
794568	1599016	2WK7	hornblendite	
794427	1598147	2WK8	hornblendite	
795634	1597837	2WK9	hornblendite	
795472	1601598	2WK12	hornblendite	
796987	1599951	WK4	hornblende gabbro	
797658	1601898	WK5	hornblende gabbro	
798731	1603105	WK6	hornblende gabbro	
797743	1603105	WK7	hornblende gabbro	
798315	1602019	WK8	hornblende gabbro	
794605	1598514	2WK6	hornblende microgabbro & hornblendite	
795079	1602682	2WK14	biotite granite&spotted slate	biotite granite
792765	1603009	3WK6	biotite granite	
793579	1602545	3WK7	biotite granite	
794265	1602682	3WK8	biotite granite	
794692	1602616	3WK9	biotite granite	
799208	1603665	3WK10	biotite granite	
798708	1603648	3WK11	biotite granite	
798576	1603882	3WK12	biotite granite	
797301	1603056	WKG1	biotite granite	
798878	1603632	2WK10	biotite granite	
809124	1587459	3WK19	hornblende diorite	hornblende granite
807213	1588362	3WK20	hornblende granite	
804800	1587214	3WK23	hornblende diorite	
806188	1585002	3WK24	hornblende diorite	
808110	1586484	2WK1	hornblende diorite	
806067	1585784	3WK26	hornblende diorite	
809260	1583423	3WK28	hornblende diorite	
809151	1583749	3WK27	hornblende granite	
804863	1590387	3WK30	hornblende diorite	
805912	1585216	2WK4	hornblende diorite	

Table 2.1 (cont.)

Sample location		Sample no.	Rock type	Rock unit
Easting	Northing			
805995	1589493	3WK21	hornblende diorite	hornblende granite
809968	1587579	3WK18	hornblende granite	
805991	1587632	3WK22	hornblende diorite	
806273	1586840	2WK2	hornblende diorite	
806569	1585761	3WK25	hornblende diorite	
806100	1584729	2WK3	hornblende diorite	
808658	1583765	3WK29	hornblende diorite	
803410	1589768	3WK31	hornblende diorite	
796392	1602725	2WK11	biotite-hornblende diorite	biotite-hornblende granite
796001	1602401	2WK13	biotite-hornblende diorite	
795873	1602788	2WK15	biotite-hornblende granite	
786709	1601488	3WK1	biotite-hornblende diorite	
788490	1601954	3WK2	biotite-hornblende diorite	
791099	1602109	3WK3	biotite-hornblende diorite	
791788	1602889	3WK4	biotite-hornblende diorite	
792354	1603210	3WK5	biotite-hornblende granite	

CHAPTER 3

MAFIC-ULTRAMAFIC PLUTONIC ROCKS

Mafic- ultramafic plutonic rocks in the Wang Nam Khiao area, Nakhon Ratchasima were investigated and will be reported in 6 main parts including field observation, petrography, mineral chemistry, whole- rock geochemistry, geothermobarometry and zircon U-Pb geochronology. These results can be used to discuss on intrusion depths, magma genesis, petrogenesis, and age of rock formation.

The main parts of this study have been published in the Journal of Asian Earth Sciences, Volume 130, 15 November 2016, Pages 239-255, under the title ***" Petrochemistry and mineral chemistry of Late Permian hornblendite and hornblende gabbro from the Wang Nam Khiao area, Nakhon Ratchasima, Thailand: Indication of Palaeo-Tethyan subduction"***.

3.1 Field observation

The mafic – ultramafic plutonic rocks in the study area are found within the mapped area as Late Permian hornblende gabbro and hornblendite (Fig. 2.3) in the northern part of the study area which is contact with the Carboniferous biotite granite to the north, Triassic biotite- hornblende granite to the northwest, the Permian sedimentary rocks to the south, and the Mesozoic sedimentary rocks of Khorat Group to the east (Fig. 2.3). However, most contacts of mafic – ultramafic plutonic rocks with other rocks are not clear. The exposures of these rocks cover about 5 km wide and 6 km long. These mafic – ultramafic plutonic rocks can be classified into the hornblendite, hornblende gabbro and hornblende microgabbro (Fig. 3.1), based on the field investigation and detailed petrographic classification. Hornblendite is characterized by the coarse-grained dark colored massive rock (Fig. 3.1a, b) with some weak foliations (Fig. 3.1c) in some locations together with marble lens (Fig. 3.1d), particularly near the pluton rim, which are mainly found in the western part of pluton (Fig. 2.3). Hornblende gabbro (Fig. 3.1e, f) are exposed in the northwest of pluton (Fig. 2.3) which is usually characterized by coarse- to medium-grained and dark grayish rock

with weak foliation (Fig. 3.1f) in some locations. In addition, the hornblendite is cut by the dike of medium- to fine-grained hornblende microgabbro (Fig. 3.1a, b) in some locations. The hornblendite and hornblende gabbro are clearly isolate exposures in the pluton which is rolling land (Fig. 2.4).

Figure 3.1 Photographs of mafic-ultramafic exposures in the Wang Nam Khiao area, Nakhon Ratchasima including (a, b) hornblende microgabbro occurred as a dike cutting hornblendite (sample 2WK6), (c) weak foliation of hornblendite, (d)

hornblendite and marble contact, (e) hornblende gabbro with (f) weak foliation of hornblende gabbro.

3.2 Petrography

The mafic-ultramafic plutonic rocks in this study are classified, based on petrographic study, as hornblendite and related hornblende gabbro. The details of petrographic characters are reported below.

Hornblendite: comprises mostly hornblende (more than 90%) (Figs. 3.2a, b and c) with some accessory plagioclase (5%), clinopyroxene (2-3%), and less abundant (1-2%) chlorite, epidote, calcite, apatite, muscovite and opaque minerals (pyrite, magnetite) with/without scapolite and sphene in some samples. Euhedral shape of greenish hornblende shows very coarse- to coarse-grained (1 mm to 1 cm). In addition, the tiny inclusions of apatite are usually found in these hornblendes. Plagioclase shows as the medium- to coarse-grained crystals which are found between the hornblende grains. Moreover, between the coarse-grained hornblende and plagioclase are usually discovered the fine-grained plagioclase, epidote, chlorite and calcite. Anhedral clinopyroxene is found as a relic in hornblende and small crystals around the very coarse- and coarse-grained hornblende. For other accessory minerals, fine-grained sphene (titanite) are presented as a subhedral to euhedral shapes while medium-grained scapolite is found only the hornblendite contact with the marble (Fig. 3.2d), which should be resulted from the metasomatism of mafic magma and host marble. Opaque minerals are also found as accessory minerals which contain magnetite (Fig. 3.3a, b) with some pyrites.

Hornblende gabbro: fine- to coarse-grained and subhedral to anhedral plagioclase (40-60%), subhedral to euhedral hornblende (40-60%) and clinopyroxene (5-10%) are presented as dominant minerals together with other epidote and apatite as accessory minerals (1-3%). The clinopyroxene shows subhedral and sometimes rounded grains which are probably corresponding to the earliest mineral formed during magmatic crystallization. The microscopic textures of subophitic and intergrowth textures of plagioclase (0.1-0.7 mm) and hornblende (0.4-1.1 mm) are found in this

rock and probably later crystallization phases are found as the matrix of clinopyroxene. These textures indicate the clear primary igneous texture (Fig. 3.2e). In addition, the foliation of medium-grained hornblende and plagioclase orientation (Fig. 3.2f) are found in some parts of the hornblende gabbro.

Hornblende microgabbro: a dike cut into hornblendite, is dominated by fine- to medium-grained (0.05-0.4 mm) hornblende (40-60%) and plagioclase (40-60%). In addition, magnetite and epidote (Figs. 3.2c, d) are presented as accessory minerals (1-5%). Subhedral to anhedral plagioclase and hornblende show primary igneous texture with some fine-grained opaque minerals. The grain boundaries of coarse-grained hornblende and plagioclase display the fine-grained epidote. Some part of this rock is also presented oriented hornblende and plagioclase.

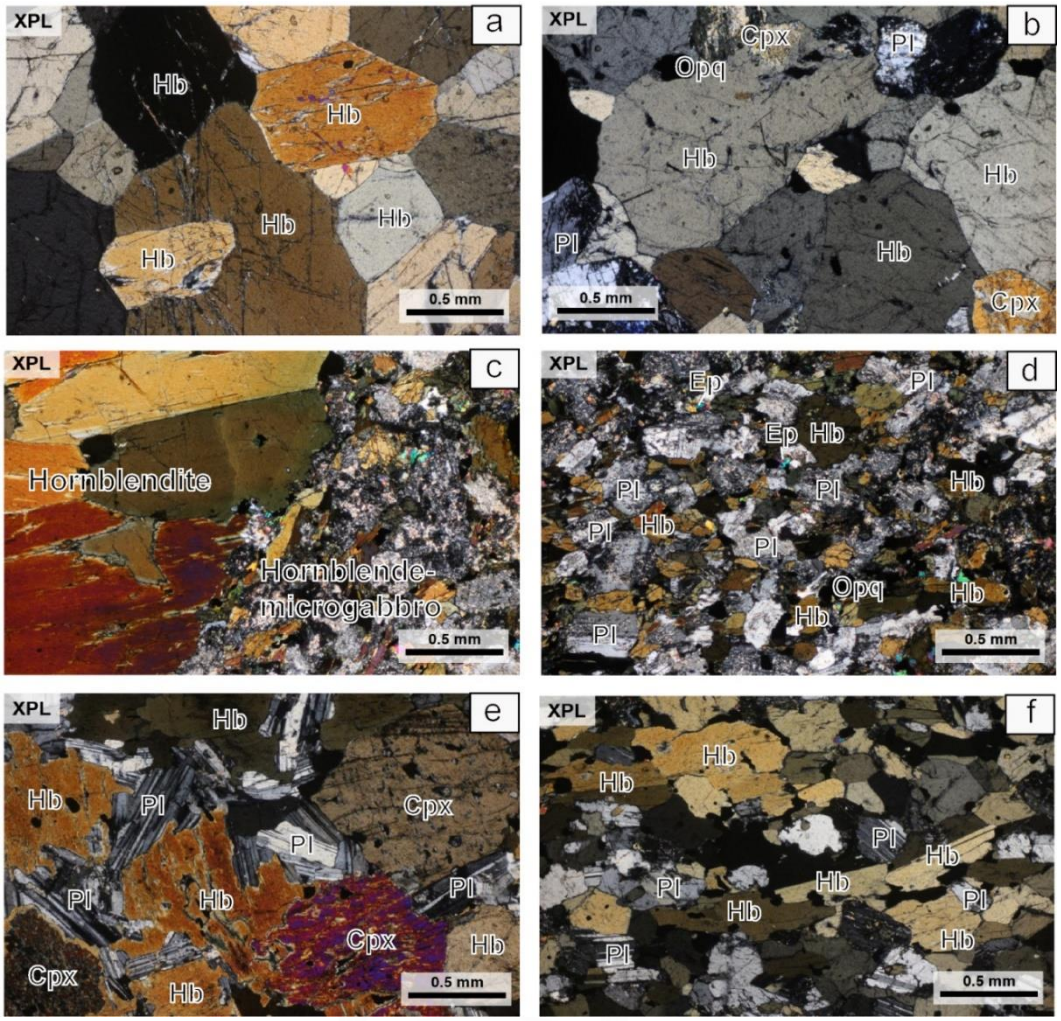

Figure 3.2 Photomicrographs of mafic-ultramafic rocks in the Wang Nam Khiao area, Nakhon Ratchasima showing typical mineral assemblages and textures. (a, b) Equigranular hornblende with some plagioclase and clinopyroxene in hornblendite. (c) A contact between hornblende microgabbro (fine-grained texture) and host hornblendite (coarse-grained texture). (d) Fine-grained hornblende and plagioclase in hornblende microgabbro. (e) Magmatic texture of hornblende gabbro with plagioclase, hornblende and clinopyroxene. (f) Hornblende gabbro with abundant oriented hornblende and plagioclase. Mineral abbreviations; Hb (hornblende), Pl (plagioclase), Cpx (clinopyroxene), Ep (epidote), Opq (opaque minerals).

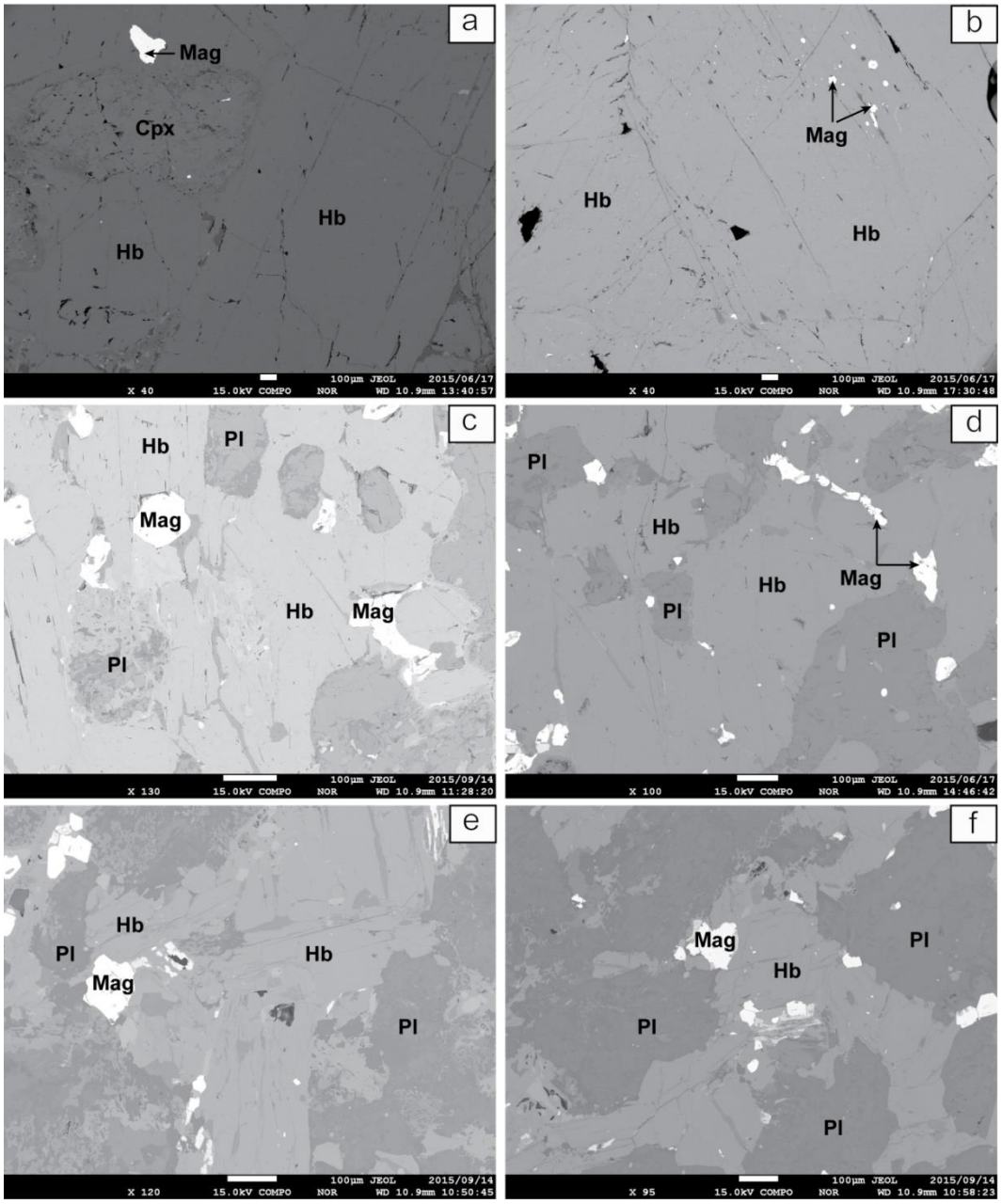

Figure 3. 3 BEI images showing opaque minerals in (a, b) hornblendite, (c, d) hornblende gabbro, and (e, f) hornblende microgabbro in the Wang Nam Khiao area, Nakhon Ratchasima. Mineral abbreviations; Hb (hornblende), Pl (plagioclase), Cpx (clinopyroxene), Ep (epidote), Mag (magnetite).

3.3 Mineral chemistry

Mineral chemical analyses can provide the important data about the characteristics of mineral composition of the mafic-ultramafic plutonic rocks in the study area. In addition, the analytical data can be discussed with other results (e.g., petrography, whole-rocks geochemistry, geochronology) to understand the genesis of rocks which can also be applied to tectonic setting. Moreover, the mineral chemistry of some coexisting minerals can be used to estimate the PT condition of rocks' crystallization (Section 3.5).

As the reported mineral compositions of these rocks, the dominant mineral assemblages, especially amphibole, plagioclase and clinopyroxene of the mafic-ultramafic plutonic rocks were presented and described in this section.

Sixteen samples (Table 2.1) of mafic-ultramafic plutonic rocks in the Wang Nam Khiao area, Nakhon Ratchasima were prepared as polished thin sections for mineral chemical analyses using Electron Probe Micro Analyzer (EPMA) (the detailed procedures in section 1.3.4). Solid-solution minerals such as calcic amphibole, plagioclase and clinopyroxene are shown in Tables 3.1 to 3.3, plotted in Fig. 3.4, and summarized below.

Calcic amphibole: The calcic amphibole is the most dominant mineral assemblages in the mafic-ultramafic plutonic rocks in the study area (Fig. 3.2). The representative analyses of calcic amphiboles and their recalculated cations based on 23 oxygens are revealed in Table 3.1.

The analyzed calcic amphiboles approximately comprise 40-42 %SiO_2, 13-15 %Al_2O_3, 13-14 %MgO, 11-12 %CaO, 10-12 %FeO_t, and 2 %Na_2O of hornblendite, 40-42 %SiO_2, 13-14 %Al_2O_3, 11-13 %MgO, 12 %CaO, 12-14 %FeO_t, and 2 %Na_2O of hornblende gabbro, and 40-42 %SiO_2, 13-14 %Al_2O_3, 9-10 %MgO, 11 %CaO, 16-17 %FeO_t, and 2 %Na_2O of hornblende microgabbro.

In term of mineral chemistry, the calcic amphiboles in the hornblendite are classified as pargasite with some edenite in component (X_{Mg} = 0.66-0.71, Si = 5.96-6.29 pfu, Al = 2.34-2.69 pfu, $(Na+K)_A$ = 0.71-0.77 pfu, and TiO2 = 1.64-1.94 wt%; Fig. 4a) based on the nomenclature of Leake et al. (1997). The hornblende gabbro and

hornblende microgabbro show the same calcic amphibole compositions which fall within the same pargasite field (Fig. 3.4a), although the latter shows slightly lower X_{Mg} (X_{Mg} = 0.60-0.66, Si = 6.09-6.22 pfu, Al = 2.23-2.52 pfu, $(Na+K)_A$ = 0.73-0.82 pfu, and TiO_2 = 1.80-1.95 wt% for hornblende gabbro and X_{Mg} = 0.50-0.52, Si = 6.18-6.45 pfu, Al = 2.23-2.47 pfu, $(Na+K)_A$ = 0.65-0.72 pfu, and TiO_2 = 1.11-1.56 wt% for hornblende microgabbro) (Table. 3.1, Fig. 3.4a).

Plagioclase: is one of the most common mineral assemblages in all hornblendite, hornblende gabbro, and hornblende microgabro (Fig. 3.2). The analytical results of plagioclase and calculated formula based on 8 oxygens are presented in the Table 3.2.

The plagioclase in hornblendite presents composition ranges of about 44-45% SiO_2, 35% Al_2O_3, 18-19% CaO, 1% Na_2O, while the hornblende gabbro shows plagioclase composition varying about 45-46% SiO_2, 34-35% Al_2O_3, 18% CaO, 1% Na_2O, and the hornblende gabbro reveals plagioclase composition ranges of 45-57% SiO_2, 27-35% Al_2O_3, 10-18% CaO, 1-6% Na_2O.

The plagioclase in hornblendite presents significantly higher anorthite (An) contents (An_{92-94}, which is classified as anorthite) than that in hornblende gabbro (corresponding to labradorite to anorthite in composition, An_{88-91}), while composition of plagioclase in hornblende microgabbro reveals the lowest anorthite contents (An_{47-57}) indicating andesine to labradorite composition (Table 3.2, Fig. 3.4b). The anorthite contents of these plagioclase exhibit decreasing from hornblendite to hornblende gabbro and hornblende microgabbro; on the other hand, their mineral assemblages appear to be increasing amount of plagioclase and decreasing amounts of clinopyroxene and calcic-amphibole, representatively. These evidences may indicate their relationship of fractional crystallization.

Clinopyroxene: is found as minor mineral compositions in hornblendite and hornblende gabbro (Fig. 3.2) while the clinopyroxene is not presented in the hornblende microgabbro. The analytical results of clinopyroxene and calculated formula based on 6 oxygens are presented in the Table 3.3.

All the analyzed clinopyroxenes from hornblendite and hornblende gabbro reveal nearly consistent Mg-rich composition, classified as diopside, in term of Fe-Mg

ratio (Fig. 3.4c), although clinopyroxene in hornblendite is slightly enriched in X_{Mg} (X_{Mg} = 0.76-0.78) than that in hornblende gabbro (X_{Mg} = 0.70-0.78) (Table 3.3, Fig. 3.4c).

Table 3.1 Representative EPMA analyses of hornblende in hornblendite, hornblende gabbro and hornblende microgabbro in the Wang Nam Khiao, Nakhon Ratchasima, Thailand.

Rock type	Hornblendite					Hornblende gabbro		
Sample no.	WK2-1	WK2-1	WK3-1	WK3-1	WK9-6	WK4-2	WK4-2	WK4-2
Remark	Core	Rim	Core	Rim	Rim	Core	Rim	Core
SiO_2	39.96	41.72	39.91	41.08	42.47	41.02	40.62	40.68
Al_2O_3	15.18	13.34	15.28	14.22	13.44	12.86	13.48	13.70
TiO_2	1.87	1.64	1.94	1.69	1.87	1.93	1.95	1.88
Cr_2O_3	0.02	0.00	0.00	0.04	0.02	0.02	0.01	0.00
FeO	11.75	11.14	10.39	10.32	10.12	13.62	13.67	13.56
MnO	0.16	0.12	0.13	0.13	0.12	0.20	0.20	0.25
MgO	12.65	13.55	13.51	13.83	13.69	11.90	11.46	11.74
CaO	12.20	12.26	12.02	12.21	11.46	11.71	11.84	11.65
Na_2O	2.17	2.14	2.25	2.12	2.24	2.29	2.26	2.30
K_2O	0.63	0.52	0.61	0.56	0.57	0.68	0.77	0.73
Cl	0.05	0.01	0.01	0.00	0.04	0.07	0.08	0.05
F	0.02	0.01	0.01	0.02	0.03	0.02	0.02	0.02
Total	96.67	96.44	96.07	96.22	96.07	96.31	96.34	96.55
23 (O)								
Si	5.969	6.206	5.956	6.107	6.290	6.200	6.145	6.132
Al	2.672	2.338	2.686	2.491	2.345	2.290	2.403	2.432
Ti	0.210	0.183	0.218	0.189	0.209	0.219	0.221	0.213
Cr	0.003	0.000	0.000	0.004	0.003	0.002	0.001	0.000
Fe3+	0.000	0.000	0.000	0.000	0.000	0.000	0.000	0.000
Fe2+	1.467	1.386	1.297	1.283	1.254	1.721	1.729	1.709
Mn	0.020	0.015	0.017	0.016	0.016	0.026	0.026	0.032
Mg	2.815	3.002	3.004	3.063	3.019	2.679	2.582	2.635
Ca	1.952	1.953	1.921	1.944	1.818	1.896	1.919	1.881
Na	0.628	0.617	0.650	0.612	0.643	0.671	0.663	0.671
K	0.121	0.098	0.116	0.107	0.108	0.131	0.148	0.141
Total	15.858	15.799	15.866	15.816	15.703	15.835	15.837	15.845
Mg/(Fe+Mg)	0.66	0.68	0.70	0.70	0.71	0.61	0.60	0.61
Na+K	0.75	0.71	0.77	0.72	0.75	0.80	0.81	0.81

Table 3.1 (cont.).

Rock type	Hornblende gabbro			Hornblende microgabbro	
Sample no.	WK4-2	WK4-1	WK4-1	2WK6	2WK6
Remark	Rim	Core	Rim	Core	Rim
SiO_2	40.48	40.50	41.64	40.47	42.44
Al_2O_3	14.21	14.40	12.58	13.75	12.50
TiO_2	1.81	1.85	1.80	1.56	1.11
Cr_2O_3	0.01	0.00	0.01	0.03	0.01
FeO	13.04	11.65	13.70	17.01	16.20
MnO	0.20	0.18	0.21	0.29	0.30
MgO	11.74	12.94	11.93	9.42	9.79
CaO	11.86	11.78	11.94	11.26	11.38
Na_2O	2.35	2.40	2.06	2.03	1.81
K_2O	0.70	0.59	0.67	0.64	0.60
Cl	0.00	0.01	0.01	0.10	0.00
F	0.03	0.03	0.04	0.05	0.05
Total	96.43	96.34	96.59	96.61	96.18
23 (O)					
Si	6.093	6.060	6.266	6.183	6.450
Al	2.521	2.539	2.231	2.475	2.239
Ti	0.204	0.208	0.204	0.179	0.126
Cr	0.001	0.000	0.001	0.004	0.001
Fe^{3+}	0.000	0.000	0.000	0.000	0.000
Fe^{2+}	1.642	1.457	1.724	2.172	2.058
Mn	0.026	0.023	0.026	0.037	0.039
Mg	2.633	2.885	2.675	2.143	2.217
Ca	1.912	1.888	1.924	1.843	1.851
Na	0.685	0.696	0.601	0.599	0.532
K	0.134	0.113	0.129	0.125	0.115
Total	15.851	15.868	15.780	15.761	15.628
Mg/(Fe+Mg)	0.62	0.66	0.61	0.50	0.52
Na+K	0.82	0.81	0.73	0.72	0.65

Table 3.2 Representative EPMA analyses of plagioclase in hornblendite, hornblende gabbro and hornblende microgabbro in the Wang Nam Khiao, Nakhon Ratchasima, Thailand.

Rock type	Hornblendite				Hornblende gabbro			
Analysis no.	WK2-1	WK2-1	WK2-2	WK2-2	WK4-2	WK4-2	WK4-1	WK4-3
Remark	Pl 129	Pl 134	Pl 137	Pl 138	Pl 146	Pl147	Pl 143	Pl 148
SiO_2	44.55	44.82	44.78	43.75	45.99	46.14	45.98	44.99
Al_2O_3	34.78	34.67	35.14	34.86	34.11	34.07	34.34	34.61
TiO_2	0.00	0.01	0.00	0.02	0.00	0.00	0.00	0.00
FeO*	0.27	0.39	0.28	0.26	0.32	0.25	0.24	0.28
MnO	0.00	0.01	0.00	0.00	0.00	0.03	0.03	0.04
MgO	0.00	0.02	0.03	0.01	0.00	0.00	0.02	0.00
CaO	18.92	18.80	18.83	18.23	17.68	17.69	17.86	18.33
Na_2O	0.68	0.77	0.66	0.92	1.37	1.36	1.22	0.99
K_2O	0.02	0.02	0.00	0.00	0.00	0.01	0.00	0.00
Total	99.26	99.56	99.76	98.08	99.46	99.54	99.76	99.25
8 (O)								
Si	2.075	2.082	2.073	2.061	2.129	2.134	2.123	2.093
Al	1.909	1.897	1.917	1.935	1.861	1.856	1.868	1.896
Ti	0.000	0.000	0.000	0.001	0.000	0.000	0.000	0.000
Fe3+	0.000	0.000	0.000	0.000	0.000	0.000	0.000	0.000
Fe2+	0.011	0.015	0.011	0.010	0.012	0.010	0.009	0.011
Mn	0.000	0.001	0.000	0.000	0.000	0.001	0.001	0.001
Mg	0.000	0.002	0.002	0.000	0.000	0.000	0.001	0.000
Ca	0.944	0.935	0.934	0.920	0.877	0.876	0.883	0.913
Na	0.061	0.069	0.059	0.084	0.122	0.122	0.109	0.089
K	0.001	0.001	0.000	0.000	0.000	0.000	0.000	0.000
Total	5.002	5.004	4.998	5.012	5.002	5.000	4.997	5.004
An	0.94	0.93	0.94	0.92	0.88	0.88	0.89	0.91
Ab	0.06	0.07	0.06	0.08	0.12	0.12	0.11	0.09
Or	0.00	0.00	0.00	0.00	0.00	0.00	0.00	0.00

Table 3.2 (cont.).

Rock type	Hornblende gabbro		Hornblende microgabbro	
Analysis no.	WK6-2	WK6-2	2WK6	2WK6
Remark	Pl 151	Pl 152	Pl 169	Pl 170
SiO_2	45.82	46.39	53.90	56.77
Al_2O_3	34.41	34.48	29.20	27.40
TiO_2	0.00	0.00	0.00	0.07
FeO*	0.25	0.18	0.11	0.06
MnO	0.03	0.03	0.00	0.00
MgO	0.00	0.00	0.03	0.02
CaO	17.97	17.63	11.65	9.68
Na_2O	1.29	1.34	4.92	6.02
K_2O	0.02	0.01	0.05	0.06
Total	99.83	100.08	99.85	100.07
8 (O)				
Si	2.116	2.132	2.439	2.546
Al	1.872	1.867	1.557	1.448
Ti	0.000	0.000	0.000	0.002
Fe3+	0.000	0.000	0.000	0.000
Fe2+	0.010	0.007	0.004	0.002
Mn	0.001	0.001	0.000	0.000
Mg	0.000	0.000	0.002	0.001
Ca	0.889	0.868	0.564	0.465
Na	0.115	0.119	0.431	0.523
K	0.001	0.001	0.003	0.003
Total	5.006	4.995	5.000	4.991
An	0.88	0.88	0.57	0.47
Ab	0.11	0.12	0.43	0.53
Or	0.00	0.00	0.00	0.00

Table 3.3 Representative EPMA analyses of clinopyroxene in hornblendite and hornblende gabbro in the Wang Nam Khiao, Nakhon Ratchasima, Thailand.

Rock type	Hornblendite				Hornblende gabbro							
Analysis no.	WK3-1	WK3-1	WK3-3	WK3-3	WK4-2	WK4-2	WK4-1	WK4-1	WK6-2	WK6-2	WK8-3	WK8-3
Remark	Core	Rim	Core	Rim	Core	Rim	Core	Rim	Core	Rim	Core	Rim
SiO_2	49.15	48.62	50.38	50.18	50.47	53.08	49.10	50.73	48.91	49.11	51.86	50.43
Al_2O_3	6.48	6.27	4.74	5.25	4.31	2.29	5.59	3.58	5.49	5.45	3.04	4.35
TiO_2	0.71	0.72	0.52	0.63	0.38	0.44	0.77	0.55	0.74	0.73	0.29	0.58
Cr_2O_3	0.04	0.07	0.00	0.00	0.00	0.00	0.03	0.05	0.00	0.04	0.01	0.00
FeO	7.35	7.51	7.02	7.14	8.63	6.83	9.08	8.18	8.52	8.64	7.97	8.45
MnO	0.19	0.13	0.11	0.16	0.27	0.23	0.29	0.26	0.25	0.24	0.21	0.28
MgO	13.36	13.31	13.63	13.73	12.85	13.94	12.01	12.68	12.79	13.09	14.09	13.59
CaO	22.80	22.61	23.93	22.99	23.28	24.53	22.72	24.04	22.17	22.17	22.36	21.77
Na_2O	0.31	0.28	0.19	0.28	0.48	0.33	0.43	0.33	0.41	0.44	0.42	0.50
K_2O	0.00	0.00	0.00	0.00	0.00	0.00	0.01	0.01	0.01	0.00	0.01	0.01
Total	100.44	99.52	100.51	100.37	99.54	99.54	100.03	100.41	99.29	99.91	100.29	99.96
6 (O)												
Si	1.822	1.821	1.866	1.858	1.880	1.940	1.844	1.894	1.844	1.840	1.924	1.882
Al	0.283	0.277	0.207	0.229	0.189	0.099	0.247	0.158	0.244	0.241	0.133	0.191
Ti	0.020	0.020	0.014	0.018	0.011	0.012	0.022	0.015	0.021	0.021	0.008	0.016
Cr	0.001	0.002	0.000	0.000	0.000	0.000	0.001	0.001	0.000	0.001	0.000	0.000
Fe3+	0.000	0.000	0.000	0.000	0.000	0.000	0.000	0.000	0.000	0.000	0.000	0.000
Fe2+	0.228	0.235	0.217	0.221	0.269	0.209	0.285	0.255	0.269	0.271	0.247	0.264
Mn	0.006	0.004	0.004	0.005	0.009	0.007	0.009	0.008	0.008	0.008	0.007	0.009
Mg	0.738	0.743	0.752	0.757	0.713	0.759	0.672	0.705	0.718	0.731	0.778	0.755
Ca	0.905	0.907	0.949	0.912	0.929	0.960	0.914	0.961	0.895	0.890	0.888	0.870
Na	0.022	0.021	0.014	0.020	0.035	0.024	0.031	0.024	0.030	0.032	0.030	0.036
K	0.000	0.000	0.000	0.000	0.000	0.000	0.000	0.000	0.000	0.000	0.000	0.000
Total	4.027	4.029	4.023	4.020	4.033	4.010	4.026	4.023	4.028	4.034	4.017	4.024
Mg/(Fe+Mg)	0.760	0.760	0.780	0.770	0.730	0.780	0.700	0.730	0.730	0.730	0.760	0.740

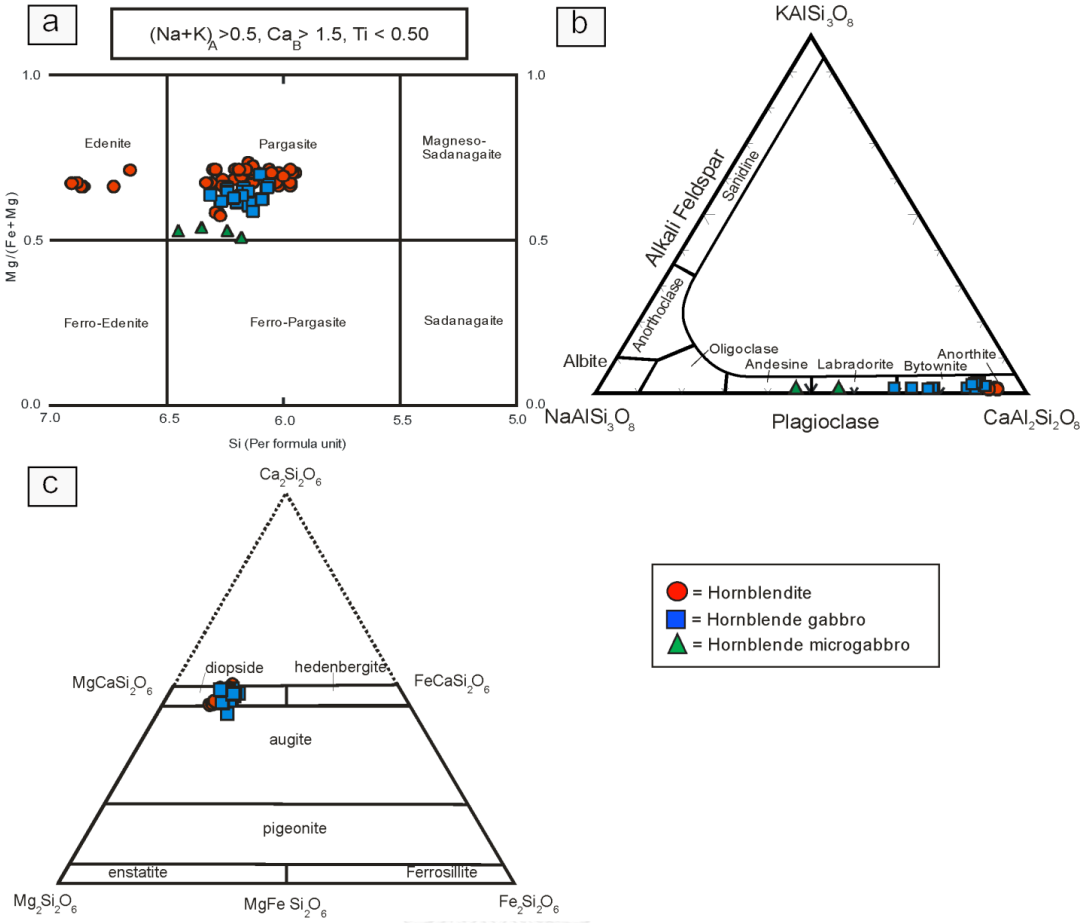

Figure 3.4 Mineral chemistry plots of (a) calcic-amphibole (Leake et al., 1997), (b) plagioclase (Smith and Brown, 1974) and (c) clinopyroxene (Morimoto et al., 1988) in the mafic- ultramafic plutonic rocks from Wang Nam Khiao area, Nakhon Ratchasima.

3.4 Whole-rock geochemistry

The representative whole- rock geochemistry of hornblendite, hornblende gabbro, and hornblende microgabbro from the Wang Nam Khiao, Nakhon Ratcharima, Thailand, are described below and summarized in Table 3.4.

The hornblendite shows major and minor compositions ranging between 41.71-43.60 % SiO_2, 1.30-1.85 % TiO_2, 12.68-14.60 % Al_2O_3, 10.24-11.90 % FeO_{total}, 0.01-0.11 % MnO, 12.04-13.37 % MgO, 11.61-14.97 % CaO, 1.79-2.30 % Na_2O, 0.48-0.72 % K_2O, 0.03-0.11 % P_2O_5, 1.36-2.13 % LOI. Their trace and rare earth elements in ppm are between 80.00-89.00 Ba, 60.00-150.00 Cr, 30.00-140.00 Cu, 13.00-42.00 Ni, 93.00-115.00 Sc, 290.00-337.00 Sr, 491.00-658.00 V, 36.00-50.00 Zn, 4.70-5.40 Ce, 60.50-81.40 Co, 0.20-0.20 Cs, 2.64-3.52 Dy, 1.34-1.71 Er, 0.74-0.91 Eu, 12.00-14.00 Ga, 2.53-3.27 Gd, 0.70 Hf, 0.49- 0.62 Ho, 1.50-1.60 La, 0.14-0.20 Lu, 0.60-1.00 Nb, 5.30-6.40 Nd, 0.93-1.07 Pr, 2.30-3.30 Rb, 0.50 Sb, 1.96-2.50 Sm, 2.00 Sn, 0.42-0.56 Tb, 0.10-0.16 Th, 0.18-0.26 Tm, 0.05 U, 84.00-95.00 W, 12.50-16.50 Y, 1.00-1.40 Yb, and 18.90-22.00 Zr.

The hornblende gabbro presents major and minor compositions between 37.92-45.25 % SiO_2, 0.90-1.84 % TiO_2, 13.37-20.27 % Al_2O_3, 11.78-19.29 % FeO_{total}, 0.15-0.19 % MnO, 7.01-10.17 % MgO, 12.74-14.38 % CaO, 1.19-1.74 % Na_2O, 0.31-0.47 % K_2O, 0.02-0.04 % P_2O_5, 0.61-2.41 % LOI. Their trace and rare earth elements in ppm are between 63.00-120.00 Ba, 20.00-250.00 Cr, 40.00-100.00 Cu, 20.00-110.00 Ni, 35.00-52.00 Sc, 378.00-670.00 Sr, 413.00-683.00 V, 70.00-80.00 Zn, 5.22-8.16 Ce, 41.00-54.00 Co, 0.20-0.50 Cs, 2.42-3.31 Dy, 1.33-1.77 Er, 0.68-1.01 Eu, 15.00-18.00 Ga, 2.40-3.45 Gd, 0.70-0.80 Hf, 0.46-0.64 Ho, 1.65-2.79 La, 0.16-0.23 Lu, 0.70-1.30 Nb, 5.85-8.47 Nd, 0.93-1.50 Pr, 4.00-6.00 Rb, 0.50-4.40 Sb, 1.90-2.94 Sm, 1.00 Sn, 0.40-0.57 Tb, 0.09-0.12 Th, 0.18-0.25 Tm, 0.02-0.03 U, 0.70-1.00 W, 11.70-16.20 Y, 1.05-1.58 Yb, and 22.00-23.00 Zr.

A representative hornblende microgabbro reveals the major and minor compositions of 45.63 % SiO_2, 1.15 % TiO_2, 22.18 % Al_2O_3, 9.96 % FeO_{total}, 0.10 % MnO, 3.05 % MgO, 10.25 % CaO, 3.41 % Na_2O, 1.16 % K_2O, 0.05 % P_2O_5, 2.24 % LOI. Its trace and rare earth elements in ppm are of 210.00 Ba, 30.00 Cr, 40.00 Cu, 20 Ni, 14.00 Sc, 1281.00 Sr, 182.00 V, 110.00 Zn, 17.70 Ce, 17.00 Co, 0.90 Cs, 2.07 Dy,

0.92 Er, 1.37 Eu, 23.00 Ga, 3.31 Gd, 2.20 Hf, 0.35 Ho, 6.58 La, 0.11 Lu, 2.10 Nb, 14.80 Nd, 2.78 Pr, 22.00 Rb, 0.60 Sb, 3.87 Sm, 1.00 Sn, 0.42 Tb, 0.15 Th, 0.12 Tm, 0.09 U, 0.80 W, 9.50 Y, 0.72 Yb, and 120.00 Zr.

Major compositions of all hornblendite, hornblende gabbro and hornblende microgabbro show low SiO_2 contents varying from 41.71-43.60 wt%, 37.92-45.25 wt% and 45.63 wt%, respectively. The Na_2O+K_2O contents of hornblendite and hornblende gabbro are 2.27-3.02 wt% and 1.50-2.21 wt%, respectively, whereas hornblende microgabbro shows higher Na_2O+K_2O content (4.57 wt%) and consistents with abundance and composition of plagioclase. In term of Mg# (100*Mg/Mg+Fe), hornblendite shows high Mg# (51.39-54.34), TiO_2 (1.30-1.85 wt%), and FeO_t content (10.24-11.90 wt%) whereas both hornblende gabbro and hornblende microgabbro display lower Mg# (29.64-46.33 for hornblende gabbro and 23.44 for hornblende microgabbro) with high FeO_t (11.78-19.29 wt% for hornblende gabbro and 9.96 wt% for hornblende microgabbro) and varying TiO_2 (0.90-1.84 wt% for hornblende gabbro and 1.15 wt% for hornblende microgabbro). In addition, high CaO (11.61-14.97 wt%) and Al_2O_3 (12.68-14.60 wt%) contents are of hornblendite, corresponding to their high abundances of calcic-amphibole, plagioclase, and clinopyroxene. Also hornblende gabbro and hornblende microgabbro display high CaO (12.74-14.38 wt% and 10.25 wt%, respectively) and Al_2O_3 (13.37-20.07 wt% and 22.13 wt%) contents, consistent with assemblages of calcic-amphibole, plagioclase, clinopyroxene and apatite. In the total alkali (Na_2O+K_2O) vs. silica TAS diagram (Cox et al., 1979) (Fig. 3.5), hornblendite data are plotted in ultrabasic-alkali gabbro field whereas hornblende gabbro and hornblende microgabbro fall within gabbro field varying from ultrabasic to basic compositions, consistent with the abundances of hornblende, pyroxene, and plagioclase. Regarding to Harker variation diagrams (Harker, 1909) (Fig. 3.6), all the samples exhibit some correlations between MgO and other major oxides; Al_2O_3, MnO, Na_2O and K_2O show negative correlations (Figs. 3.6b, d, g and h), whereas TiO_2 and CaO exhibit positive correlations (Figs. 3.6e and f) against increasing of MgO. SiO_2 and FeO_t values present scattered distribution (Fig. 3.6a and c). These variation diagrams are compatible with mineral assemblages and An content in plagioclase which exhibit decreasing of clinopyroxene and increasing of plagioclase with lowering An content in plagioclase from hornblendite, hornblende gabbro, and hornblende

microgabbro. These variation plots agree well to support the genesis model of magma fractional crystallization of these rocks.

In the primitive mantle-normalized spider (Fig. 3.7a), most rock samples show positive Ba, K, Sr anomalies, and negative Th, U, Nb, Ta, Zr anomalies. The large ion lithophile elements (LILE) are highly enriched (e.g. Ba, K, Sr). In addition, most samples also show marked depletion of Nb, Ta and Zr (Fig. 3.7a).

The hornblendite samples show $(La/Yb)_N$ ratios ranging from 0.77 to 1.13 which are similar to those of hornblende gabbro (1.00 to 1.54). On the other hand, hornblende microgabbro shows higher ratio (6.56). The $(La/Sm)_N$ ratios of hornblendite range from 0.39 to 0.53 while hornblende gabbro and hornblende microgabbro yield higher ranges of 0.50-0.76 and 1.10, respectively. These rocks exhibit weakly light-REE (LREE) enrichment in chondrite-normalized spider diagram for hornblendite and hornblende gabbro and higher light-REE for hornblende microgabbro which indicate the crystallization sequences from hornblendite to hornblende gabbro and hornblende microgabbro, respectively. However, these REE patterns, in overall, are similar patterns with those of typical arc setting reported by Togashi et al. (1992), Woodhead et al. (1998) and Greene et al. (2006) (Fig. 3.7b). All hornblendite, hornblende gabbro and hornblende microgabbro show similar pattern, the slightly curved patterns with broad enrichment of Pr-Nd, suggesting that hornblende megacrysts may have equilibrated with LREE-enriched basaltic melt (Irving and Frey, 1984). The La, Ce to Pr and Nd depletions are affected by the mineralogical compositions of cumulated hornblende which are effected by hornblende/liquid partitioning coefficients (Schnetzler and Philpotts, 1970).

Table 3.4 Representative whole-rock geochemical analyses of hornblendite, hornblende gabbro and hornblende microgabbro in the Wang Nam Khiao, Nakhon Ratchasima, Thailand (Major and minor oxide in wt%, trace elements and REE in ppm).

Rock type	Hornblendite			Hornblende gabbro			Hornblende microgabbro
Composition	WK9-1	WK2-2	WK3-3	WK4-2	WK6-2	WK8-3	2WK6
SiO_2	42.8	43.6	41.7	37.9	38.6	45.3	45.6
TiO_2	1.85	1.30	1.66	1.46	1.84	0.90	1.15
Al_2O_3	14.6	12.7	14.5	20.1	13.4	15.9	22.2
FeO_t	11.2	10.2	11.9	16.6	19.3	11.8	9.96
MnO	0.01	0.01	0.11	0.15	0.19	0.17	0.10
MgO	13.4	12.0	12.6	7.01	9.21	10.2	3.05
CaO	11.6	15.0	12.3	12.7	14.4	13.0	10.3
Na_2O	2.30	1.79	2.01	1.74	1.19	1.31	3.41
K_2O	0.72	0.48	0.54	0.47	0.31	0.35	1.16
P_2O_5	0.11	0.09	0.03	0.04	0.02	< 0.01	0.55
LOI	1.36	1.92	2.13	2.41	1.49	0.61	2.24
Total	100	99.1	99.5	101	99.9	99.5	99.7
Ba	80.0	80.0	89.0	122	63.0	80.0	210
Be	<5.00	<5.00	< 1.00	< 1.00	< 1.00	< 1.00	< 1.00
Cr	150	140	60.0	20.0	40.0	250	30.0
Cu	140	30.0	100	40.0	50.0	100	40.0
Ni	42.0	13.0	40.0	< 20.0	20.0	110	< 20.0
Sc	115	93.0	103	35.0	52.0	49.0	14.0
Sr	290	320	337	670	378	522	1281
V	658	491	589	413	683	433	182
Zn	43.0	36.0	50.0	80.0	80.0	70.0	110
Ag	< 1.00	< 1.00	< 0.50	< 0.50	< 0.50	< 0.50	< 0.50
As	<5.00	<5.00	<5.00	<5.00	<5.00	<5.00	<5.00
Bi	<0.10	<0.10	<0.10	<0.10	<0.10	<0.10	<0.10
Ce	5.40	4.70	4.89	8.16	5.22	6.37	17.7
Co	81.4	60.50	61.0	41.0	54.0	50.0	17.0
Cs	<0.10	0.20	< 0.10	0.20	0.50	0.30	0.90
Dy	3.52	2.72	2.64	3.31	2.67	2.42	2.07

Table 3.4 (cont.)

Rock type	Hornblendite			Hornblende gabbro			Hornblende microgabbro
Composition	WK9-1	WK2-2	WK3-3	WK4-2	WK6-2	WK8-3	2WK6
Er	1.71	1.34	1.38	1.77	1.48	1.33	0.92
Eu	0.91	0.74	0.77	1.01	0.80	0.68	1.37
Ga	14.0	14.0	12.0	18.0	16.0	15.0	23.0
Gd	3.27	2.68	2.53	3.45	2.53	2.40	3.31
Ge	2.00	2.00	1.40	1.00	1.40	1.40	0.80
Hf	<1.00	<1.00	0.70	0.80	0.70	0.70	2.20
Ho	0.62	0.49	0.51	0.64	0.53	0.46	0.35
In	<0.20	<0.20	< 0.10	< 0.10	0.10	< 0.10	< 0.10
La	1.50	1.50	1.60	2.79	1.65	2.25	6.58
Lu	0.20	0.14	0.14	0.23	0.17	0.16	0.11
Mo	<2.00	<2.00	<2.00	<2.00	<2.00	<2.00	<2.00
Nb	1.00	<1	0.60	1.30	0.70	0.80	2.10
Nd	6.40	5.30	5.73	8.47	5.85	5.85	14.8
Pb	<5.00	<5.00	<5.00	<5.00	<5.00	<5.00	<5.00
Pr	1.07	0.93	0.96	1.50	0.93	1.05	2.78
Rb	3.30	2.30	3.00	4.00	5.00	6.00	22.0
Sb	<0.10	<0.10	0.50	0.50	4.40	0.50	0.60
Sm	2.50	2.10	1.96	2.94	2.14	1.90	3.87
Sn	2.00	2.00	< 1.00	< 1.00	1.00	1.00	1.00
Ta	<0.50	<0.50	< 0.01	0.04	< 0.01	0.04	0.06
Tb	0.56	0.43	0.42	0.57	0.43	0.40	0.42
Th	0.10	0.10	0.16	< 0.05	0.09	0.12	0.15
Tl	<0.50	<0.50	< 0.05	< 0.05	< 0.05	< 0.05	0.10
Tm	0.26	0.19	0.18	0.25	0.20	0.18	0.12
U	<0.05	<0.05	0.05	0.02	0.02	0.03	0.09
W	84.0	95.0	<0.50	1.00	<0.50	0.70	0.80
Y	16.5	12.8	12.5	16.2	13.0	11.7	9.50
Yb	1.40	1.00	1.02	1.58	1.18	1.05	0.72
Zr	18.9	19.8	22.0	23.0	22.0	22.0	120

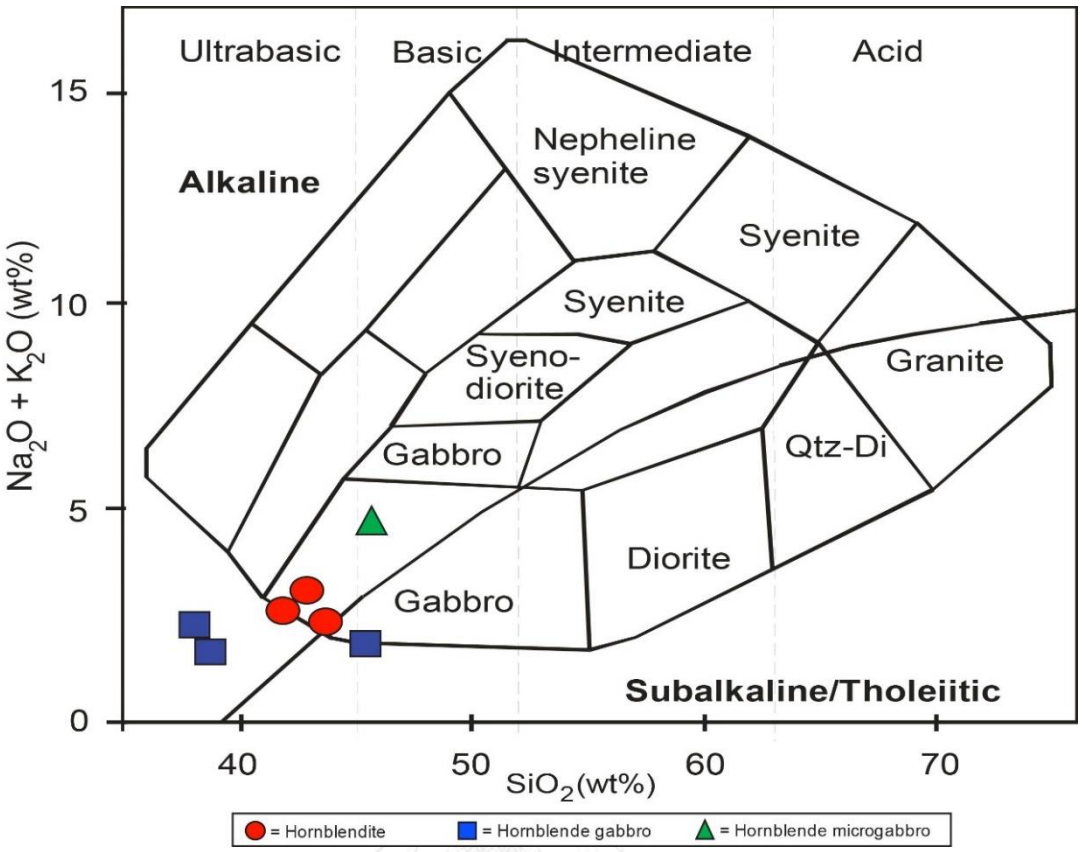

Figure 3.5 SiO_2 and Na_2O+K_2O discrimination diagram showing the classification of plutonic rocks after Cox et al. (1979). The analyzed mafic-ultramafic rocks mostly fall close to the gabbro field.

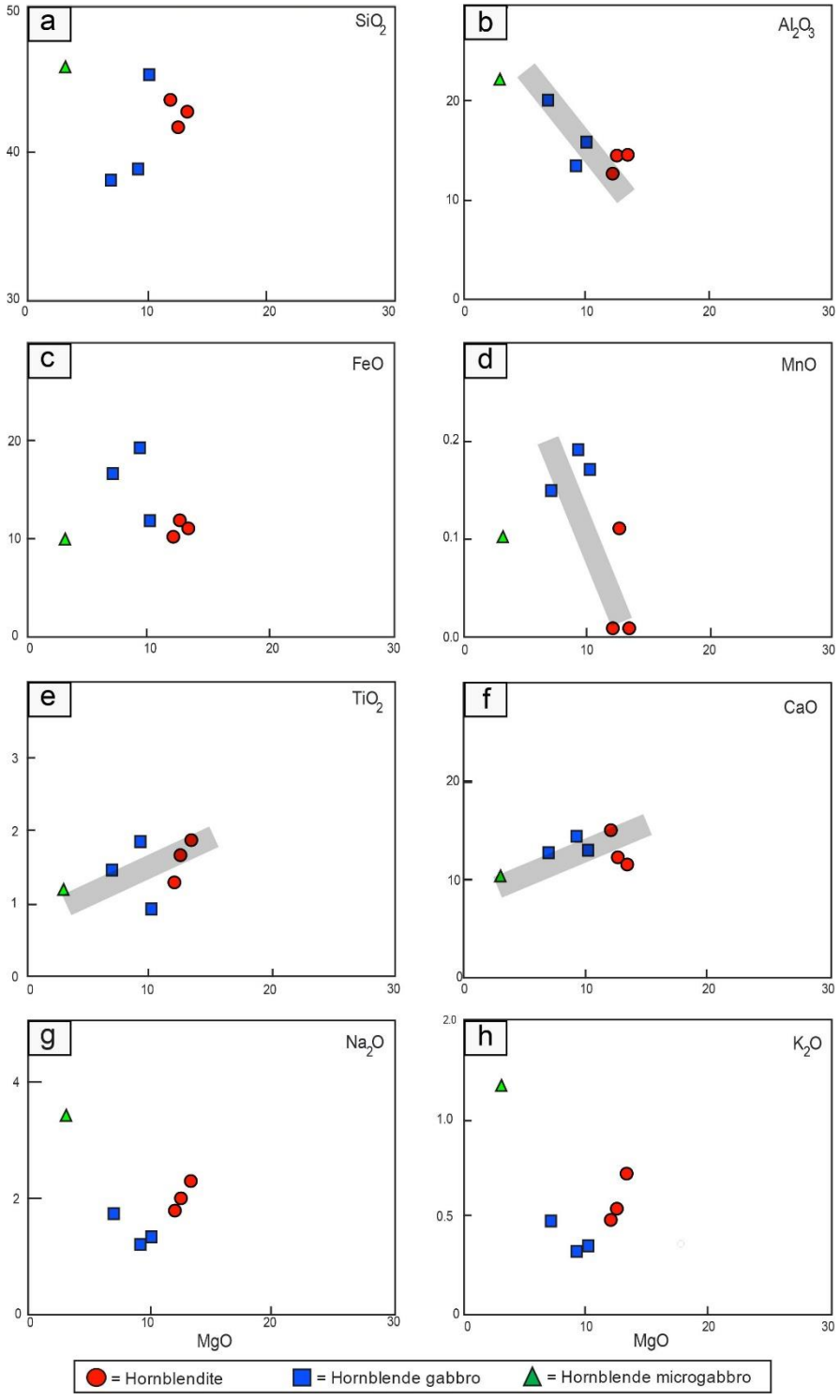

Figure 3.6 Harker variation diagrams of the mafic-ultramafic rocks from the Wang Nam Khiao area, Nakhon Ratchasima, Thailand.

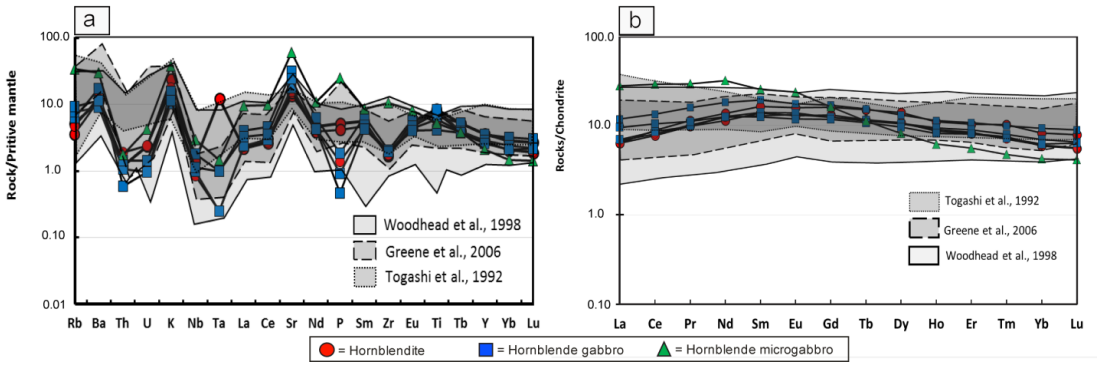

Figure 3.7 (a) Primitive mantle-normalized spider diagrams (primitive mantle values from Sun and McDonough (1989)) and (b) chondrite-normalized REE patterns (chondrite values from Sun and McDonough (1989)) of hornblendite, hornblende gabbro and hornblende microgabbro from the Wang Nam Khiao area, Nakhon Ratchasima, Thailand comparing to typical arc setting by shade patterns, data from Togashi et al. (1992), Woodhead et al. (1998) and Greene et al. (2006).

3.5 Geothermobarometry

The several geothermobarometers have been purposed for pressure and temperature (P-T) conditions of amphibole crystallization (Smith and Brown, 1974; Blundy and Holland, 1990; Holland and Blundy, 1994; Anderson and Smith, 1995; Anderson, 1996; Ague, 1997; Stein and Dietl, 2001).

Based on the mineral assemblages, hornblende and plagioclase are significant in all hornblendite, hornblende gabbro and hornblende microgabbro. Therefore, the P-T calculation should be carried out using hornblende-plagioclase geothermometer and Al-in-hornblende geobarometer.

The temperature calculation can be commonly applied for the coexisting minerals of hornblende and plagioclase (Blundy and Holland, 1990; Holland and Blundy, 1994). Based on the experimental data of hornblende-plagioclase, edenite-tremolite reaction (edenite + 4quartz = tremolite + albite) and edenite-richterite reaction (edenite + albite = richterite + anorthite) were suggested for geothermometers for quartz-bearing igneous rocks and quartz-free igneous rocks, respectively (Holland and Blundy, 1994) with reported uncertain calibration of ± 40 ^{o}C. Thus, the temperatures of crystallization of

these mafic-ultramafic plutonic rocks are calculated using the edenite-richterite thermometer (Table 3.5). The calculated results for hornblendite, hornblende gabbro and hornblende microgabbro show temperature ranges of 670-1,000 ºC, 850-950 ºC and 750-850 ºC, respectively.

For the crystallization pressure of rocks, the Al in hornblende has been widely used to calculate the crystallization pressure of magmatic rocks (Hammarstrom and Zen, 1986; Hollister et al., 1987; Schmidt, 1992). The correlation of the total Al content of calcic amphibole and the pressure was employed to calculate the pressure and was confirmed by the experimental studies (Hollister et al., 1987; Johnson and Rutherford, 1989; Schmidt, 1992; Anderson and Smith, 1995). The calibration equation of Schmidt (1992), P (± 0.6 kbar) = -3.01 + 4.76 Al^{tot}, is experimentally calibrated the amount of Al in hornblende in tonalite under H_2O-saturated conditions which is then chosen to estimate the pressure of crystallization (Table 3.5). The results present pressure ranges from 5.3 to 9.8 kbar for hornblendite, 7.6 to 9.0 kbar for hornblende gabbro and 7.6 to 8.8 kbar for hornblende microgabbro, respectively.

Table 3.5 Geothermobarometry of the mafic-ultramafic plutonic rocks in the Wang Nam Khiao area, Nakhon Ratchasima.

Rock type	Hornblendite				Hornblende gabbro				Hornblende microgabbro			
Sample No.	WK2-1- 8	WK2-1-10	WK2-1-12	WK2-2-16	WK4-2-35	WK4-3- 39	WK6-2-49	WK8-3- 56	2WK6-75	2WK6-76	2WK6-77	2WK6- 78
Mineral Name	Hb	Hb	Hb	Hb	Hb	Hb	Hb	Hb	Hb	Hb	Hb	Hb
No. oxygen	23	23	23	23	23	23	23	23	23	23	23	23
SiO_2	41.72	41.89	40.39	41.24	41.02	41.22	41.30	42.04	41.16	41.72	40.47	42.44
Al_2O_3	13.34	14.73	14.82	14.52	12.86	13.40	13.76	13.40	13.19	12.91	13.75	12.50
TiO_2	1.64	1.30	1.48	1.31	1.93	1.97	1.98	2.37	1.92	1.10	1.56	1.11
Cr_2O_3	0.00	0.00	0.03	0.02	0.02	0.00	0.00	0.04	0.00	0.00	0.03	0.01
FeO_t	11.14	10.43	11.16	11.62	13.62	12.83	12.29	12.03	16.48	16.13	17.01	16.20
MnO	0.12	0.10	0.10	0.15	0.20	0.19	0.22	0.16	0.28	0.31	0.29	0.30
MgO	13.55	13.36	12.95	13.00	11.90	12.00	12.45	12.56	9.83	10.01	9.42	9.79
CaO	12.26	12.61	12.38	12.31	11.71	12.01	11.92	11.47	11.35	11.51	11.26	11.38
Na_2O	2.14	2.01	2.01	1.98	2.29	1.58	2.00	1.94	2.16	1.93	2.03	1.81
K_2O	0.52	0.37	0.48	0.47	0.68	0.67	0.58	0.63	0.49	0.68	0.64	0.60
Total	96.42	96.80	95.81	96.62	96.22	95.86	96.50	96.64	96.86	96.28	96.45	96.14
Formula 23(O)												
Si	6.13	6.10	5.97	6.04	6.14	6.14	6.10	6.18	6.18	6.28	6.11	6.39
Al	2.31	2.53	2.58	2.51	2.27	2.35	2.39	2.32	2.33	2.29	2.44	2.22
Ti	0.18	0.14	0.16	0.14	0.22	0.22	0.22	0.26	0.22	0.12	0.18	0.13
Cr	0.00	0.00	0.00	0.00	0.00	0.00	0.00	0.01	0.00	0.00	0.00	0.00
Fe_{3+}	0.53	0.48	0.63	0.64	0.47	0.55	0.51	0.44	0.45	0.46	0.57	0.40
Fe_{2+}	0.84	0.79	0.75	0.78	1.24	1.04	1.00	1.04	1.62	1.57	1.58	1.64
Mn	0.02	0.01	0.01	0.02	0.03	0.02	0.03	0.02	0.04	0.04	0.04	0.04
Mg	2.97	2.90	2.85	2.84	2.65	2.66	2.74	2.75	2.20	2.25	2.12	2.20
Ca	1.93	1.97	1.96	1.93	1.88	1.92	1.89	1.81	1.82	1.86	1.82	1.84
Na	0.61	0.57	0.57	0.56	0.66	0.46	0.57	0.55	0.63	0.56	0.59	0.53
K	0.10	0.07	0.09	0.09	0.13	0.13	0.11	0.12	0.09	0.13	0.12	0.11
Total	15.62	15.56	15.59	15.56	15.67	15.48	15.57	15.51	15.58	15.56	15.57	15.49
Geobarometer (Schmidt, 1992)												
P(kbar)(+0.6 kbar)	**8.12**	**9.16**	**9.45**	**9.10**	**7.89**	**8.32**	**8.52**	**8.15**	**8.21**	**8.00**	**8.77**	**7.65**
Depth (km)	**30**	**33**	**34**	**33**	**29**	**30**	**31**	**30**	**30**	**29**	**32**	**28**
Geothermometer (Holland & Blundy, 1994)												
cum	-0.0212	-0.0387	-0.0383	-0.0240	0.0019	-0.0139	-0.0002	0.0210	0.0286	0.0139	0.0275	0.0138
XTSi	0.5336	0.5262	0.4928	0.5110	0.5344	0.5339	0.5250	0.5462	0.5445	0.5709	0.5267	0.5983
XTAl	0.4664	0.4738	0.5072	0.4890	0.4656	0.4661	0.4750	0.4538	0.4555	0.4291	0.4733	0.4017
XMAl	0.2226	0.3175	0.2765	0.2759	0.2021	0.2431	0.2473	0.2535	0.2556	0.2873	0.2757	0.3063
XK	0.0966	0.0688	0.0909	0.0884	0.1295	0.1262	0.1083	0.1184	0.0942	0.1304	0.1239	0.1145
XBlk	0.3839	0.4361	0.4134	0.4405	0.3277	0.5160	0.4336	0.4999	0.4236	0.4359	0.4367	0.5086
XNa	0.5195	0.4951	0.4958	0.4711	0.5428	0.3578	0.4581	0.3817	0.4822	0.4337	0.4394	0.3769
XMNa	0.0452	0.0357	0.0396	0.0460	0.0606	0.0494	0.0572	0.0863	0.0736	0.0651	0.0763	0.0754
XMCa	0.9654	0.9837	0.9796	0.9660	0.9385	0.9575	0.9429	0.9033	0.9121	0.9280	0.9099	0.9177
XPlAb (0.1-0.9)	**0.07**	**0.06**	**0.06**	**0.06**	**0.12**	**0.09**	**0.12**	**0.22**	**0.43**	**0.43**	**0.53**	**0.53**
XPlAn	0.93	0.94	0.94	0.94	0.88	0.91	0.88	0.78	0.57	0.57	0.47	0.47
Y1	7.3788	7.6032	7.6032	7.6032	6.2928	6.9372	6.2928	4.3008	0.8988	0.8988	0.0000	0.0000
Y2	-7.3200	-7.5600	-7.5600	-7.5600	-6.1200	-6.8400	-6.1200	-3.7200	1.3200	1.3200	3.0000	3.0000
KD1	0.0062	0.0062	0.0051	0.0062	0.0088	0.0157	0.0132	0.0366	0.0476	0.0606	0.0618	0.1124
KD2	0.3006	0.2661	0.2593	0.3289	0.2292	0.2520	0.2073	0.1719	0.0539	0.0522	0.0349	0.0458
T2(° C)(+40 °C)	**963**	**916**	**965**	**969**	**949**	**918**	**920**	**881**	**833**	**791**	**815**	**754**

3.6 Zircon U-Pb geochronology

The zircon U-Pb geochronology is widely used to determine the ages of rocks (Faure, 1986; Rollinson, 1993; Schoene, 2014) which is applied to determine the crystallization ages of plutonic rocks in the Wang Nam Khiao area, Nakhon Ratchasima. The representative mafic-ultramafic plutonic rocks (hornblende microgabbro) are geochronologically studied by the separated zircons as reported below.

Sixteen zircon grains extracted from hornblende microgabbro (sample no. 2WK6), which cut into hornblendite, were analyzed by LA-ICP-MS to determine the minimum U-Pb age of the magmatic event. Field occurrence of the sample suggests its close genetic relation with hornblendite and hornblende gabbro (Fig. 2.3). Among the twenty-three analyzed spots plotted on Concordia diagram (Fig. 3.9a, Table 3.6), eleven zircons are less than 10 percent discordance as summarized in Fig. 3.9b. Analytical spots and ^{238}U-^{206}Pb dating results of the eleven grains are shown in cathodoluminescence (CL) images (Fig. 3.8). In general, these zircon grains are medium-grained (100-300 μm), anhedral to euhedral in shape, and show clear oscillatory zoning or homogeneous grain, suggesting crystallization from magma. Two CL-dark zircons, in the bottom line of Fig. 3.8 (analytical spots 03 to 09), yielded older ages (over 420 Ma) that may indicate contaminated zircon grains. According to Tera-Wasserburg Concordia diagram (Fig. 3.9a) and weighted histogram and density curve for zircon U-Pb analytical spots with <10% concordance (Fig. 3.9b), the U-Pb data are separated into 2 distinctive groups. The dominant group yielded younger ages defining a weighted mean ^{238}U-^{206}Pb age of 257.1 ± 3.4 Ma (Fig. 3.9b). On the other hand, a few dark CL grains show older ages defining a weighted mean ^{238}U-^{206}Pb age of 447.0 ± 19 Ma (Fig. 3.9b).

Hornblende microgabbro appears to have close relationship with hornblende gabbro and hornblendite, based on field investigation, petrographic features, and geochemistry as reported above. Thus, the 257.1 ± 3.4 Ma ^{238}U-^{206}Pb ages defined by concordant zircons, taken from the younger microgabbro dyke, should indicate the minimum age of magmatic crystallization of mafic-ultramafic magma during Late

Permian because of cross- cutting relationship of hornblende microgabbro into hornblendite.

Table 3. 6 Zircon LA- ICP- MS U- Pb data and calculated ages of zircons in the hornblende microgabbro dike into hornblendite (2WK6).

Analytical spot number	$206Pb_c$ (1) (%)	U (ppm)	Th (ppm)	Th/U	$^{238}U/^{206}Pb^*$ (1)	$^{207}Pb^*/^{206}Pb^*$ (1)	$^{238}U/^{206}Pb^*$ age (1) (Ma)	$^{238}U/^{206}Pb^*$ age (2) (Ma)	Conc
2WK6_011	0.11	361	240	0.68	25.74 ± 0.46	0.0524 ± 0.0045	245.7 ± 4.3	245.3 ± 4.2	Conc
2WK6_022	1.20	204	108	0.54	25.51 ± 0.50	0.0494 ± 0.0069	247.9 ± 4.7	248.5 ± 4.6	Conc
2WK6_023	0.66	118	43	0.37	25.42 ± 0.86	0.0508 ± 0.0084	248.7 ± 8.3	248.9 ± 8.3	Conc
2WK6_014	0.00	419	185	0.45	24.77 ± 0.41	0.0530 ± 0.0022	255.1 ± 4.1	254.6 ± 4.2	Conc
2WK6_015	0.26	207	81	0.40	24.73 ± 0.55	0.0493 ± 0.0048	255.5 ± 5.6	256.2 ± 5.5	Conc
2WK6_025	0.00	192	60	0.32	24.26 ± 0.61	0.0571 ± 0.0035	260.4 ± 6.4	258.6 ± 6.5	Conc
2WK6_021	0.06	275	88	0.33	24.45 ± 0.47	0.0495 ± 0.0049	258.4 ± 4.9	258.6 ± 4.8	Conc
2WK6_010	1.10	452	331	0.75	24.65 ± 0.43	0.0438 ± 0.0048	256.4 ± 4.4	258.8 ± 4.3	Conc
2WK6_020	0.00	252	93	0.38	24.21 ± 0.48	0.0573 ± 0.0035	261.0 ± 5.0	259.1 ± 5.1	Conc
2WK6_018	0.00	142	42	0.30	24.04 ± 0.58	0.0586 ± 0.0050	262.7 ± 6.3	260.5 ± 6.4	Conc
2WK6_013	0.00	186	64	0.35	24.10 ± 0.60	0.0512 ± 0.0034	262.1 ± 6.4	262.1 ± 6.4	Conc
2WK6_016	0.00	134	38	0.29	23.93 ± 0.68	0.0555 ± 0.0055	263.9 ± 7.3	262.6 ± 7.5	Conc
2WK6_024	0.00	127	39	0.32	24.03 ± 0.62	0.0520 ± 0.0039	262.9 ± 6.6	262.7 ± 6.7	Conc
2WK6_026	0.03	209	98	0.48	23.93 ± 0.62	0.0544 ± 0.0063	263.9 ± 6.8	263.0 ± 6.7	Conc
2WK6_019	0.43	151	52	0.35	24.03 ± 0.64	0.0466 ± 0.0063	262.8 ± 6.9	263.9 ± 6.8	Conc
2WK6_012	0.00	115	33	0.29	23.55 ± 0.53	0.0563 ± 0.0039	268.1 ± 5.9	266.5 ± 6.0	Conc
2WK6_001	0.26	135	49	0.37	23.73 ± 0.51	0.0468 ± 0.0048	266.1 ± 5.6	266.8 ± 5.5	Conc
2WK6_003	0.00	661	397	0.62	14.41 ± 0.16	0.0539 ± 0.0011	432.6 ± 4.6	432.6 ± 4.6	Conc
2WK6_004	0.00	698	259	0.38	14.33 ± 0.16	0.0554 ± 0.0011	434.9 ± 4.6	434.9 ± 4.6	Conc
2WK6_006	0.00	317	74	0.24	13.93 ± 0.16	0.0540 ± 0.0018	446.9 ± 4.9	446.9 ± 4.9	Conc
2WK6_005	0.13	526	102	0.20	13.93 ± 0.18	0.0533 ± 0.0015	446.9 ± 5.6	447.4 ± 5.6	Conc
2WK6_009	0.26	702	239	0.35	13.30 ± 0.14	0.0564 ± 0.0019	467.3 ± 4.8	467.3 ± 4.8	Conc
2WK6_008	0.23	369	145	0.40	12.63 ± 0.21	0.0553 ± 0.0028	491.4 ± 7.7	492.4 ± 7.7	Conc

Errors are 1-sigma; Pb_c and Pb^* indicate the common and radiogenic portions, respectively.
(1) Common Pb corrected by assuming $^{206}Pb/^{238}U$-$^{208}Pb/^{232}Th$ age-concordance
(2) Common Pb corrected by assuming $^{206}Pb/^{238}U$-$^{207}Pb/^{235}U$ age-concordance

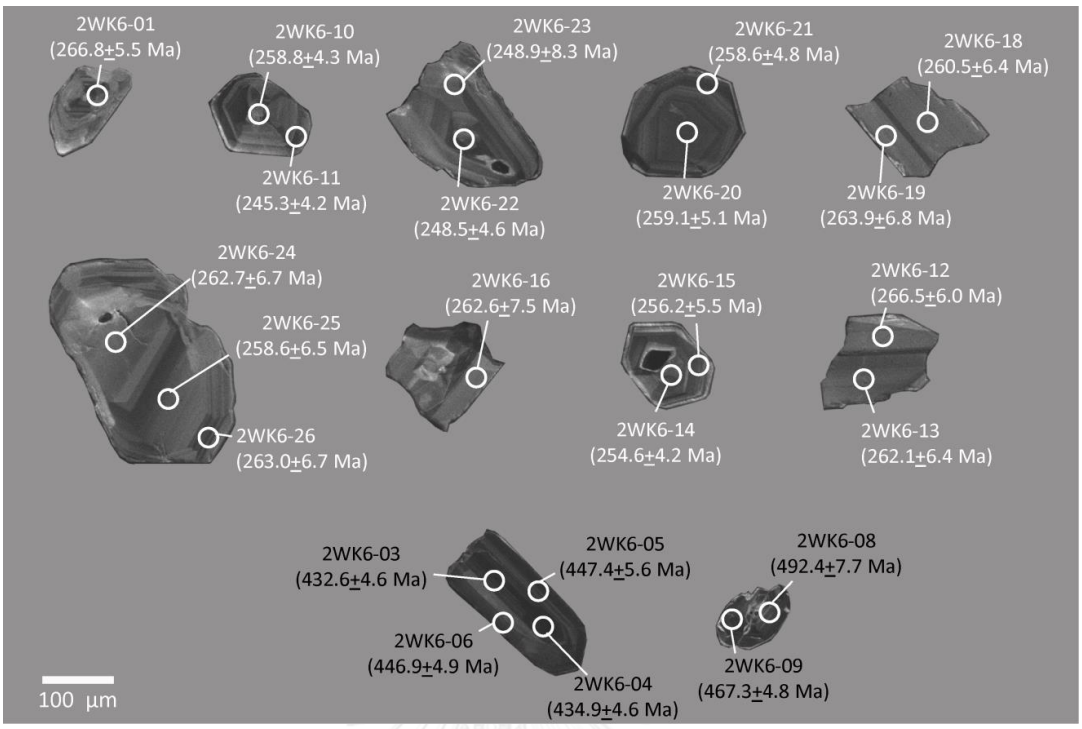

Figure 3.8 CL images of zircon from hornblende microgabbro (sample no. 2WK6) with $^{206}Pb/^{238}U$ ages. The analytical spot numbers in Table 3.6 are shown by circles.

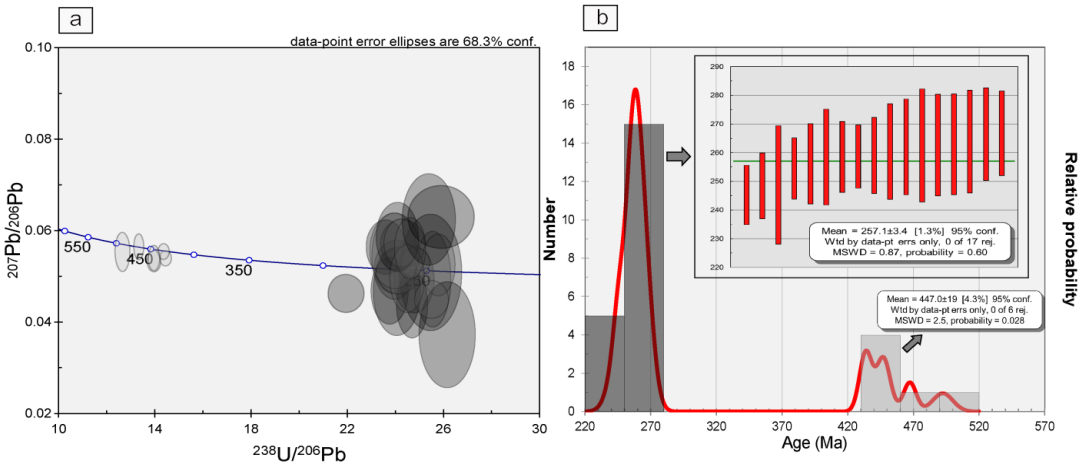

Figure 3.9 (a) The Tera-Wasserburg concordia diagram showing $^{238}U/^{206}Pb$ and $^{207}Pb/^{206}Pb$ ratio of zircons in hornblende microgabbro (sample no. 2WK6). (b) Histogram display ^{238}U - ^{206}Pb ages with a probability curve and weighted average ^{238}U-^{206}Pb ages.

3.7 Discussions

Intrusion depths: The understanding of emplacement pressure of magmatic rocks calculated from Al in hornblende (Hammarstrom and Zen, 1986; Hollister et al., 1987; Vyhnal et al., 1991; Schmidt, 1992) has been generally used to determine the intrusion depth (Schmidt, 1992; Stein and Dietl, 2001; Helmy et al., 2004; Hossain et al., 2009). The intrusion depth of both mafic-ultramafic plutonic rocks (hornblendite, related hornblende gabbro and hornblende microgabbro) were determined by the calculated pressure of hornblende rim (Fig. 3.10) using the equation P = pgh (P = pressure (GPa), p = continental crust density (2.73 kg/m^3), g = specific gravity (10.0 m/s^2), h = depth (km)).

Based on the calculated crystallization pressure from the Al-in-hornblende geobarometry of hornblendite, hornblende gabbro and hornblende microgabbro, these calculated pressures can be conversed to emplacement depths (Fig. 3.10) as averages of 31.2 km, 29.8 km and 28.9 km, respectively. The results are very consistent depth of crystallization in the lower crust (Petrini and Podladchikov, 2000) (Fig. 5.2). The calculated depth values are also consistent with the calculated hornblende-plagioclase temperatures (670-1,000 ºC, 850-950 ºC and 750-850 ºC for hornblendite, hornblende gabbro and microgabbro, respectively), that suggest magmatic crystallization took place in the lower crust (Peacock, 1993; Winter, 2001; Kelemen et al., 2003; Richards, 2003).

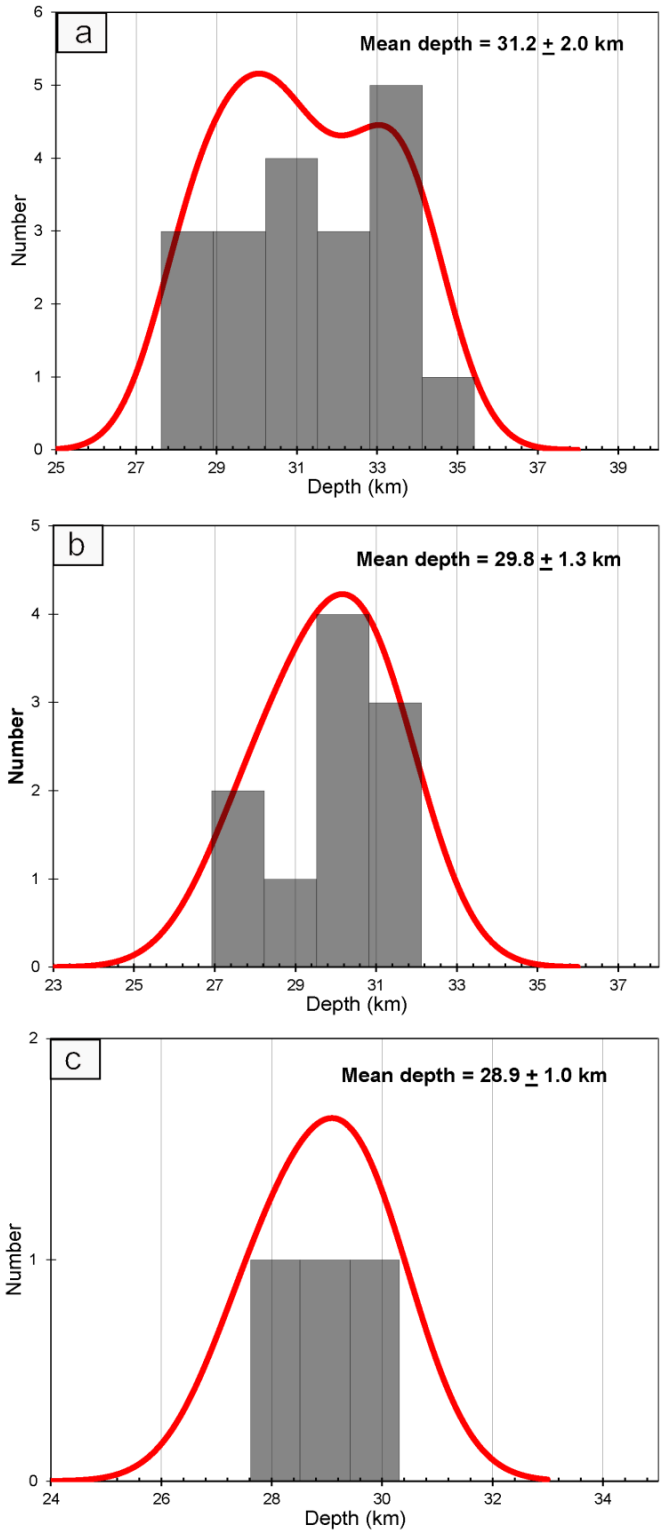

Figure 3.10 (a, b, c) The histograms of calculated intrusion depth distributions from hornblendite, hornblende gabbro and hornblende microgabbro, respectively, in the Wang Nam Khiao area, Nakhon Ratchasima, Thailand.

Magma genesis: According to the plots of Ca+Ti vs. Ti (Leterrier et al., 1982) diagram, the mineral chemistry of clinopyroxene indicates the alkalic features (Fig. 3.11). The clinopyroxenes from hornblendite and hornblende gabbro in this diagram show mostly in the alkali basalt field with minor subalkalic variety (Fig. 3.11) which is consistent with the results of the total alkali (Na_2O+K_2O) vs. silica TAS plots (Fig. 3.5).

The geochemistry data also suggest partial melting and crustal contamination for the evolution of the mafic-ultramafic rocks. La/Nb vs. La/Ba plot (Fig. 3.12a) indicates magma evolution in subduction-related setting resulted from magma-crust interaction (Fig. 3.12b). The high aluminum contents of these rocks (12.68 wt% to 22.18 wt%) implies the evolution of high aluminum basaltic magmas which is often originated from primitive magma produced by partial melting of mantle peridotite (Brophy and Marsh, 1986) above the descending oceanic slab in the mantle wedge (Brophy and Marsh, 1986; Crawford et al., 1987) and hornblende formed by reaction of pyroxene and water (Sisson and Layne, 1993). Moreover, all the geochemistry data are significantly enriched in LILE (e.g. Ba, K, Sr) and depletion of HFSE (e.g. Nb, Ta, Zr) (Fig. 3.7a) suggesting subduction zone or arc-related evolution (Pearce, 1982, 1983; Ryerson and Watson, 1987; Kelemen et al., 1990; Ringwood, 1990; Kelemen et al., 1993). The REE patterns of these rocks (Fig. 3.7b) are mostly characterized by the convex shape and slightly flat which indicate the high degree of partial melting.

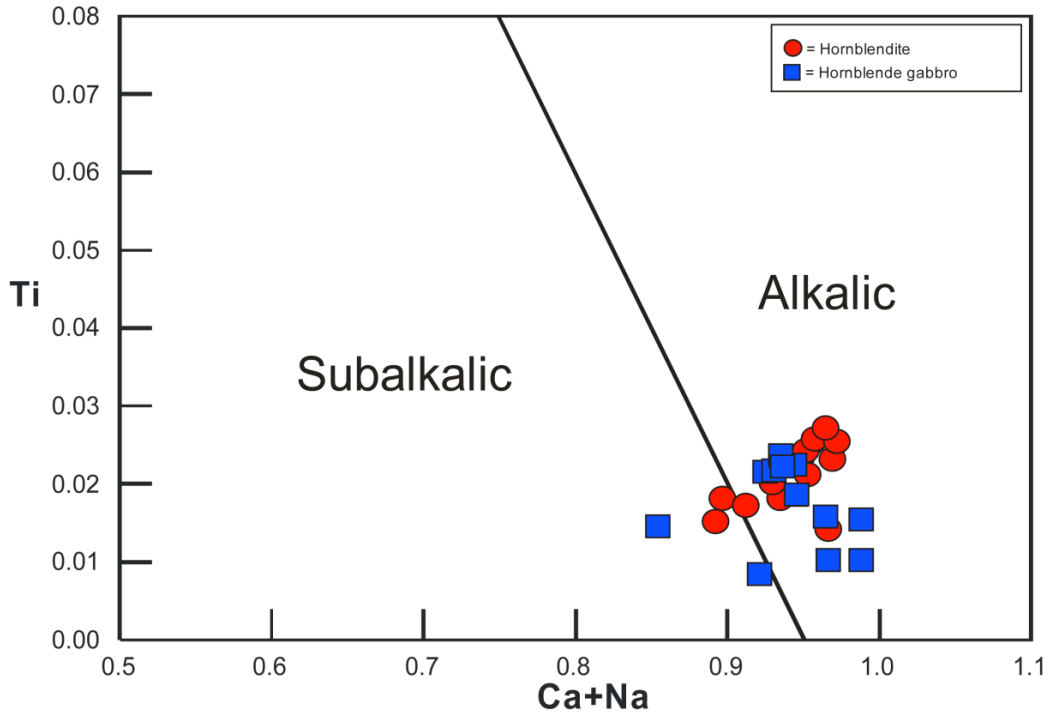

Figure 3. 11 Clinopyroxene composition plots of Ca+ Na vs. Ti (introduced by Leterrier *et al.* (1982)) showing the alkali composition.

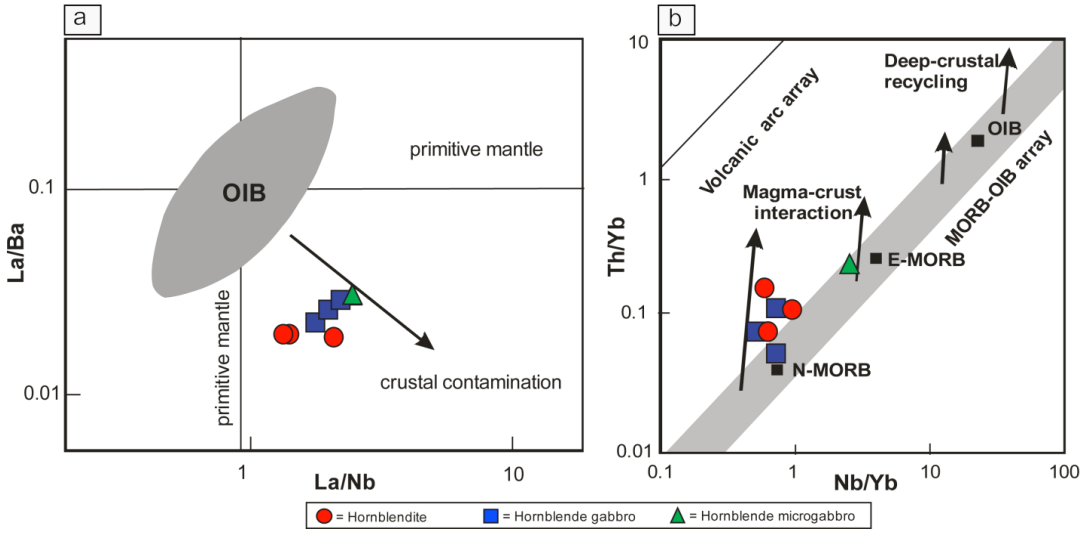

Figure 3.12 (a) Whole-rock geochemical plots of La/Nb vs. La/Ba indicate the effect of crustal contamination (Kieffer et al., 2004) and (b) Nb/Yb vs. Th/Yb plots show the magma-crust interaction in volcanic arc affinity (Pearce, 2008).

Petrogenesis: The results of petrography and mineral chemistry of the mafic-ultramafic plutonic rocks in the study area, particularly hornblende + plagioclase assemblage, cumulate texture (Fig. 3.2), and high An content of plagioclase (Fig. 3.4b) indicate the hydrous magma source for the formation of the rocks (Sisson and Layne, 1993; Sisson et al., 1996).

The clinopyroxene compositions can be used to explain the crystallization genesis using some discrimination diagrams plotting clinopyroxene compositions. The plots of clinopyroxene discrimination on TiO_2 against Al diagram suggest arc accumulate affinity (Fig. 3.13a) which is consistent with the hornblende composition plotted on Si vs. Na+K diagram (Fig. 3.13b).

The plots of major, minor, and trace elements compositions on the discrimination diagrams from all analyzed samples (hornblendite, hornblende gabbro and hornblende microgabbro), the chondrite-normalized ratios of La/Sm vs. Ba/La indicate Island arc field (IA) (Fig. 3.14a) which is also consistent with Volcanic Arc (VA) affinity in Zr vs. Ti diagram (Fig. 3.14b). Moreover, the primitive mantle-normalized spider diagram (Fig. 3.7a) shows clear Nb and Ta depletions in addition with the patterns in chondrite-normalized REE patterns (Fig. 3.7b) which suggest subduction-related magmatism in typical arc setting (Togashi et al., 1992; Woodhead et al., 1998; Greene et al., 2006).

Therefore, all the geochemical and mineral chemical features indicate that the tectonic setting of these hornblendite, hornblende gabbro and hornblende microgabbro is probably related to an arc-related magmatism, which is comparable with the Alaskan-type mafic- ultramafic intrusions (Taylor, 1967; Irvine, 1974; Snoke et al., 1981; Himmelberg and Loney, 1995; Helmy and El Mahallawi, 2003; Ishiwatari and Ichiyama, 2004; Batanova et al., 2005; Johan, 2006; Pettigrew and Hattori, 2006; Eyuboglu et al., 2010; Su et al., 2012).

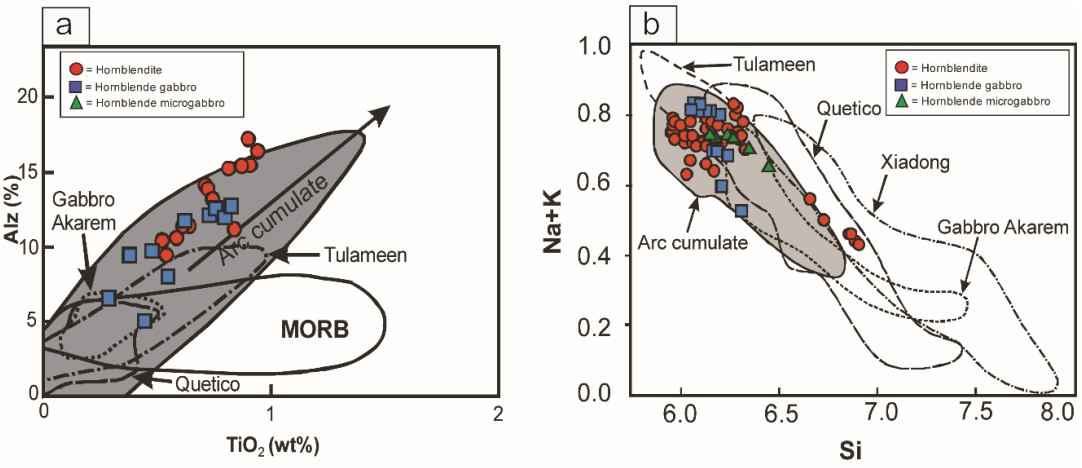

Figure 3.13 (a) Clinopyroxene compositional plots in TiO_2 and Al_z, suggesting arc accumulate trend in hydrous magmas as defined by Loucrs (1990) with comparable other hydrous arc magmatic rocks (Tulameen Complex from Rublee (1994); Gabbro Akarem Complex from Helmy and El Mahallawi (2003); Quetico Intrusions from Pettigrew and Hattori (2006)). (b) Calcic amphibole composition plot based on Si and Na+K, suggesting arc accumulate as defined by Beard and Barker (1989) together with those of arc Alaskan-type intrusion of Tulameen Complex from Rublee (1994); Gabbro Akarem Complex from Helmy and El Mahallawi (2003); Quetico Intrusions from Pettigrew and Hattori (2006); Su et al. (2012)).

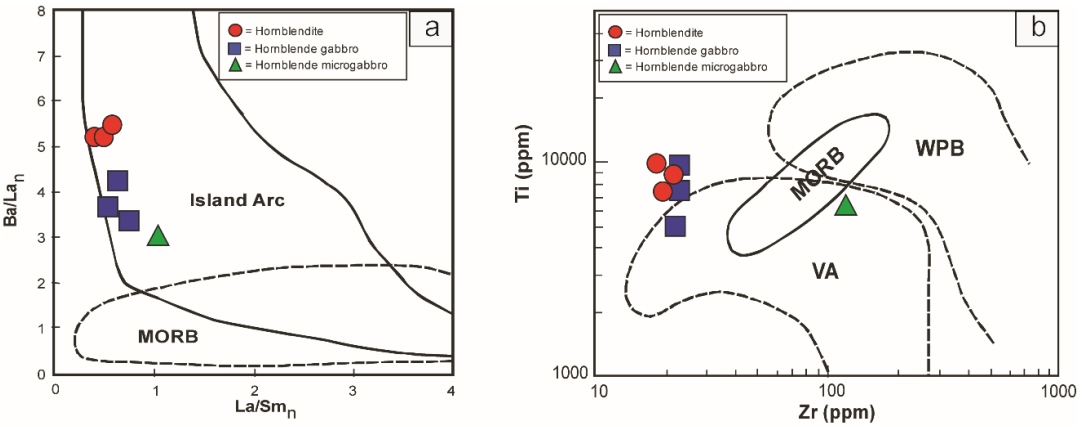

Figure 3.14 Whole-rock geochemical plots of tectonic setting discrimination diagrams: (a) normalized La/Sm vs Ba/La ratio diagram after Wood (1980)

(chondrite normalized data from Sun and McDonough (1989); (b) Zr vs. Ti diagram after Pearce and Cann (1973).

Age of rocks formation: The hornblendite, hornblende gabbro and hornblende microgabbro in the Wang Nam Khiao area show very close petrographical, mineral chemical and geochemical features, suggesting these rocks were defined by crystallization from the same magma chamber in the lower crust. Thus, the hornblende microgabbro cut into hornblendite probably reflects the latest stage of crystallization. In addition, the CL images of zircon in the hornblende microgabbro clearly show oscillatory zoning (Fig. 3.8), indicating the zircon crystallized from magma. The zircon yielded weighted mean U-Pb age of 257.1 ± 3.4 Ma (Fig. 3.9) which is probably interpreted as the timing of magmatism through subduction of Paleo-Tethys beneath the Indochina Terrane during Late Permian (Charusiri et al., 1993; Intasopa, 1993; Charusiri et al., 2002; Zaw et al., 2007; Sone and Metcalfe, 2008; Barr and Charusiri, 2011; Metcalfe, 2011b, 2013; Kamvong et al., 2014; Zaw et al., 2014). Moreover, this age is consistent with that of Late Permian/Earliest Triassic arc magmatic rocks in Loei Fold Belt (U-Pb zircon age, 254-250 Ma) (Khositanont et al., 2008; Salam et al., 2014; Zaw et al., 2014) regarding to Permian-Triassic magmatic arc which may represent Palaeo-Tethys subduction beneath western Indochina (Sone and Metcalfe, 2008; Metcalfe, 2011b, a; Sone et al., 2012; Metcalfe, 2013). On the other hand, the older zircons yielded weighted mean U-Pb age of 447.0 ± 19 Ma (Fig. 3.9) which may indicate zircon from the older arc-related magmatism of Loei Fold Belt (Khositanont et al., 2008; Boonsoong et al., 2011).

CHAPTER 4
GRANITIC ROCKS

The granitic rocks in the Wang Nam Khao area, Nakhon Ratchasima can be classified into biotite granite, hornblende granite, and biotite-hornblende granite based on the mineral assemblages. The study of the granitic rocks can be reported within 6 main parts including field observation, petrography, mineral chemistry, whole-rock geochemistry, geothermobarometry, and zircon U-Pb geochronology. These results can be subsequently discussed on the intrusion depth, magma genesis, petrogenesis, and age of rock formation.

The main parts of this study have been submitted to the Journal of Asian Earth Sciences, special issue: ASIA2016 on the topic "***Petrochemistry and zircon U-Pb geochronology of granitic rocks in the Wang Nam Khiao area, Nakhon Ratchasima, Thailand***: ***Implications for petrogenesis and tectonic setting***".

4.1 Field observation

The exposed granitic rocks in Wang Nam Khiao area, Nakhon Ratchasima consists of 3 main granitic units (Fig. 2.3): biotite granite, hornblende granite, and biotite-hornblende granite.

Biotite granite: is discovered in the northern part where it exposed as small bodies covering 2-3 km^2. These rocks are characterized by pink biotite granite (Fig. 4.1a) showing weakly foliation in some areas. The outcrop exposures are commonly found as a natural outcrop and some quarries in which they usually show exfoliation (Fig. 4.1a). The rock contact with spotted slate are clearly observed (Fig. 4.1b); this evidence indicates granite intruded into the country rock.

Hornblende granite: is found in the southern part of the study area (Fig. 2.3). This rock unit covers about 10 km wide and 8 km long. For the outcrop exposures, the natural massive outcrops are commonly present (Fig. 4.1c) with thin exfoliations. In addition, the mafic autholiths usually embed in this rock (Fig. 4.1c). These rocks show

a variety of hornblende granite to hornblende diorite (Fig. 4.5) which are characterized by dominant hornblende within mafic mineral assemblage (Figs. 4.1c, 4.2c-d).

Biotite-hornblende granite: is exposed in the northern part of the study area (Fig. 2.3) contacted with the hornblende gabbro and hornblendite and the biotite granite and surrounded by the Permian sedimentary rocks (Fig. 2.3). This rock unit covers about 10 km long and 8 km wide. The rock units vary from granite to diorite in compositions (Fig. 4.5); however, they are similarly composed of biotite and hornblende (Figs. 4.1d-f, 4.2e-f). Massive natural outcrops with the exfoliations of this rock unit is clearly observed (Fig. 4.1d). In addition, mafic autholiths (Fig. 4.1e) and quart-feldspar veins (Fig. 4.1f) are commonly found in these rocks.

Figure 4. 1 Exposures of granitic rocks in the Wang Nam Khiao area, Nakhon Ratchasima, Thailand showing (a) biotite granite with (b) contact of spotted slate, (c) hornblende granite with the typical mafic autholiths, and (d) biotite-hornblende granite with the (e) mafic autholith and (f) quartz-feldspar vein.

4.2 Petrography

The classified granitic rocks as the biotite granite, hornblende granite, and biotite-hornblende granite (Fig. 2.3) in this study are explained the details of petrography including mineral assemblages and microtextures. These features are the most important evidences to understand the genesis of rocks which can be used to discuss with other results in next section.

Biotite granite: are characterized by fine- to coarse-grained biotite granite. These rocks are dominated by quartz (30-50%), K-feldspar (20-60%), plagioclase (10-40%), and biotite (5-25%) with less abundance of opaque minerals (3-5%) (Figs. 4.3a, b), and zircon (1-2%) with/without altered minerals (<1%) e.g. sericite and chlorite. Quartz (0.2-2 mm) shows anhedral shape with strong wavy extinction. The equigranular texture of quartz, K-feldspar, and plagioclase (Figs. 4.2a, b) are presented in this rock. In addition, the foliations of fine-grained quartz with sub-grained texture between the coarse-grained, and ribbon quartzs are sometime displayed as the foliated granite. The medium- to coarse-grained (0.5-3 mm) K-feldspar and plagioclase exhibit anhedral-, and anhedral- to subhedral, respectively, as the equigranular texture. For the secondary minerals (sericite) are sometime found as fine-grained minerals in plagioclase and K-feldspar.

Hornblende granite: comprises abundances of plagioclase (25-60%), quartz (5-30%), K-feldspar (5-30%), hornblende (10-30%), biotite (5-10%) with less abundances (2-8%) of opaque minerals (Figs. 4.3c, d), titanite, zircon, and apatite. Sericite and chlorite may be observed as secondary minerals (Figs. 4.2c-d). Fine- to medium-grained (0.3-1 mm) plagioclase shows euhedral to subhedral shape. Quartz is found as fine- to medium-grain (0.1-1 mm) with anhedral shape. Anhedral to subhedral K-feldspar shows medium- to coarse-grained texture. Fine- to medium-grained (0.3-2 mm) greenish hornblende commonly occurs with some flaky fine- to medium-grained (0.1-1 mm) brown biotite. In addition, the accessory minerals, subhedral (0.2-0.5 mm) titanite (sphene) and anhedral (0.1-0.3 mm) opaque minerals (magnetite), are also presented in this rock.

Biotite-hornblende granite: contains mainly quartz (20-40%), plagioclase (10-60%), K-feldspar (5-40%), biotite (10-20%), hornblende (5-10%) (Figs. 4.2e, f) and the

minor (2-5%) assemblages of opaque minerals (Figs. 4.3e, f), zircon, and apatite. These mineral assemblages display equigranular texture of the anhedral medium- to coarse-grained quartz (0.3-2 mm), euhedral to subhedral coarse-grained plagioclase (0.5-2 mm), and subhedral coarse-grained K-feldspar (0.5-3 mm). Moreover, the zoning texture is commonly displayed in plagioclase (Fig. 4.2e). Brownish biotite shows medium-grained (0.2-1 mm) and anhedral to subhedral flaky crystals. Altered mineral, sericite, is sometime found in plagioclase.

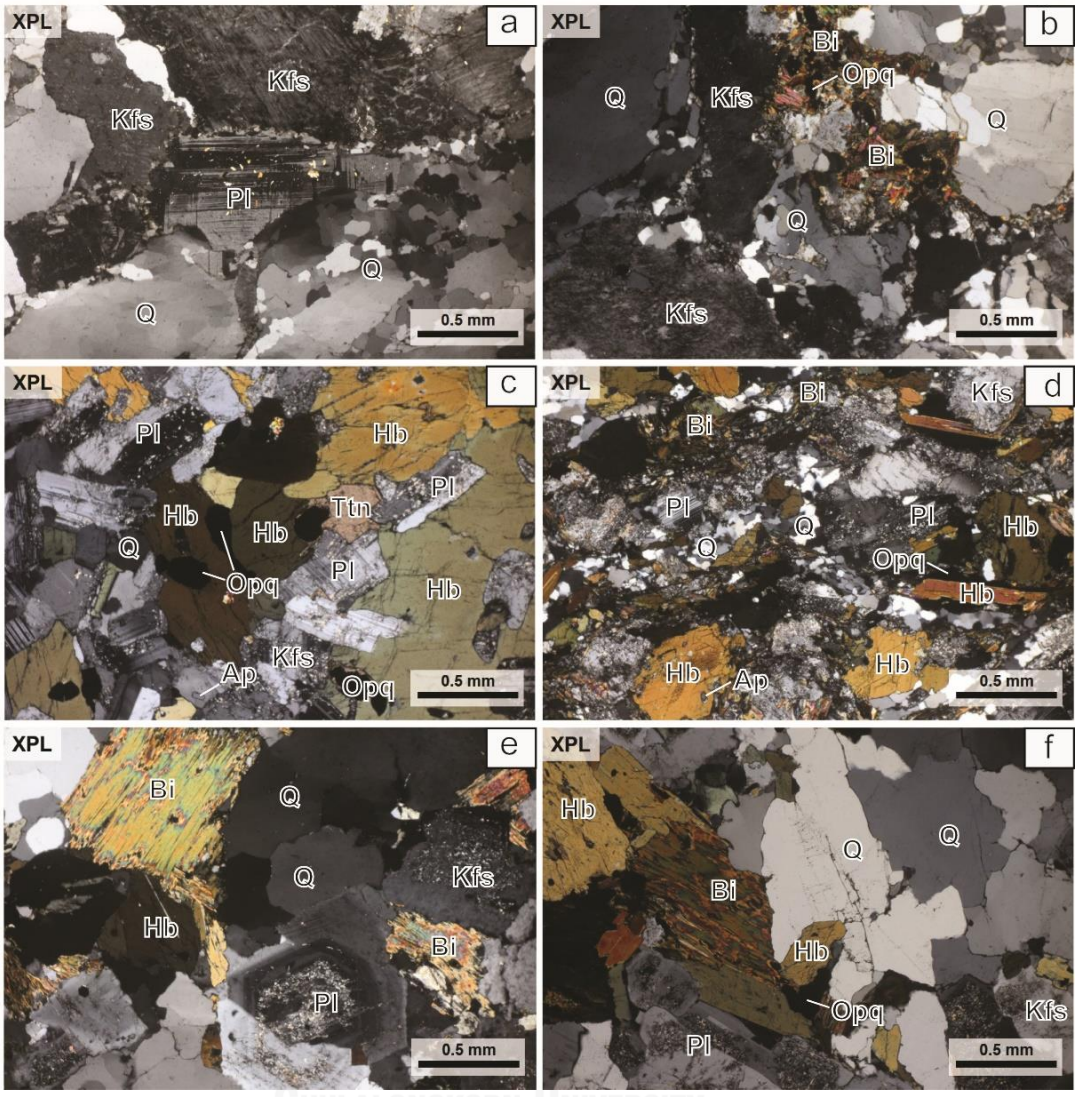

Figure 4.2 Photomicrographs of granitic rocks in the Wang Nam Khiao area showing mineral assemblages and textures. (a) coarse-grained K-feldspar, quartz, and plagioclase and (b) dominant K-feldspar, quartz, and plagioclase, with less abundant biotite and opaque minerals in the biotite granite; (c, d) equigranular texture of plagioclase, hornblende, quartz, K-feldspar with accessory minerals of titanite, opaque minerals in the hornblende granite; (e, f) equigranular texture of zoned plagioclase, K-feldspar, quartz, biotite, hornblende with opaque minerals in the biotite-hornblende granite. Mineral abbreviations, Q (quartz), Pl (plagioclase), Kfs (K-feldspar), Hb (hornblende), Bi (biotite), Ttn (titanite), Opq (opaque minerals).

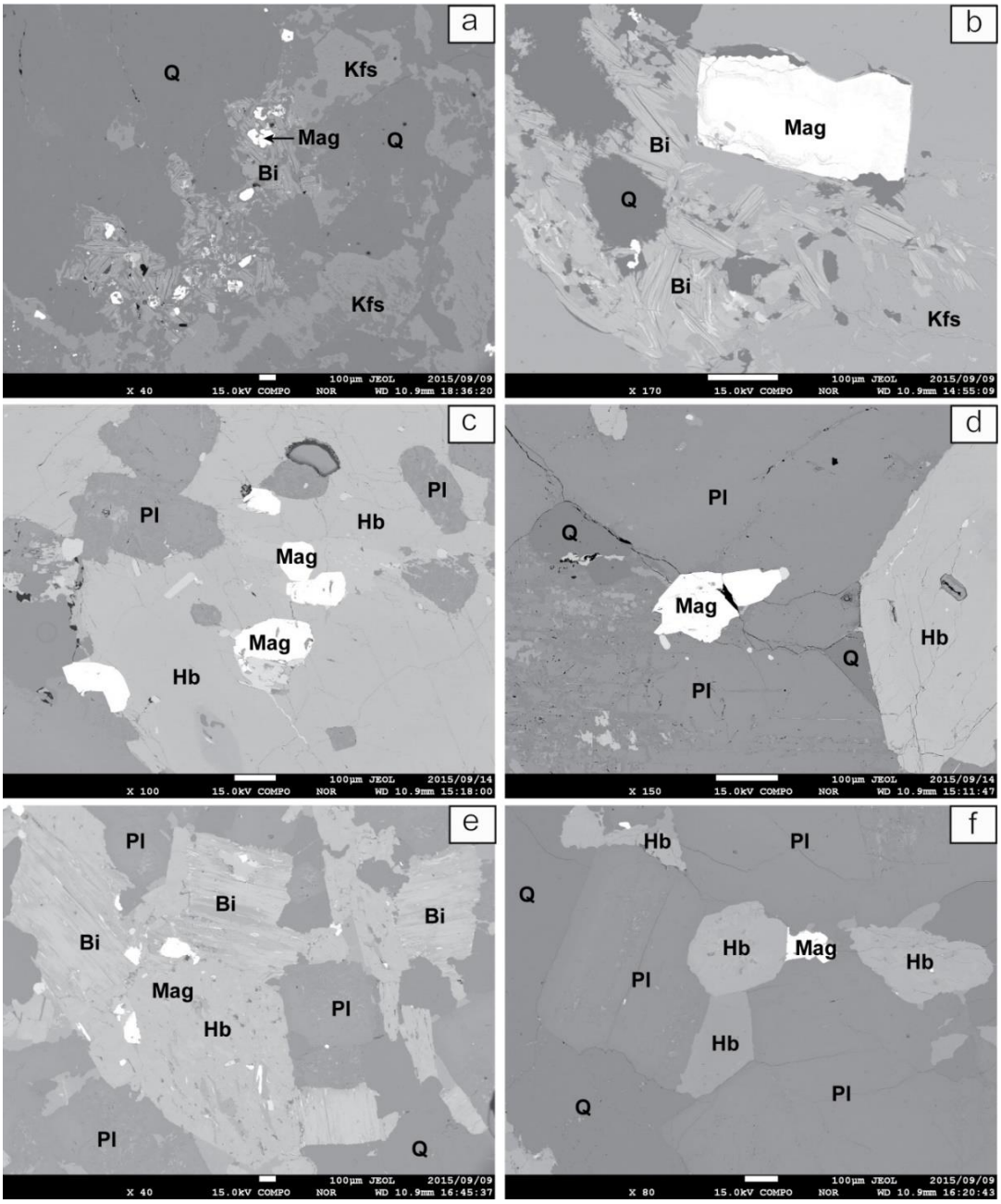

Figure 4.3 BEI images showing opaque minerals in (a, b) biotite granite, (c, d) hornblende granite, and (e, f) biotite-hornblende granite in the Wang Nam Khiao area, Nakhon Ratchasima Mineral abbreviations, Q (quartz), Pl (plagioclase), Kfs (K-feldspar), Hb (hornblende), Bi (biotite), Mag (Magnetite).

4.3 Mineral chemistry

Mineral chemistry can provide the important characteristics of mineral assemblage in studied granitic rocks. Moreover, the analytical data can be discussed with other results (e.g., petrography, whole-rocks geochemistry, geochronology) to understand the genesis of rocks and their tectonic setting. Moreover, the mineral chemistry of some coexisting minerals can be used to estimate the crystallization PT conditions (Section 4.5).

Thirty-six samples (Table 2.1) of granitic rocks inform the Wang Nam Khiao area, Nakhon Ratchasima were prepared as polished thin sections for mineral chemical analysis using Electron Probe Micro Analyzer (EPMA) as reported in sections 2.3 and 2.4).

The mineral chemistries of the solid-solutions minerals (i.e., calcic amphibole, K-feldspar, plagioclase, and biotite) are presented in Tables 4.1 to 4.3, and plotted in Fig. 4.4. Details are reported below.

Calcic amphibole: is commonly presented as a minor mineral composition in the hornblende granite and biotite-hornblende granite (Fig. 4.4). Amphibole is not found in the biotite granite. The analytical results of calcic amphiboles and their recalculated cations based on 23 oxygens are revealed in Table 4.1.

The calcic amphibole in the hornblende granite shows composition ranges of 43-48 %SiO_2, 7-11 %Al_2O_3, 9-14 %MgO, 11-12 %CaO, 14-19 %FeO_t, and 1 %Na_2O, while the calcic amphibole in the biotite-hornblende granite reveals 47-51 %SiO_2, 6-7 %Al_2O_3, 14-15 %MgO, 11-12 %CaO, 12-14 %FeO_t, and 1-2 %Na_2O in compositions.

In general, the hornblende granite and biotite-hornblende granite show a wide composition of calcic amphibole in X_{Mg} ((Mg/Mg+Fe) = 0.47–0.69), $(Na+K)_A$ (0.33–0.55 pfu), and Si (6.59–7.37 pfu) (Table 4.1). These calcic amphiboles of are mostly edenite with some ferro-edenite components for hornblende granite, whereas only edentate is presented for biotite-hornblende granites, based on the nomenclature of Leake *et al.* (1997) (Fig. 4.4a). In terms of $(Na+K)_A$, amphibole composition in the hornblende granite shows a lower value of $(Na+K)_A$ (0.33-0.55 pfu) with some compositional zoning, slightly increases from rim (0.33–0.53 pfu) to core (0.39–0.55

pfu), whereas the biotite-hornblende granite shows higher $(Na+K)_A$ value (0.39-0.52 pfu) with decreasing slightly from rim (0.40–0.52 pfu) to core (0.39–0.52 pfu). X_{Mg} of the hornblende granite (X_{Mg} = 0.47-0.64 pfu) is slightly lower than that of biotite-hornblende granite (X_{Mg} = 0.65-0.69 pfu).

Feldspars: is found as the major composition in all granitic rocks in the study area which they are composed of both plagioclase and K-feldspar (Fig. 4.4). The analytical results and their recalculated cations based on 10 oxygens of feldspars in the biotite granite, hornblende granite, and biotite-hornblende granite are summarized in Table 4.2

Plagioclase in the hornblende granite shows higher anorthite (An) contents (An_{36-52}, classified as andesine to labradorite) than that in the biotite-hornblende granite (An_{9-36}, classified as albite to andesine) and in the biotite granite (An_{0-9}, which is classified as albite) (Fig. 4.4b). K-feldspar in biotite granite shows high orthoclase contents (Or_{92-97}) (Fig. 4.4b).

Biotite: is accessory mineral of all granitic rocks. It was analyzed and recalculated cations based on 10 oxygens as summarized in Table 4.3.

The analyzed biotites in all granites under this study show similar compositions (Table 4.3) which are classified as annite-siderophyllite (Fig. 4.4c). These biotites are plotted in the Mg-biotite field (Fig. 4.4d) based on the classification of Foster (1960). It shows Mg-rich (X_{Mg} = 0.47-063). The biotite-hornblende granite shows a higher X_{Mg} (0.59-0.63) than those in hornblende granite (X_{Mg} = 0.47-0.57) and biotite granites (X_{Mg} = 0.47-0.58). Moreover, Ti content of the biotite-hornblende granite reveals higher Ti content (Ti = 0.15-0.20) than that of hornblende granite (Ti = 0.12-0.21) and biotite granites (Ti = 0.04-0.15). However, the FeO contents biotite in the biotite-hornblende granite are lower (FeO_{total} = 15.70-16.96 wt%) than that in hornblende granite (FeO_{total} = 17.31-22.81 wt%) and biotite granites (FeO_{total} = 16.41-17.92 wt%), in terms of FeO_{total}.

Table 4.1 Representative EPMA analyses of hornblende in granitic rocks from the Wang Nam Khiao, Nakhon Ratchasima, Thailand.

Rock unit	Hornblende granite							
Sample no.	2WK1_5	2WK1_6	2WK1_8	2WK1_9	2WK1_11	2WK1_12	2WK2_13	2WK2_14
Remark	Core	Rim	Core	Rim	Rim	Core	Core	Rim
SiO_2	44.90	46.59	46.05	46.43	46.91	44.24	44.22	43.16
Al_2O_3	9.59	8.41	9.01	8.31	8.09	10.20	9.24	10.20
TiO_2	1.80	1.24	1.41	1.29	1.03	1.82	1.30	0.86
Cr_2O_3	0.02	0.03	0.03	0.04	0.02	0.00	0.00	0.00
FeO	14.09	14.14	14.22	14.23	13.57	14.63	17.91	18.61
MnO	0.34	0.36	0.36	0.38	0.36	0.31	0.96	0.84
MgO	12.50	13.16	12.87	12.99	13.60	12.06	10.00	9.28
CaO	11.91	11.81	11.82	11.80	11.97	11.92	11.71	11.67
Na_2O	1.26	1.12	1.28	1.18	1.11	1.44	1.04	0.94
K_2O	0.68	0.49	0.53	0.45	0.53	0.73	1.09	1.18
Cl	0.00	0.05	0.04	0.10	0.02	0.09	0.00	0.00
F	0.07	0.07	0.08	0.09	0.10	0.07	0.10	0.12
Total	97.09	97.35	97.58	97.10	97.19	97.35	97.47	96.74
23 (O)								
Si	6.681	6.881	6.799	6.882	6.924	6.593	6.707	6.622
Al	1.681	1.464	1.567	1.451	1.407	1.791	1.651	1.844
Ti	0.201	0.138	0.156	0.144	0.114	0.204	0.148	0.099
Cr	0.002	0.004	0.004	0.005	0.002	0.000	0.000	0.000
Fe^{3+}	0.000	0.000	0.000	0.000	0.000	0.000	0.000	0.000
Fe^{2+}	1.753	1.746	1.755	1.763	1.674	1.823	2.271	2.387
Mn	0.043	0.045	0.045	0.048	0.045	0.039	0.123	0.109
Mg	2.770	2.895	2.830	2.868	2.990	2.677	2.259	2.121
Ca	1.898	1.868	1.869	1.873	1.892	1.903	1.902	1.918
Na	0.363	0.321	0.366	0.339	0.317	0.416	0.306	0.279
K	0.129	0.092	0.100	0.085	0.100	0.139	0.211	0.231
Total	15.522	15.454	15.492	15.458	15.466	15.585	15.578	15.61 1
Mg/(Fe+Mg)	0.613	0.624	0.617	0.619	0.641	0.595	0.499	0.470
Na+K	0.492	0.413	0.466	0.424	0.417	0.555	0.516	0.510
P (kbar)	5.0	4.0	4.5	3.9	3.7	5.5	4.9	5.8
Depth (Km)	18	14	16	14	13	20	18	21

Table 4.1 (cont.).

Rock unit	Hornblende granite							
Sample no.	2WK2_15	2WK2_16	2WK2_18	2WK2_19	2WK3_25	2WK3_26	2WK3_27	2WK3_28
Remark	Core	Rim	Core	Rim	Core	Rim	Core	Rim
SiO_2	45.14	43.40	45.28	44.37	46.86	45.76	45.85	45.54
Al_2O_3	8.34	10.24	8.78	9.56	7.47	8.32	8.27	8.44
TiO_2	1.39	1.14	1.24	0.96	1.53	1.36	1.50	0.97
Cr_2O_3	0.00	0.00	0.00	0.00	0.02	0.03	0.00	0.03
FeO	17.99	18.77	17.25	18.11	14.57	15.47	14.93	15.52
MnO	0.91	0.89	0.83	0.85	0.53	0.60	0.51	0.55
MgO	10.36	9.36	10.63	10.84	12.68	11.71	12.46	11.97
CaO	11.42	11.66	11.83	11.04	11.76	11.83	11.93	11.93
Na_2O	0.77	1.01	0.93	0.62	1.04	0.96	1.20	1.03
K_2O	0.83	1.19	0.93	0.76	0.68	0.96	0.95	0.84
Cl	0.02	0.05	0.05	0.09	0.03	0.04	0.00	0.00
F	0.08	0.11	0.08	0.07	0.11	0.17	0.18	0.05
Total	97.15	97.66	97.70	97.11	97.14	97.00	97.60	96.82
23 (O)								
Si	6.837	6.601	6.804	6.714	6.962	6.861	6.822	6.843
Al	1.488	1.835	1.555	1.705	1.308	1.470	1.450	1.494
Ti	0.158	0.130	0.140	0.109	0.171	0.153	0.168	0.110
Cr	0.000	0.000	0.000	0.000	0.002	0.004	0.000	0.004
Fe^{3+}	0.000	0.000	0.000	0.000	0.000	0.000	0.000	0.000
Fe^{2+}	2.278	2.387	2.167	2.291	1.810	1.939	1.857	1.950
Mn	0.117	0.115	0.106	0.109	0.067	0.076	0.064	0.070
Mg	2.337	2.121	2.379	2.443	2.806	2.615	2.761	2.679
Ca	1.852	1.899	1.904	1.789	1.871	1.900	1.901	1.920
Na	0.226	0.298	0.271	0.182	0.299	0.279	0.346	0.300
K	0.160	0.231	0.178	0.147	0.129	0.184	0.180	0.161
Total	15.454	15.616	15.503	15.489	15.426	15.480	15.549	15.529
Mg/(Fe+Mg)	0.506	0.470	0.523	0.516	0.608	0.574	0.598	0.579
Na+K	0.386	0.528	0.449	0.328	0.428	0.462	0.526	0.461
P (kbar)	4.1	5.7	4.4	5.1	3.2	4.0	3.9	4.1
Depth (Km)	15	21	16	19	12	14	14	15

Table 4.1 (cont.).

Rock unit	Hornblende granite							
Sample no.	2WK3_29	2WK3_47	2WK4_33	2WK4_34	2WK4_35	2WK4_36	2WK4_40	2WK4_41
Remark	Core	Core	Core	Rim	Core	Rim	Rim	Core
SiO_2	47.14	46.39	47.72	44.84	47.03	47.28	44.89	46.44
Al_2O_3	7.29	7.51	7.32	9.41	7.41	7.24	9.21	8.02
TiO_2	1.38	1.70	1.59	1.01	1.61	1.58	1.00	1.85
Cr_2O_3	0.00	0.00	0.00	0.01	0.00	0.01	0.03	0.00
FeO	14.59	14.58	13.65	16.33	13.91	14.86	16.16	13.95
MnO	0.56	0.59	0.55	0.52	0.55	0.68	0.50	0.58
MgO	12.85	12.91	13.46	11.42	13.30	12.89	11.57	13.21
CaO	11.91	11.66	11.66	12.13	11.36	11.33	11.94	11.43
Na_2O	0.95	1.08	1.10	0.92	1.29	1.25	0.98	1.33
K_2O	0.70	0.65	0.52	0.93	0.55	0.53	0.96	0.56
Cl	0.00	0.00	0.04	0.00	0.02	0.00	0.03	0.00
F	0.13	0.14	0.14	0.05	0.16	0.15	0.06	0.16
Total	97.37	97.07	97.57	97.52	97.01	97.65	97.24	97.37
23 (O)								
Si	6.987	6.907	7.010	6.722	6.967	6.987	6.743	6.867
Al	1.273	1.318	1.267	1.662	1.294	1.261	1.630	1.397
Ti	0.154	0.190	0.176	0.114	0.179	0.176	0.113	0.206
Cr	0.000	0.000	0.000	0.001	0.000	0.001	0.004	0.000
Fe^{3+}	0.000	0.000	0.000	0.000	0.000	0.000	0.000	0.000
Fe^{2+}	1.808	1.815	1.676	2.047	1.723	1.836	2.029	1.724
Mn	0.070	0.074	0.068	0.066	0.069	0.085	0.064	0.073
Mg	2.837	2.863	2.945	2.550	2.935	2.838	2.589	2.909
Ca	1.891	1.859	1.834	1.948	1.802	1.793	1.921	1.810
Na	0.273	0.312	0.313	0.267	0.370	0.358	0.285	0.381
K	0.132	0.123	0.097	0.178	0.104	0.100	0.184	0.106
Total	15.425	15.461	15.387	15.555	15.444	15.435	15.562	15.473
Mg/(Fe+Mg)	0.611	0.612	0.637	0.555	0.630	0.607	0.561	0.628
Na+K	0.405	0.435	0.410	0.445	0.474	0.458	0.469	0.487
P (kbar)	3.1	3.3	3.0	4.9	3.1	3.0	4.7	3.6
Depth (Km)	11	12	11	18	11	11	17	13

Table 4.1 (cont.).

Rock unit	Biotite-hornblende granite							
Sample no.	2WK11_59	2WK11_60	2WK11_66	2WK13_71	2WK13_81	2WK15_95	2WK15_96	2WK15_98
Remark	Core	Core	Core	Rim	Rim	Core	Rim	Rim
SiO_2	47.27	48.63	48.46	50.87	48.05	47.36	47.73	48.80
Al_2O_3	7.46	6.45	6.65	6.57	6.49	7.46	7.17	6.05
TiO_2	0.90	0.81	0.76	0.59	0.79	0.94	0.84	0.77
Cr_2O_3	0.09	0.07	0.08	0.02	0.08	0.07	0.04	0.07
FeO	13.32	12.62	12.97	12.09	13.55	13.38	13.00	12.54
MnO	0.43	0.45	0.47	0.36	0.44	0.41	0.45	0.39
MgO	13.84	14.49	14.57	13.81	14.03	13.79	14.11	14.69
CaO	11.65	11.49	11.77	11.02	11.62	11.25	11.51	11.48
Na_2O	1.37	1.31	1.22	0.94	1.19	1.54	1.46	1.18
K_2O	0.44	0.23	0.25	1.41	0.32	0.39	0.34	0.40
Cl	0.02	0.13	0.06	0.07	0.01	0.07	0.05	0.07
F	0.03	0.03	0.03	0.02	0.03	0.03	0.03	0.02
Total	96.77	96.55	97.20	97.68	96.56	96.59	96.65	96.37
23 (O)								
Si	6.997	7.161	7.108	7.365	7.118	7.016	7.052	7.198
Al	1.301	1.119	1.149	1.121	1.133	1.302	1.248	1.052
Ti	0.100	0.090	0.084	0.064	0.088	0.105	0.093	0.085
Cr	0.011	0.008	0.009	0.002	0.009	0.008	0.005	0.008
Fe^{3+}	0.000	0.000	0.000	0.000	0.000	0.000	0.000	0.000
Fe^{2+}	1.648	1.554	1.591	1.463	1.678	1.657	1.606	1.546
Mn	0.054	0.056	0.058	0.044	0.055	0.051	0.056	0.049
Mg	3.052	3.178	3.183	2.978	3.096	3.043	3.105	3.228
Ca	1.847	1.812	1.849	1.709	1.844	1.785	1.821	1.814
Na	0.393	0.374	0.347	0.264	0.342	0.442	0.418	0.337
K	0.083	0.043	0.047	0.260	0.060	0.074	0.064	0.075
Total	15.485	15.394	15.425	15.271	15.424	15.482	15.469	15.393
Mg/(Fe+Mg)	0.649	0.672	0.667	0.671	0.648	0.647	0.659	0.676
Na+K	0.476	0.417	0.394	0.524	0.402	0.516	0.482	0.413
P (kbar)	3.2	2.3	2.5	2.3	2.4	3.2	2.9	2.0
Depth (Km)	12	8	9	8	9	12	11	7

Table 4.2 Representative EPMA analyses of feldspar in granitic rocks from the Wang Nam Khiao, Nakhon Ratchasima, Thailand.

Rock unit	Biotite granite							
Analysis no.	WKG1_19	WKG1_20	WKG1_21	WKG1_22	WKG1_23	2WK10_69	2WK10_70	2WK10_71
Remark	Pl-Core	Pl-Rim	Kfs	Kfs	Pl	Kfs	Pl	Pl
SiO_2	68.40	68.68	64.44	65.50	67.56	64.90	67.75	67.84
Al_2O_3	19.47	19.29	18.23	18.47	20.20	18.38	20.31	20.05
TiO_2	0.02	0.04	0.00	0.03	0.00	0.00	0.00	0.04
FeO*	0.00	0.05	0.02	0.06	0.13	0.01	0.08	0.04
MnO	0.00	0.00	0.01	0.00	0.00	0.00	0.00	0.00
MgO	0.00	0.00	0.00	0.00	0.00	0.00	0.00	0.00
CaO	0.14	0.06	0.01	0.02	0.72	0.00	1.00	1.19
Na_2O	11.42	11.68	0.43	0.92	10.79	0.51	11.02	10.92
K_2O	0.14	0.07	16.31	15.60	0.32	15.91	0.08	0.07
Total	99.59	99.88	99.44	100.60	99.71	99.73	100.24	100.15
8 (O)								
Si	2.998	3.003	2.998	3.001	2.964	3.002	2.958	2.964
Al	1.005	0.994	0.999	0.997	1.044	1.002	1.045	1.032
Ti	0.001	0.001	0.000	0.001	0.000	0.000	0.000	0.001
Fe^{3+}	0.000	0.000	0.000	0.000	0.000	0.000	0.000	0.000
Fe^{2+}	0.000	0.002	0.001	0.002	0.005	0.000	0.003	0.001
Mn	0.000	0.000	0.000	0.000	0.000	0.000	0.000	0.000
Mg	0.000	0.000	0.000	0.000	0.000	0.000	0.000	0.000
Ca	0.007	0.003	0.000	0.001	0.034	0.000	0.047	0.056
Na	0.970	0.989	0.038	0.082	0.917	0.046	0.932	0.924
K	0.008	0.004	0.967	0.912	0.018	0.938	0.004	0.004
Total	4.988	4.996	5.005	4.996	4.982	4.989	4.988	4.983
An	0.01	0.00	0.00	0.00	0.04	0.00	0.05	0.06
Ab	0.99	0.99	0.04	0.08	0.95	0.05	0.95	0.94
Or	0.01	0.00	0.96	0.92	0.02	0.95	0.00	0.00

Table 4.2 (cont.).

Rock unit	Biotite granite							
Analysis no.	2WK10_73	2WK10_74	2WK14_111	2WK14_112	2WK14_114	2WK14_115	2WK14_116	2WK14_117
Remark	Pl	Pl	Kfs	Pl	Pl	Pl	Kfs	Pl
SiO_2	68.38	68.28	64.62	67.43	66.86	67.82	64.81	67.87
Al_2O_3	19.87	20.07	18.01	19.77	20.69	19.89	18.58	19.86
TiO_2	0.00	0.00	0.02	0.08	0.00	0.00	0.00	0.04
FeO^*	0.05	0.05	0.04	0.41	0.02	0.05	0.04	0.03
MnO	0.03	0.00	0.01	0.01	0.00	0.00	0.00	0.01
MgO	0.02	0.02	0.03	0.00	0.00	0.00	0.00	0.03
CaO	0.57	0.78	0.00	0.72	1.83	0.81	0.25	0.60
Na_2O	11.17	11.16	0.32	10.95	10.50	10.88	2.50	11.08
K_2O	0.12	0.08	16.35	0.11	0.10	0.09	13.32	0.06
Total	100.20	100.44	99.45	99.50	100.06	99.55	99.49	99.60
8 (O)								
Si	2.981	2.972	3.006	2.968	2.930	2.976	2.986	2.976
Al	1.021	1.029	0.987	1.025	1.068	1.028	1.008	1.026
Ti	0.000	0.000	0.001	0.002	0.000	0.000	0.000	0.001
Fe^{3+}	0.000	0.000	0.000	0.000	0.000	0.000	0.000	0.000
Fe^{2+}	0.002	0.002	0.001	0.015	0.001	0.002	0.001	0.001
Mn	0.001	0.000	0.000	0.000	0.000	0.000	0.000	0.000
Mg	0.001	0.002	0.002	0.000	0.000	0.000	0.000	0.002
Ca	0.027	0.036	0.000	0.034	0.086	0.038	0.012	0.028
Na	0.944	0.941	0.029	0.934	0.892	0.925	0.223	0.941
K	0.007	0.004	0.970	0.006	0.005	0.005	0.782	0.003
Total	4.983	4.986	4.998	4.986	4.984	4.975	5.013	4.981
An	0.03	0.04	0.00	0.03	0.09	0.04	0.01	0.03
Ab	0.97	0.96	0.03	0.96	0.91	0.96	0.22	0.97
Or	0.01	0.00	0.97	0.01	0.01	0.00	0.77	0.00

Table 4.2 (cont.).

Rock unit	Hornblende granite							
Analysis no.	2WK1_26	2WK1_27	2WK1_28	2WK1_30	2WK1_31	2WK1_32	2WK1_33	2WK2_34
Remark	Pl-Core	Pl-Rim	Pl	Pl-Core	Pl-Rim	Pl-Rim	Pl	Pl
SiO_2	54.55	56.37	55.11	54.61	59.95	56.62	55.69	57.62
Al_2O_3	29.40	28.32	28.39	29.24	25.58	27.35	28.38	27.27
TiO_2	0.00	0.01	0.00	0.02	0.00	0.00	0.00	0.00
FeO*	0.26	0.17	0.10	0.19	0.13	0.15	0.16	0.19
MnO	0.00	0.00	0.01	0.00	0.04	0.04	0.00	0.03
MgO	0.02	0.00	0.00	0.02	0.02	0.01	0.02	0.00
CaO	11.81	10.36	10.82	11.68	7.40	9.73	10.80	9.33
Na_2O	4.82	5.77	5.48	5.04	7.27	5.98	5.48	6.08
K_2O	0.15	0.13	0.13	0.09	0.15	0.14	0.10	0.33
Total	101.01	101.14	100.04	100.92	100.57	100.03	100.63	100.83
8 (O)								
Si	2.442	2.509	2.484	2.446	2.659	2.544	2.494	2.565
Al	1.551	1.485	1.508	1.543	1.337	1.448	1.498	1.431
Ti	0.000	0.000	0.000	0.001	0.000	0.000	0.000	0.000
Fe^{3+}	0.000	0.000	0.000	0.000	0.000	0.000	0.000	0.000
Fe^{2+}	0.010	0.006	0.004	0.007	0.005	0.006	0.006	0.007
Mn	0.000	0.000	0.000	0.000	0.001	0.002	0.000	0.001
Mg	0.001	0.000	0.000	0.001	0.001	0.001	0.001	0.000
Ca	0.566	0.494	0.523	0.560	0.351	0.468	0.518	0.445
Na	0.418	0.498	0.479	0.437	0.625	0.521	0.476	0.524
K	0.008	0.007	0.007	0.005	0.009	0.008	0.006	0.019
Total	4.996	5.000	5.005	5.003	4.989	4.997	4.998	4.991
An	0.57	0.49	0.52	0.56	0.36	0.47	0.52	0.45
Ab	0.42	0.50	0.47	0.44	0.63	0.52	0.48	0.53
Or	0.01	0.01	0.01	0.01	0.01	0.01	0.01	0.02

Table 4.2 (cont.).

Rock unit	Hornblende granite							
Analysis no.	2WK2_36	2WK2_39	2WK2_40	2WK3_44	2WK3_45	2WK3_46	2WK3_47	2WK3_49
Remark	Pl-Rim	Pl-Core	Pl-Rim	Pl-Core	Pl-Rim	Pl-Core	Pl-Rim	Pl
SiO_2	58.42	58.07	57.45	56.35	58.85	58.42	58.90	58.27
Al_2O_3	26.40	27.04	27.46	27.53	25.77	25.52	25.84	26.16
TiO_2	0.01	0.00	0.00	0.03	0.00	0.01	0.00	0.00
FeO*	0.18	0.13	0.07	0.19	0.17	0.16	0.16	0.06
MnO	0.03	0.00	0.00	0.02	0.00	0.00	0.00	0.00
MgO	0.00	0.00	0.00	0.03	0.00	0.00	0.00	0.00
CaO	8.53	9.25	8.95	10.06	7.94	8.00	7.89	8.62
Na_2O	6.74	6.08	6.08	5.80	6.92	6.85	6.97	6.58
K_2O	0.23	0.37	0.39	0.21	0.29	0.33	0.26	0.18
Total	100.54	100.94	100.41	100.21	99.94	99.29	100.05	99.87
8 (O)								
Si	2.604	2.580	2.564	2.530	2.633	2.633	2.632	2.611
Al	1.386	1.416	1.444	1.457	1.359	1.355	1.361	1.381
Ti	0.000	0.000	0.000	0.001	0.000	0.000	0.000	0.000
Fe^{3+}	0.000	0.000	0.000	0.000	0.000	0.000	0.000	0.000
Fe^{2+}	0.007	0.005	0.003	0.007	0.006	0.006	0.006	0.002
Mn	0.001	0.000	0.000	0.001	0.000	0.000	0.000	0.000
Mg	0.000	0.000	0.000	0.002	0.000	0.000	0.000	0.000
Ca	0.407	0.440	0.428	0.484	0.380	0.386	0.378	0.414
Na	0.582	0.523	0.526	0.504	0.600	0.598	0.603	0.571
K	0.013	0.021	0.022	0.012	0.017	0.019	0.015	0.010
Total	5.001	4.984	4.987	4.998	4.995	4.998	4.996	4.989
An	0.41	0.45	0.44	0.48	0.38	0.38	0.38	0.42
Ab	0.58	0.53	0.54	0.50	0.60	0.60	0.61	0.57
Or	0.01	0.02	0.02	0.01	0.02	0.02	0.01	0.01

Table 4.2 (cont.).

Rock unit	Hornblende granite							
Analysis no.	2WK3_50	2WK3_51	2WK4_59	2WK4_60	2WK4_61	2WK4_62	2WK4_64	2WK4_65
Remark	Pl-Core	Pl-Rim	Pl-Core	Pl-Rim	Pl-Core	Pl-Rim	Pl-Rim	Pl-Core
SiO_2	58.64	58.18	57.53	58.17	57.98	58.20	58.91	56.41
Al_2O_3	26.01	26.36	27.60	26.80	26.61	26.78	26.16	27.86
TiO_2	0.00	0.00	0.01	0.00	0.00	0.00	0.00	0.01
FeO^*	0.09	0.09	0.17	0.11	0.22	0.06	0.11	0.15
MnO	0.00	0.04	0.00	0.00	0.00	0.01	0.00	0.00
MgO	0.00	0.00	0.00	0.01	0.00	0.00	0.00	0.00
CaO	8.24	8.58	9.36	8.97	8.57	8.85	8.08	10.12
Na_2O	6.80	6.71	6.05	6.42	6.56	6.47	6.87	5.65
K_2O	0.25	0.18	0.18	0.14	0.26	0.16	0.17	0.22
Total	100.03	100.14	100.90	100.63	100.19	100.56	100.32	100.41
8 (O)								
Si	2.622	2.602	2.557	2.589	2.593	2.591	2.624	2.526
Al	1.370	1.389	1.445	1.405	1.402	1.405	1.373	1.470
Ti	0.000	0.000	0.000	0.000	0.000	0.000	0.000	0.000
Fe^{3+}	0.000	0.000	0.000	0.000	0.000	0.000	0.000	0.000
Fe^{2+}	0.003	0.003	0.006	0.004	0.008	0.002	0.004	0.006
Mn	0.000	0.001	0.000	0.000	0.000	0.000	0.000	0.000
Mg	0.000	0.000	0.000	0.001	0.000	0.000	0.000	0.000
Ca	0.394	0.411	0.446	0.427	0.410	0.422	0.385	0.485
Na	0.589	0.581	0.521	0.553	0.568	0.558	0.593	0.490
K	0.014	0.010	0.010	0.008	0.015	0.009	0.010	0.012
Total	4.994	4.999	4.986	4.988	4.997	4.989	4.990	4.990
An	0.40	0.41	0.46	0.43	0.41	0.43	0.39	0.49
Ab	0.59	0.58	0.53	0.56	0.57	0.56	0.60	0.50
Or	0.01	0.01	0.01	0.01	0.01	0.01	0.01	0.01

Table 4.2 (cont.).

Rock unit	Hornblende granite							
Analysis no.	2WK11_79	2WK11_80	2WK11_81	2WK11_82	2WK11_85	2WK11_86	2WK11_87	2WK11_89
Remark	Pl-Core	Pl-Rim	Pl-Core	Pl-Rim	Pl-Rim	Pl-Core	Pl-Rim	Pl-Core
SiO_2	58.68	63.04	59.36	63.74	61.93	62.42	63.39	59.89
Al_2O_3	25.12	22.98	24.67	21.67	23.06	22.67	22.11	24.44
TiO_2	0.00	0.00	0.01	0.00	0.05	0.00	0.00	0.00
FeO^*	0.15	0.14	0.13	0.15	0.11	0.15	0.06	0.12
MnO	0.00	0.03	0.00	0.01	0.02	0.00	0.00	0.02
MgO	0.00	0.01	0.00	0.00	0.01	0.00	0.00	0.00
CaO	7.44	4.54	6.55	3.48	4.61	4.42	3.76	6.48
Na_2O	7.04	8.84	7.33	9.37	8.78	8.67	9.40	7.40
K_2O	0.29	0.14	0.37	0.20	0.31	0.32	0.11	0.34
Total	98.72	99.74	98.42	98.62	98.89	98.66	98.83	98.71
8 (O)								
Si	2.654	2.796	2.686	2.851	2.776	2.799	2.831	2.700
Al	1.339	1.201	1.315	1.142	1.218	1.198	1.163	1.298
Ti	0.000	0.000	0.000	0.000	0.002	0.000	0.000	0.000
Fe^{3+}	0.000	0.000	0.000	0.000	0.000	0.000	0.000	0.000
Fe^{2+}	0.005	0.005	0.005	0.006	0.004	0.005	0.002	0.004
Mn	0.000	0.001	0.000	0.000	0.001	0.000	0.000	0.001
Mg	0.000	0.001	0.000	0.000	0.001	0.000	0.000	0.000
Ca	0.360	0.216	0.318	0.167	0.221	0.212	0.180	0.313
Na	0.617	0.759	0.643	0.812	0.763	0.753	0.813	0.647
K	0.017	0.008	0.021	0.011	0.018	0.018	0.006	0.019
Total	4.993	4.987	4.988	4.989	5.003	4.987	4.996	4.983
An	0.36	0.22	0.32	0.17	0.22	0.22	0.18	0.32
Ab	0.62	0.77	0.65	0.82	0.76	0.77	0.81	0.66
Or	0.02	0.01	0.02	0.01	0.02	0.02	0.01	0.02

Table 4.2 (cont.).

Rock unit	Biotite-hornblende granite							
Analysis no.	2WK11_92	2WK11_93	2WK11_94	2WK11_95	2WK11_97	2WK11_98	2WK11_99	2WK11_100
Remark	Pl-Core	Pl-Rim	Pl-Core	Pl-Rim	Pl-Core	Pl-Rim	Pl-Core	Pl-Rim
SiO_2	60.61	62.09	63.82	64.47	60.54	60.55	59.54	59.43
Al_2O_3	24.71	23.03	20.05	22.00	24.64	24.15	24.91	25.81
TiO_2	0.00	0.00	0.00	0.00	0.00	0.00	0.00	0.00
FeO^*	0.19	0.24	0.06	0.18	0.12	0.15	0.12	0.17
MnO	0.00	0.00	0.00	0.00	0.00	0.01	0.00	0.01
MgO	0.05	0.15	0.02	0.00	0.01	0.02	0.00	0.00
CaO	6.23	3.07	1.37	3.39	6.42	6.39	6.98	7.55
Na_2O	7.67	8.34	5.55	9.54	7.34	7.62	7.36	7.25
K_2O	0.38	1.14	7.77	0.14	0.73	0.17	0.22	0.18
Total	99.85	98.05	98.63	99.74	99.79	99.06	99.17	100.42
8 (O)								
Si	2.702	2.800	2.918	2.850	2.703	2.717	2.676	2.643
Al	1.298	1.224	1.080	1.146	1.296	1.277	1.319	1.353
Ti	0.000	0.000	0.000	0.000	0.000	0.000	0.000	0.000
Fe^{3+}	0.000	0.000	0.000	0.000	0.000	0.000	0.000	0.000
Fe^{2+}	0.007	0.009	0.002	0.007	0.004	0.006	0.005	0.006
Mn	0.000	0.000	0.000	0.000	0.000	0.000	0.000	0.000
Mg	0.003	0.010	0.001	0.000	0.001	0.001	0.000	0.000
Ca	0.298	0.148	0.067	0.161	0.307	0.307	0.336	0.359
Na	0.663	0.729	0.492	0.817	0.635	0.663	0.641	0.625
K	0.021	0.065	0.453	0.008	0.042	0.010	0.012	0.010
Total	4.991	4.985	5.014	4.989	4.987	4.981	4.990	4.998
An	0.30	0.16	0.07	0.16	0.31	0.31	0.34	0.36
Ab	0.68	0.77	0.49	0.83	0.65	0.68	0.65	0.63
Or	0.02	0.07	0.45	0.01	0.04	0.01	0.01	0.01

Table 4.2 (cont.).

Rock unit	Biotite-hornblende granite							
Analysis no.	2WK13_102	2WK13_103	2WK13_104	2WK13_105	2WK13_107	2WK13_109	2WK13_110	2WK13_119
Remark	Pl-Core	Pl-Rim	Pl-Core	Pl-Rim	Pl-Core	Pl-Core	Pl-Rim	Pl-Rim
SiO_2	61.25	65.87	60.61	64.19	60.47	60.05	61.66	62.64
Al_2O_3	24.20	21.03	25.21	21.98	24.50	25.01	23.52	22.78
TiO_2	0.00	0.00	0.01	0.00	0.00	0.01	0.00	0.00
FeO*	0.14	0.14	0.18	0.13	0.24	0.15	0.13	0.11
MnO	0.02	0.01	0.00	0.00	0.00	0.00	0.00	0.00
MgO	0.00	0.00	0.01	0.02	0.15	0.00	0.01	0.00
CaO	5.86	2.36	6.80	3.26	4.42	6.90	5.27	4.55
Na_2O	7.88	10.19	7.55	9.77	7.42	7.60	8.14	8.71
K_2O	0.34	0.12	0.25	0.14	1.41	0.25	0.32	0.20
Total	99.72	99.72	100.62	99.53	98.61	99.97	99.06	99.02
8 (O)								
Si	2.729	2.903	2.683	2.846	2.726	2.678	2.759	2.798
Al	1.271	1.092	1.315	1.148	1.301	1.315	1.240	1.199
Ti	0.000	0.000	0.000	0.000	0.000	0.000	0.000	0.000
Fe^{3+}	0.000	0.000	0.000	0.000	0.000	0.000	0.000	0.000
Fe^{2+}	0.005	0.005	0.007	0.005	0.009	0.006	0.005	0.004
Mn	0.001	0.000	0.000	0.000	0.000	0.000	0.000	0.000
Mg	0.000	0.000	0.000	0.001	0.010	0.000	0.001	0.000
Ca	0.280	0.111	0.322	0.155	0.213	0.330	0.253	0.218
Na	0.680	0.871	0.648	0.839	0.648	0.657	0.706	0.754
K	0.019	0.007	0.014	0.008	0.081	0.014	0.018	0.011
Total	4.986	4.989	4.990	5.003	4.988	5.000	4.983	4.985
An	0.29	0.11	0.33	0.15	0.23	0.33	0.26	0.22
Ab	0.69	0.88	0.66	0.84	0.69	0.66	0.72	0.77
Or	0.02	0.01	0.01	0.01	0.09	0.01	0.02	0.01

Table 4.2 (cont.).

Rock unit	Biotite-hornblende granite							
Analysis no.	2WK15_120	2WK15_121	2WK15_122	2WK15_123	2WK15_124	2WK15_125	2WK15_127	2WK15_128
Remark	Pl-Core	Pl-Rim	Pl-Core	Pl-Rim	Pl-Core	Pl-Rim	Pl-Core	Pl-Rim
SiO_2	63.52	62.42	61.75	64.51	62.68	63.84	60.40	60.93
Al_2O_3	23.11	23.39	23.54	22.33	22.63	21.37	24.83	23.88
TiO_2	0.04	0.02	0.00	0.00	0.05	0.03	0.00	0.00
FeO^*	0.12	0.14	0.14	0.10	0.22	0.08	0.08	0.14
MnO	0.00	0.00	0.00	0.00	0.04	0.00	0.00	0.00
MgO	0.00	0.02	0.03	0.00	0.01	0.00	0.00	0.00
CaO	4.42	4.95	5.23	3.74	4.37	2.82	6.38	5.79
Na_2O	8.95	8.64	8.24	9.08	8.95	10.04	7.51	7.75
K_2O	0.28	0.20	0.21	0.23	0.18	0.11	0.38	0.38
Total	100.43	99.79	99.14	100.00	99.12	98.28	99.58	98.87
8 (O)								
Si	2.798	2.772	2.760	2.843	2.799	2.863	2.698	2.736
Al	1.200	1.224	1.240	1.160	1.191	1.129	1.307	1.264
Ti	0.001	0.001	0.000	0.000	0.002	0.001	0.000	0.000
Fe^{3+}	0.000	0.000	0.000	0.000	0.000	0.000	0.000	0.000
Fe^{2+}	0.004	0.005	0.005	0.004	0.008	0.003	0.003	0.005
Mn	0.000	0.000	0.000	0.000	0.002	0.000	0.000	0.000
Mg	0.000	0.001	0.002	0.000	0.000	0.000	0.000	0.000
Ca	0.209	0.235	0.250	0.177	0.209	0.136	0.305	0.278
Na	0.764	0.743	0.714	0.775	0.774	0.873	0.650	0.675
K	0.016	0.011	0.012	0.013	0.010	0.006	0.022	0.022
Total	4.991	4.993	4.983	4.971	4.996	5.011	4.984	4.980
An	0.21	0.24	0.26	0.18	0.21	0.13	0.31	0.29
Ab	0.77	0.75	0.73	0.80	0.78	0.86	0.67	0.69
Or	0.02	0.01	0.01	0.01	0.01	0.01	0.02	0.02

Table 4.3 Representative EPMA analyses of biotite in granitic rocks from the Wang Nam Khiao, Nakhon Ratchasima, Thailand.

Rock unit	Biotite granite					Hornblende granite				
Analysis no.	2WK10_46	2WK14_85	2WK14_86	2WK14_87	2WK14_88	2WK2_17	2WK2_23	2WK2_24	2WK4_37	2WK4_38
Remark	Bi	Bi	Bi	Bi	Bi	Bi	Bi	Bi	Bi	Bi
SiO_2	36.76	36.92	36.95	35.88	37.04	31.76	33.66	32.51	35.91	35.46
Al_2O_3	16.79	18.51	18.14	17.82	17.47	16.21	15.72	15.41	14.83	15.81
TiO_2	1.31	0.73	2.35	1.52	2.75	2.17	2.64	3.82	3.36	2.75
FeO^*	16.43	17.25	15.35	17.92	16.41	22.81	21.89	21.95	17.31	17.57
MnO	0.41	0.54	0.52	0.50	0.57	0.69	0.66	0.67	0.43	0.56
MgO	12.63	8.49	8.77	10.02	9.86	12.05	10.84	11.08	11.65	12.91
CaO	0.44	0.16	0.37	0.17	0.35	0.10	0.13	0.97	0.13	0.14
Na_2O	0.10	0.05	0.03	0.03	0.02	0.04	0.05	0.06	0.10	0.05
K_2O	3.95	4.34	4.21	4.38	4.87	3.98	6.32	4.73	8.85	7.21
Total	88.82	86.99	86.69	88.24	89.34	89.81	91.91	91.21	92.57	92.50
8 (O)										
Si	2.604	2.672	2.659	2.584	2.618	2.340	2.434	2.364	2.544	2.493
Al	1.402	1.579	1.538	1.512	1.455	1.407	1.339	1.320	1.238	1.310
Ti	0.070	0.040	0.127	0.082	0.146	0.120	0.143	0.209	0.179	0.145
Fe^{3+}	0.000	0.000	0.000	0.000	0.000	0.253	0.227	0.316	0.218	0.197
Fe^{2+}	0.973	1.044	0.924	1.079	0.970	1.153	1.097	1.018	0.807	0.836
Mn	0.025	0.033	0.032	0.030	0.034	0.043	0.040	0.041	0.026	0.033
Mg	1.333	0.915	0.940	1.075	1.038	1.323	1.168	1.200	1.229	1.352
Ca	0.033	0.012	0.029	0.013	0.026	0.008	0.010	0.076	0.010	0.011
Na	0.014	0.007	0.004	0.004	0.003	0.006	0.007	0.008	0.014	0.007
K	0.357	0.401	0.386	0.402	0.439	0.374	0.583	0.439	0.800	0.646
Total	6.810	6.703	6.640	6.781	6.729	7.026	7.048	6.991	7.065	7.032
Mg/(Fe+Mg)	0.58	0.47	0.50	0.50	0.52	0.48	0.47	0.47	0.55	0.57

Table 4.3 (cont.).

Rock unit	Biotite-hornblende granite									
Analysis no.	2WK11_56	2WK11_57	2WK11_62	2WK11_63	2WK13_72	2WK13_73	2WK13_74	2WK13_79	2WK13_80	2WK15_93
Remark	Bi	Bi	Bi	Bi	Bi	Bi	Bi	Bi	Bi	Bi
SiO_2	36.64	36.39	37.47	37.18	36.54	36.22	37.31	37.21	36.59	34.22
Al_2O_3	13.71	13.79	13.75	14.13	13.89	13.75	13.79	14.21	14.07	14.21
TiO_2	3.45	3.34	3.46	3.02	3.37	3.25	3.42	3.78	3.17	2.75
FeO^*	15.70	15.81	15.85	15.70	16.59	16.96	16.43	15.68	16.65	16.84
MnO	0.25	0.28	0.28	0.29	0.21	0.28	0.26	0.25	0.25	0.28
MgO	13.40	13.79	13.45	14.16	13.75	13.70	13.39	13.01	14.29	15.72
CaO	0.04	0.06	0.03	0.04	0.05	0.03	0.01	0.00	0.05	0.27
Na_2O	0.08	0.08	0.10	0.08	0.08	0.09	0.08	0.09	0.07	0.04
K_2O	9.08	9.02	9.39	8.66	8.91	8.45	9.35	9.43	8.11	5.88
Total	92.44	92.64	94.03	93.46	93.46	92.83	94.09	93.78	93.38	90.32
8 (O)										
Si	2.580	2.560	2.595	2.578	2.553	2.549	2.588	2.581	2.547	2.451
Al	1.138	1.143	1.122	1.155	1.144	1.140	1.127	1.161	1.154	1.199
Ti	0.183	0.177	0.180	0.157	0.177	0.172	0.178	0.197	0.166	0.148
Fe^{3+}	0.282	0.297	0.283	0.267	0.303	0.310	0.284	0.257	0.299	0.350
Fe^{2+}	0.642	0.633	0.635	0.643	0.666	0.688	0.669	0.652	0.669	0.658
Mn	0.015	0.017	0.016	0.017	0.012	0.017	0.015	0.015	0.015	0.017
Mg	1.406	1.445	1.388	1.463	1.431	1.436	1.384	1.344	1.482	1.677
Ca	0.003	0.005	0.002	0.003	0.004	0.002	0.001	0.000	0.004	0.021
Na	0.011	0.011	0.013	0.011	0.011	0.012	0.011	0.012	0.009	0.006
K	0.815	0.809	0.829	0.766	0.794	0.758	0.827	0.834	0.720	0.537
Total	7.079	7.100	7.078	7.070	7.099	7.091	7.087	7.061	7.072	7.070
Mg/(Fe+Mg)	0.60	0.61	0.60	0.62	0.60	0.59	0.59	0.60	0.60	0.62

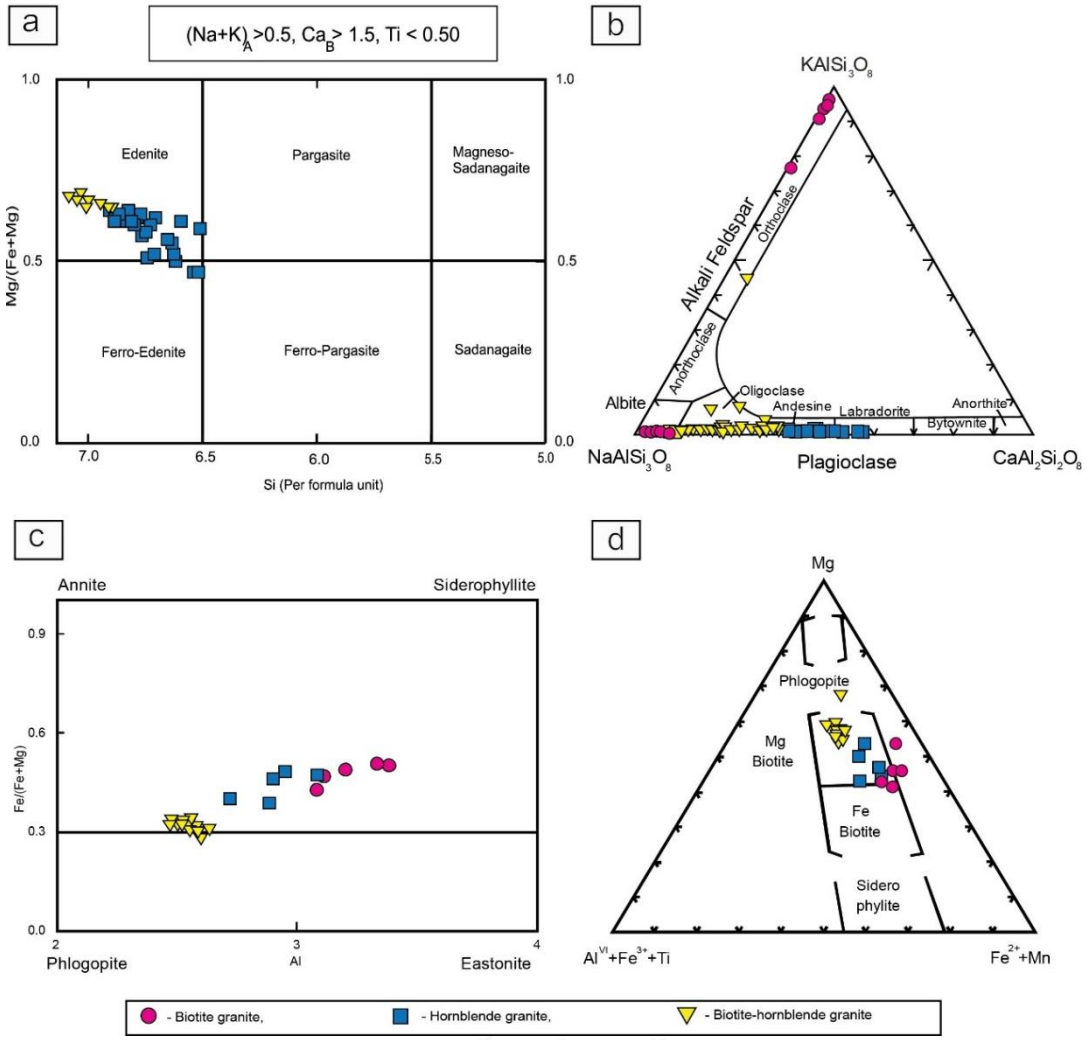

Figure 4.4 Plots of mineral chemistry (a) calcic-amphibole (Leake et al., 1997), (b) plagioclase (Smith and Brown, 1974), and (c) biotite (Morimoto et al., 1988), and (d) biotite classification (Foster, 1960) of the granitic rocks from the Wang Nam Khiao area, Nakhon Ratchasima.

4.4 Whole-rock geochemistry

The whole-rock geochemistries, major, minor, and trace compositions, of the biotite granite, hornblende granite, and biotite-hornblende granite from the Wang Nam Khiao area, Nakhon Ratchasima, Thailand were analyzed and studied (Table 4.4).

The biotite granites reveal the major and minor compositions between 72.12-74.51 % SiO_2, 0.10-0.21 % TiO_2, 12.66-14.86 % Al_2O_3, 1.14-1.75 % FeO_{total}, 0.32-0.83 % MgO, 0.48-0.91 % CaO, 3.04-5.23 % Na_2O, 2.04-4.48 % K_2O, 0.89-1.18 % LOI, with trace and rare earth elements in ppm between 1.64-5.81 Li, 1.26-2.13 Be, 2.61-19.95 V, 15.59-25.56 Cr, 2.53-4.94 Sc, 2.92-7.37 Ni, 2.58-32.16 Cu, 127.26-558.53 Mn, 0.98-1.63 As, 51.72-110.49 Co, 20.21-34.78 Zn, 12.03-16.30 Ga, 78.19-161.63 Rb, 109.89-198.77 Sr, 14.35-25.96 Y, 96.41-110.51 Zr, 0.87-3.49 Sn, 0.15-0.28 Sb, 0.50-1.11 Cs, 266.57-930.63 Ba, 22.15-46.48 La, 37.36-80.35 Ce, 3.76-7.47 Pr, 14.42-26.77 Nd, 2.73-4.93 Sm, 2.17-3.90 Gd, 0.36-0.65 Tb, 2.00-3.55 Dy, 0.31-0.56 Ho, 1.14-2.07 Er, 0.17-0.35 Tm, 1.01-2.39 Yb, 0.17-0.40 Lu, 3.97-25.56 Nb, 1.55-9.57 Ta, 7.50-13.07 Pb, 0.02-0.10 Bi, 9.65-27.85 Th, 3.17-6.68 U, 1.04-2.53 Mo, 0.50-0.97 Eu, 1.81-3.97 Hf, 0.01-0.02 Re.

The hornblende granites show the major and minor compositions between 54.74-73.04 % SiO_2, 0.19-0.95 % TiO_2, 11.17-16.38 % Al_2O_3, 1.73-8.78 % FeO_{total}, 0.69-10.89 % MgO, 1.54-8.59 % CaO, 2.86-4.34 % Na_2O, 2.86-4.36 % K_2O, 0.81-1.25 % LOI, with trace and rare earth elements in ppm between 5.24-9.82 Li, 0.73-1.36 Be, 8.81-193.62 V, 7.02-515.72 Cr, 3.51-25.17 Sc, 2.64-191.24 Ni, 1.95-100.16 Cu, 426.84-1556.72 Mn, 0.96-3.88 As, 35.73-64.98 Co, 23.84-69.00 Zn, 11.89-18.78 Ga, 16.10-57.35 Rb, 169.41-1048.50 Sr, 9.16-27.86 Y, 87.17-102.19 Zr, 0.67-4.05 Sn, 0.12-0.41 Sb, 0.18-0.73 Cs, 55.97-852.40 Ba, 9.96-60.39 La, 18.88-51.16 Ce, 2.33-5.73 Pr, 9.78-22.61 Nd, 1.94-5.10 Sm, 1.49-3.95 Gd, 0.24-0.72 Tb, 1.28-3.99 Dy, 0.20-0.63 Ho, 0.69-2.21 Er, 0.11-0.38 Tm, 0.76-2.48 Yb, 0.13-0.41 Lu, 3.22-13.58 Nb, 1.35-8.09 Ta, 2.57-10.02 Pb, 0.02-0.05 Bi, 1.06-5.87 Th, 0.51-1.67 U, 0.42-1.70 Mo, 0.64-1.69 Eu, 0.48-1.98 Hf, 0.00-0.01 Re.

The biotite-hornblende granites present the major and minor compositions between 62.52-68.87 % SiO_2, 0.27-0.50 % TiO_2, 14.34-15.66 % Al_2O_3, 2.14-5.03 % FeO_{total}, 1.60-5.55 % MgO, 0.93-5.18 % CaO, 3.44-4.17 % Na_2O, 1.62-4.56 % K_2O,

0.99-1.35 % LOI, with trace and rare earth elements in ppm between 5.33-12.71 Li, 1.14-2.55 Be, 20.39-113.34 V, 16.56-157.68 Cr, 6.03-12.84 Sc, 6.77-58.04 Ni, 2.64-9.14 Cu, 313.82-712.48 Mn, 1.02-1.69 As, 50.41-65.29 Co, 33.26-63.40 Zn, 18.42-20.06 Ga, 41.06-158.66 Rb, 172.14-1091.22 Sr, 10.63-11.56 Y, 87.65-115.29 Zr, 0.84-4.01 Sn, 0.13-0.28 Sb, 0.59-0.78 Cs, 275.43-312.41 Ba, 13.01-44.69 La, 26.63-93.28 Ce, 3.03-8.05 Pr, 13.36-28.47 Nd, 2.68-5.00 Sm, 1.90-3.82 Gd, 0.30-0.48 Tb, 1.54-1.93 Dy, 0.23-0.26 Ho, 0.78-0.93 Er, 0.12-0.15 Tm, 0.80-1.07 Yb, 0.13-0.19 Lu, 3.10-12.33 Nb, 0.95-6.01 Ta, 5.66-17.11 Pb, 0.02-0.05 Bi, 2.24-24.36 Th, 0.83-3.84 U, 0.60-0.76 Mo, 0.84-0.96 Eu, 0.76-4.19 Hf, 0.11 Re.

According to the major and minor compositions of these granitic rocks, they show a range of SiO_2 composition (Table 4.4) from diorite to granite (Fig. 4.5). The biotite granite presents between 72.12 and 74.51 wt% whereas the hornblende and biotite-hornblende granites have lower contents of 58.23 to 73.04 wt% and 62.52 to 68.87 wt%, respectively. In term of Na_2O+K_2O contents, the biotite granite shows higher Na_2O+K_2O contents (7.27-8.21 wt%) than those of the hornblende granite (4.54-7.33 wt%), and biotite-hornblende granite (5.54-7.99 wt%). However, the biotite granite reveals lower CaO contents (0.48-0.91 wt%) than in those of the hornblende granite (1.54-8.59 wt%), and biotite-hornblende granite (0.93-5.18 wt%). In addition, the biotite granite shows low Mg# (MgO/MgO+FeO = 0.21-0.37), TiO_2 (0.10-0.21 wt%), and FeO_t (1.14-1.75 wt%) than those of the hornblende granite (Mg# = 0.28-0.58, TiO_2 = 0.19-0.95 wt%, FeO_t = 1.73-8.78 wt%), and biotite-hornblende granites (Mg# = 0.43-0.53, TiO_2 = 0.27-0.50 wt%, FeO_t = 2.14-5.03 wt%). These whole-rock chemistries corresponese to the main mineral assemblages including plagioclase, hornblende, and biotite. Based on the TAS diagram of Cox et al. (1979), the biotite granites are plotted in the granite field (acid rock) whereas the hornblende granite and biotite-hornblende granite fall within diorite to granite fields (intermediate to acid rocks) (Fig. 4.5). Overall, they seem to have positive correlation between silicon and total alkai contents. Harker variation diagram, plots of SiO_2 against other major and minor compositions of all granitic sample groups, (Fig. 4.6) show negative correlations between SiO_2 and TiO_2, FeO_t, MgO, MnO, CaO (Figs. 4.6a, 4.6c, 4.6d, 4.6e, 4.6f), whereas Na_2O and K_2O reveal positive correlations (Figs. 4.6g, h). Al_2O_3 exhibits scattered distribution (Fig. 4.6b). These are compatible to their mineral assemblages,

particularly K-feldspar, plagioclase, calcic amphibole and biotite. Although, in general, all granitic groups appear to have correlations as reported above, each granitic group reveal some differences in detail. Negative correlations of SiO_2 against TiO_2, FeO, MgO, CaO and positive correlation of SiO_2 against Na_2O and K_2O are observed in hornblende granite and biotite-hornblende granite, whereas those of biotite granite are unclearly correlated. These may indicate that these magmas should not have conformable magmatic process, particularly magma differentiation or partial melting. In addition, FeO, MgO, and CaO compositions seem to be negative correlation among all granitic groups (dashed line), each group still displays individual trend which may introduce that these rocks may be formed different magmatic sources and/or diferent degree of partial melting.

The primitive mantle-normalized (Sun and McDonough, 1989) spider diagram (Fig. 4.7) shows enrichment of large ion lithophile elements (LILE) (e.g. K, Rb, Th, U) and depletion of high field strength elements (HFSE) (e.g. Nb, Ti) in all rock units. The biotite granite shows similar $(La/Yb)_N$ ratio (9.95-33.02) to those hornblende granite (4.36-20.98) and biotite-hornblende granite (11.49-29.85). In term of $(La/Sm)_N$ ratios, the biotite granite reveals high $(La/Sm)_N$ ratios (4.94-8.62) whereas the hornblende granite and biotite-hornblende granites show lower ranges of 1.90-7.65 and 2.98-5.77, respectively. These rocks exhibit slightly high light-REE (LREE) in chondrite-normalized REE pattern similar to typical arc setting, reported by Blein et al. (2001) (Fig. 4.7).

Table 4.4 Representative whole-rock geochemical analyses of the Carboniferous biotite granite, Late Permian hornblende granite, and Triassic biotite-hornblende granite from the Wang Nam Khiao, Nakhon Ratchasima, Thailand (Major and minor oxide in wt%, trace elements and REE in ppm).

Rock type:	Biotite-hornblende granite				Biotite granite							
Sample no:	2WK11	2WK13	2WK15	3WK5	2WK14	3WK6	3WK7	3WK9	3WK10	3WK11	WKG1	2WK10
Major and minor oxide (%)												
SiO_2	63.61	62.52	63.79	68.87	72.15	72.24	72.37	72.84	74.18	72.12	73.23	74.51
TiO_2	0.45	0.50	0.46	0.27	0.14	0.17	0.17	0.17	0.12	0.10	0.21	0.11
Al_2O_3	14.34	14.40	14.77	15.66	14.48	14.86	14.08	14.04	13.64	13.72	12.66	13.84
FeO	4.35	5.03	4.61	2.14	1.29	1.48	1.75	1.47	1.14	1.22	1.29	1.23
MnO	0.00	0.00	0.00	0.00	0.00	0.00	0.00	0.00	0.00	0.00	0.00	0.00
MgO	4.82	5.55	5.02	1.60	0.61	0.83	0.66	0.64	0.32	0.33	0.76	0.44
CaO	4.52	5.18	4.52	0.93	0.84	0.87	0.84	0.91	0.48	0.75	0.71	0.67
Na_2O	4.00	3.93	4.17	3.44	3.81	5.23	3.96	3.85	4.07	3.93	3.04	4.38
K_2O	1.77	1.62	1.65	4.56	4.28	2.04	4.03	4.18	4.07	4.29	4.48	3.60
P_2O_5	0.18	0.20	0.00	0.09	0.00	0.00	0.00	0.00	0.00	0.00	0.00	0.00
LOI	0.99	1.00	1.35	1.00	1.18	1.11	1.06	1.06	1.03	1.11	0.89	1.02
Total	99.01	99.92	100.34	98.54	98.78	98.83	98.94	99.18	99.05	97.56	97.28	99.79
Trace elements and REE (ppm)												
Li	11.73	12.31	12.71	5.33	5.28	3.19	4.21	5.57	4.23	5.81	1.64	2.39
Be	1.21	1.14	1.16	2.55	1.39	2.13	1.65	1.74	1.26	1.70	1.28	1.59
V	96.77	113.34	101.52	20.39	7.10	19.95	8.29	8.74	3.27	2.61	6.28	5.20
Cr	126.20	157.68	141.00	16.56	18.77	16.44	19.77	15.59	25.56	23.34	20.81	22.39
Sc	10.96	12.84	12.01	6.03	2.53	3.18	4.94	3.08	3.25	3.10	2.97	3.26
Ni	47.68	58.04	53.14	6.77	7.37	3.94	3.88	4.70	3.91	2.92	3.38	5.15
Cu	3.14	6.17	2.64	9.14	4.08	3.43	2.58	4.86	2.68	2.64	20.35	32.16
Mn	608.50	712.48	648.89	313.82	363.34	155.73	335.04	558.53	169.02	388.19	127.26	187.77
As	1.07	1.02	1.02	1.69	0.98	1.28	1.63	1.16	1.21	1.22	1.56	1.36
Co	53.49	50.41	65.29	60.54	63.44	79.77	79.86	86.70	110.49	75.89	51.72	108.75
Zn	46.56	63.40	47.37	33.26	34.78	22.87	27.19	34.17	20.21	30.47	27.08	34.52
Ga	19.18	20.06	19.84	18.42	12.87	16.30	15.29	13.57	12.03	14.05	12.99	13.69
Rb	41.28	42.80	41.06	158.66	135.07	78.19	131.94	161.63	145.18	142.44	136.21	102.36
Sr	975.25	1091.22	1049.04	172.14	173.30	185.63	146.82	198.77	109.89	168.02	182.38	170.36
Y	10.63	11.16	11.46	11.56	15.56	16.83	25.96	16.55	14.35	24.55	17.76	14.79
Zr	88.01	88.10	87.65	115.29	97.69	110.51	101.70	101.28	100.65	101.83	96.41	101.52
Sn	0.84	0.89	1.76	4.01	1.13	0.96	2.40	1.26	3.49	0.90	0.87	1.72
Sb	0.14	0.13	0.16	0.28	0.17	0.17	0.28	0.24	0.26	0.15	0.16	0.28
Cs	0.65	0.59	0.70	0.78	0.75	0.59	0.67	1.11	0.94	0.93	0.50	0.69
Ba	275.43	312.41	284.56	301.06	266.57	639.92	378.39	753.34	500.09	930.63	409.61	676.42
La	13.01	13.28	13.76	44.69	24.77	46.48	39.85	28.76	22.17	32.50	28.06	22.15

Table 4.4 (cont.).

Rock type:	Biotite-hornblende granite				Biotite granite							
Sample no:	2WK11	2WK13	2WK15	3WK5	2WK14	3WK6	3WK7	3WK9	3WK10	3WK11	WKG1	2WK10
Trace elements and REE (ppm)												
Ce	26.63	27.44	27.98	93.28	43.38	80.35	74.75	52.60	37.36	50.92	51.50	42.46
Pr	3.03	3.15	3.28	8.05	4.20	7.47	7.07	4.86	3.76	5.51	5.05	4.02
Nd	13.36	14.29	14.82	28.47	15.91	25.34	26.77	18.16	14.42	21.53	19.37	15.29
Sm	2.68	2.86	2.98	5.00	2.80	3.48	4.93	3.13	2.73	4.06	3.46	2.89
Gd	1.90	2.03	2.11	3.82	2.25	2.57	3.90	2.50	2.17	3.32	2.73	2.24
Tb	0.30	0.32	0.34	0.48	0.38	0.36	0.65	0.41	0.37	0.58	0.44	0.39
Dy	1.54	1.63	1.71	1.93	2.07	2.00	3.55	2.19	2.02	3.19	2.37	2.16
Ho	0.23	0.23	0.25	0.26	0.32	0.33	0.56	0.34	0.31	0.49	0.37	0.33
Er	0.78	0.80	0.85	0.93	1.20	1.26	2.07	1.27	1.14	1.78	1.37	1.27
Tm	0.12	0.13	0.13	0.15	0.21	0.17	0.35	0.22	0.20	0.30	0.23	0.23
Yb	0.80	0.83	0.85	1.07	1.44	1.01	2.39	1.56	1.36	2.00	1.57	1.60
Lu	0.13	0.13	0.13	0.19	0.24	0.17	0.40	0.27	0.23	0.33	0.26	0.27
Nb	8.41	5.60	3.10	12.33	12.67	25.56	3.97	9.99	5.77	10.06	12.18	6.20
Ta	5.84	0.95	6.01	4.59	3.15	5.28	1.55	9.57	8.32	7.65	2.10	9.57
Pb	7.00	5.66	6.67	17.11	11.55	7.50	12.71	12.44	13.07	12.11	11.22	8.80
Bi	0.02	0.02	0.02	0.05	0.06	0.04	0.03	0.10	0.02	0.05	0.03	0.07
Th	2.64	2.24	2.99	24.36	10.19	27.85	17.13	10.56	11.40	11.10	9.65	13.49
U	1.09	0.83	0.98	3.84	3.31	6.68	3.79	4.10	3.17	3.62	3.35	3.82
Mo	0.64	0.60	0.69	0.76	1.15	1.05	1.12	1.17	1.33	1.04	1.42	2.53
Eu	0.84	0.90	0.94	0.96	0.50	0.97	0.85	0.55	0.51	0.70	0.51	0.56
Hf	0.80	0.76	0.78	4.19	2.04	3.97	2.91	2.36	2.42	2.62	1.81	2.61
Re	0.01	0.01	0.01	0.01	0.02	0.02	0.01	0.02	0.02	0.02	0.01	0.02

Table 4.4 (cont.).

Rock type:	Hornblende granite										
Sample no:	3WK20	3WK23	3WK24	3WK26	3WK27	2WK4	3WK21	3WK18	3WK22	2WK2	3WK25
Major and minor oxide (%)											
SiO_2	68.37	58.23	59.17	60.27	73.04	54.74	57.03	66.74	57.80	58.59	58.69
TiO_2	0.40	0.95	0.60	0.56	0.19	0.64	0.87	0.33	0.85	0.69	0.59
Al_2O_3	14.24	14.23	16.25	16.38	13.87	16.25	11.17	14.94	14.57	15.46	15.27
FeO	3.55	8.37	7.12	6.12	1.73	7.71	7.83	3.69	8.78	8.02	6.64
MnO	0.00	0.14	0.17	0.16	0.00	0.16	0.11	0.12	0.15	0.20	0.17
MgO	1.92	4.88	3.31	2.99	0.69	5.20	10.89	1.75	5.11	3.84	4.54
CaO	2.38	6.97	7.35	7.17	1.54	8.59	6.15	3.58	7.18	7.30	7.98
Na_2O	3.71	2.86	4.08	4.01	4.36	3.65	2.92	4.33	2.93	2.98	3.51
K_2O	3.34	1.74	1.15	1.19	2.97	0.98	1.66	1.51	1.61	2.02	1.07
P_2O_5	0.12	0.30	0.28	0.24	0.00	0.29	0.26	0.21	0.24	0.35	0.27
LOI	0.81	1.11	1.02	1.25	1.03	1.17	1.25	1.08	1.05	1.08	1.03
Total	98.83	99.79	100.50	100.33	99.42	99.38	100.14	98.27	100.28	100.54	99.77
Trace elements and REE (ppm)											
Li	6.95	8.09	6.97	7.14	5.84	7.96	9.82	7.20	9.02	6.83	5.24
Be	1.34	1.06	0.79	0.80	1.36	0.73	0.83	1.04	0.89	0.87	0.73
V	41.82	193.62	147.42	138.05	8.81	192.45	185.89	18.34	185.59	149.72	167.36
Cr	24.41	47.72	25.03	22.92	49.04	26.70	515.72	9.49	20.26	7.02	23.52
Sc	8.08	25.17	10.39	9.80	3.51	14.08	20.81	4.10	22.34	10.72	12.28
Ni	4.04	23.25	11.78	11.85	4.80	12.19	191.24	3.51	43.73	2.64	11.95
Cu	5.63	100.16	5.58	10.62	2.59	16.35	72.14	1.95	41.82	4.46	18.55
Mn	520.44	1087.87	1182.21	1134.89	426.84	1178.31	831.62	733.80	1260.54	1556.72	1250.69
As	1.91	2.66	1.31	1.41	0.96	1.00	3.88	1.72	2.33	1.74	1.06
Co	64.20	37.88	49.14	52.20	64.98	53.70	50.49	48.84	42.27	35.73	53.80
Zn	34.06	69.00	66.14	64.38	23.84	66.55	47.94	46.87	68.18	63.93	66.22
Ga	13.16	16.39	17.79	17.81	11.89	18.78	17.75	14.43	17.50	16.91	18.58
Rb	57.35	50.76	19.91	21.49	54.25	17.84	41.65	31.10	50.71	35.57	16.10
Sr	298.43	514.78	901.29	956.26	169.41	996.81	729.08	467.42	566.95	742.06	1048.50
Y	27.16	26.08	9.16	11.85	19.55	9.83	15.54	12.61	22.46	27.86	12.77
Zr	97.13	87.64	88.34	87.70	96.95	88.93	102.19	89.58	87.17	87.96	88.91
Sn	2.67	1.82	1.67	1.22	4.05	0.67	1.07	1.85	1.64	1.03	1.01
Sb	0.23	0.22	0.17	0.15	0.17	0.13	0.41	0.37	0.22	0.16	0.12
Cs	0.73	0.61	0.50	0.49	0.43	0.36	0.18	0.47	0.70	0.57	0.22
Ba	852.40	115.21	55.97	94.90	529.51	165.20	277.58	167.75	221.24	161.00	643.72
La	27.22	60.39	9.96	12.05	24.31	10.11	12.02	19.44	17.05	14.21	12.24

Table 4.4 (cont.).

Rock type:	Hornblende granite										
Sample no:	3WK20	3WK23	3WK24	3WK26	3WK27	2WK4	3WK21	3WK18	3WK22	2WK2	3WK25
Trace elements and REE (ppm)											
La	27.22	60.39	9.96	12.05	24.31	10.11	12.02	19.44	17.05	14.21	12.24
Ce	51.16	42.71	19.07	23.97	46.04	18.88	23.17	38.75	35.21	30.60	23.08
Pr	5.73	5.32	2.33	2.95	4.99	2.33	3.41	4.52	4.34	4.43	2.97
Nd	22.21	22.61	9.78	12.53	18.44	10.02	15.75	18.03	18.82	20.09	12.80
Sm	4.68	5.10	1.94	2.58	3.51	2.08	3.57	3.32	4.26	4.82	2.70
Gd	3.81	3.95	1.49	1.96	2.80	1.60	2.62	2.42	3.31	3.84	2.06
Tb	0.68	0.69	0.24	0.33	0.49	0.27	0.44	0.38	0.58	0.72	0.34
Dy	3.77	3.68	1.28	1.72	2.69	1.41	2.27	1.90	3.12	3.99	1.82
Ho	0.61	0.57	0.20	0.26	0.43	0.22	0.34	0.29	0.48	0.63	0.28
Er	2.21	1.95	0.69	0.90	1.57	0.75	1.10	0.98	1.67	2.17	0.95
Tm	0.38	0.32	0.11	0.15	0.28	0.13	0.17	0.16	0.27	0.36	0.16
Yb	2.48	2.06	0.76	0.96	1.88	0.84	1.01	1.03	1.77	2.34	1.01
Lu	0.41	0.33	0.13	0.16	0.32	0.14	0.16	0.17	0.29	0.38	0.17
Nb	4.21	13.58	5.70	4.86	5.46	5.01	8.96	3.22	10.30	9.28	5.46
Ta	7.24	5.14	1.35	4.69	8.09	2.81	4.32	3.97	3.87	3.26	2.36
Pb	8.34	5.91	2.57	4.75	10.02	4.05	6.24	4.36	5.53	3.25	5.28
Bi	0.04	0.05	0.03	0.03	0.02	0.03	0.04	0.02	0.03	0.04	0.03
Th	5.87	5.08	1.10	1.46	5.75	1.06	1.62	2.24	4.42	2.00	1.29
U	1.67	1.61	0.52	0.60	1.56	0.51	0.58	0.67	1.52	0.96	0.57
Mo	1.70	1.70	0.71	1.05	0.98	0.86	0.42	0.60	1.17	0.87	0.80
Eu	1.19	1.26	0.76	0.98	0.64	0.80	1.13	1.09	1.15	1.69	1.00
Hf	1.53	0.61	0.64	0.57	1.73	0.72	1.98	0.59	0.48	0.67	0.74
Re	0.01	0.00	0.01	0.01	0.01	0.01	0.00	0.01	0.01	0.01	0.01

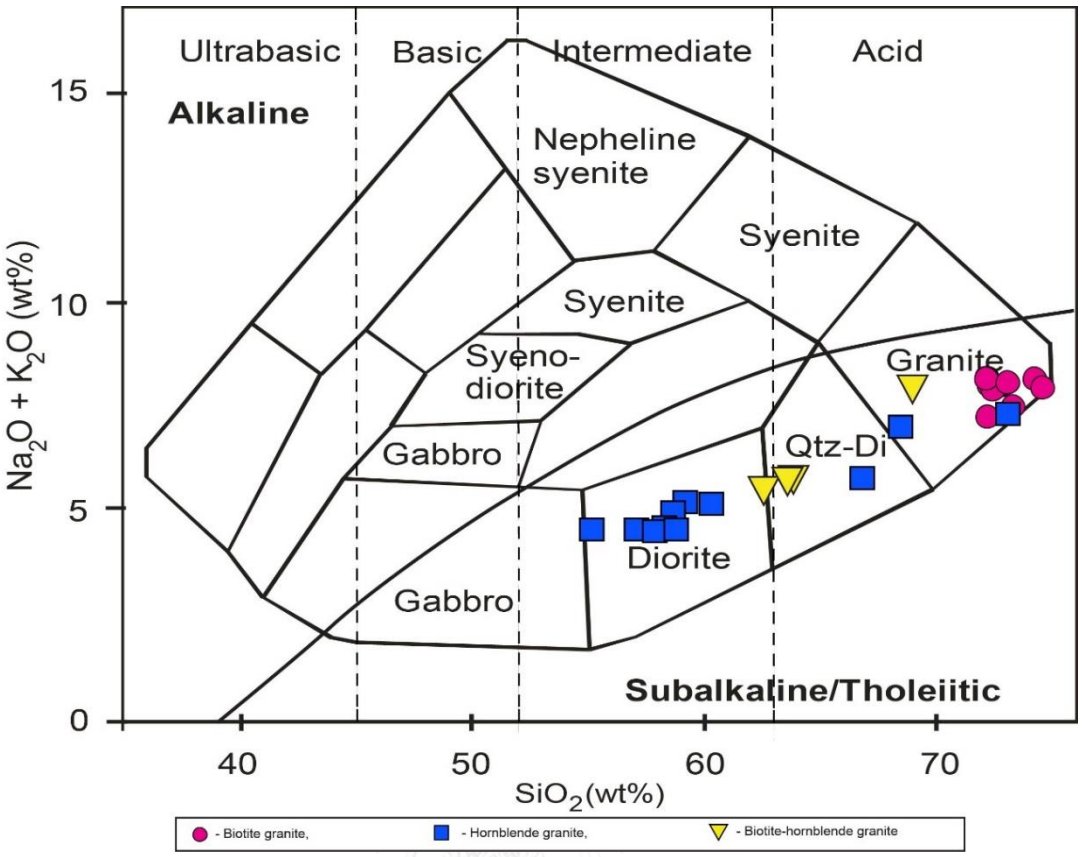

Figure 4.5 Discrimination diagram, SiO_2 and Na_2O+K_2O, showing the classification of plutonic rocks (after Cox et al. (1979)). The biotite granite falls in the granite field whereas the hornblende granite and biotite-hornblende granite range between granite to diorite fields.

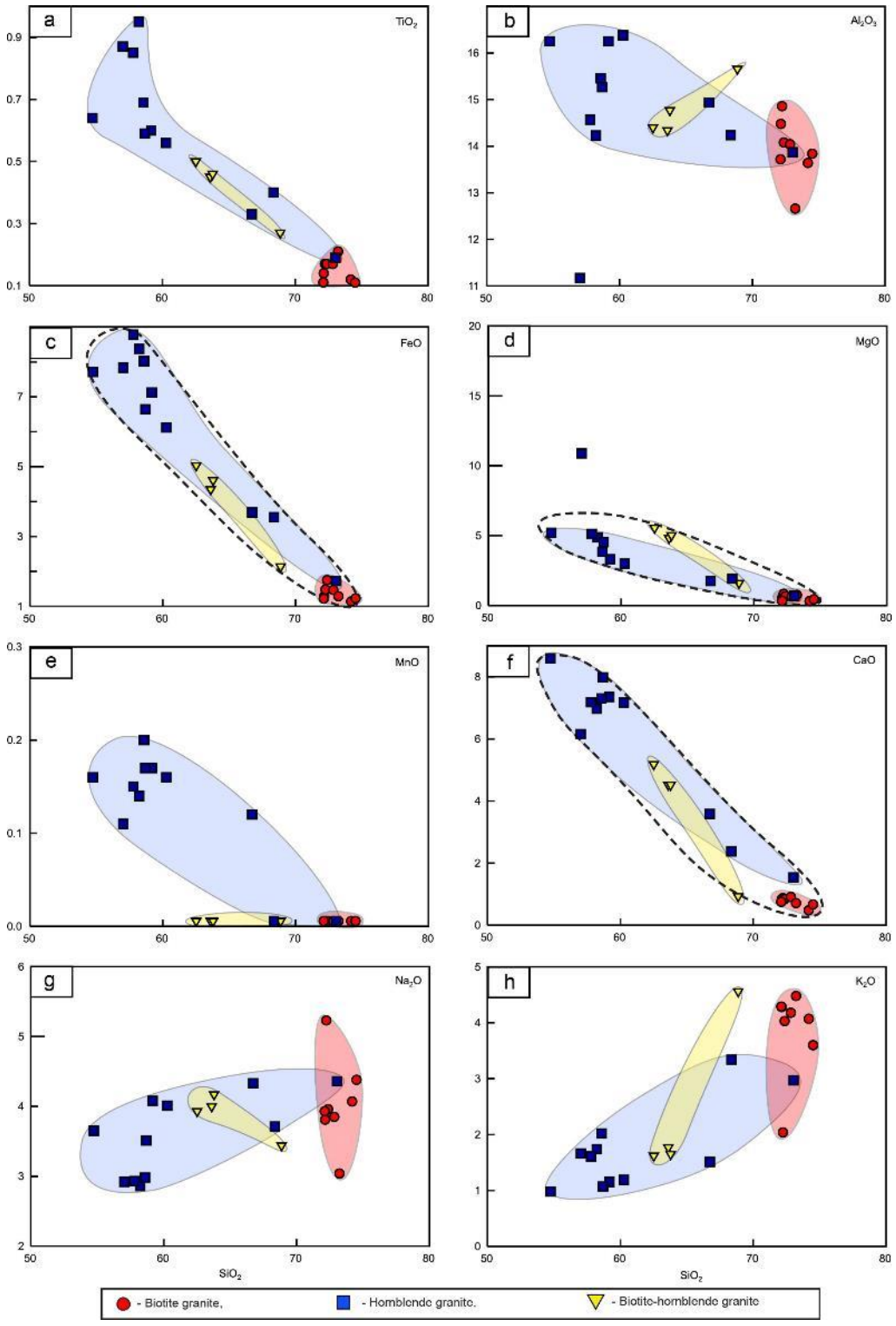

Figure 4.6 Harker variation diagrams (Harker, 1909) plotting between SiO_2 vs. other oxides of granitic rocks from the Wang Nam Khiao area, Nakhon Ratchasima, Thailand.

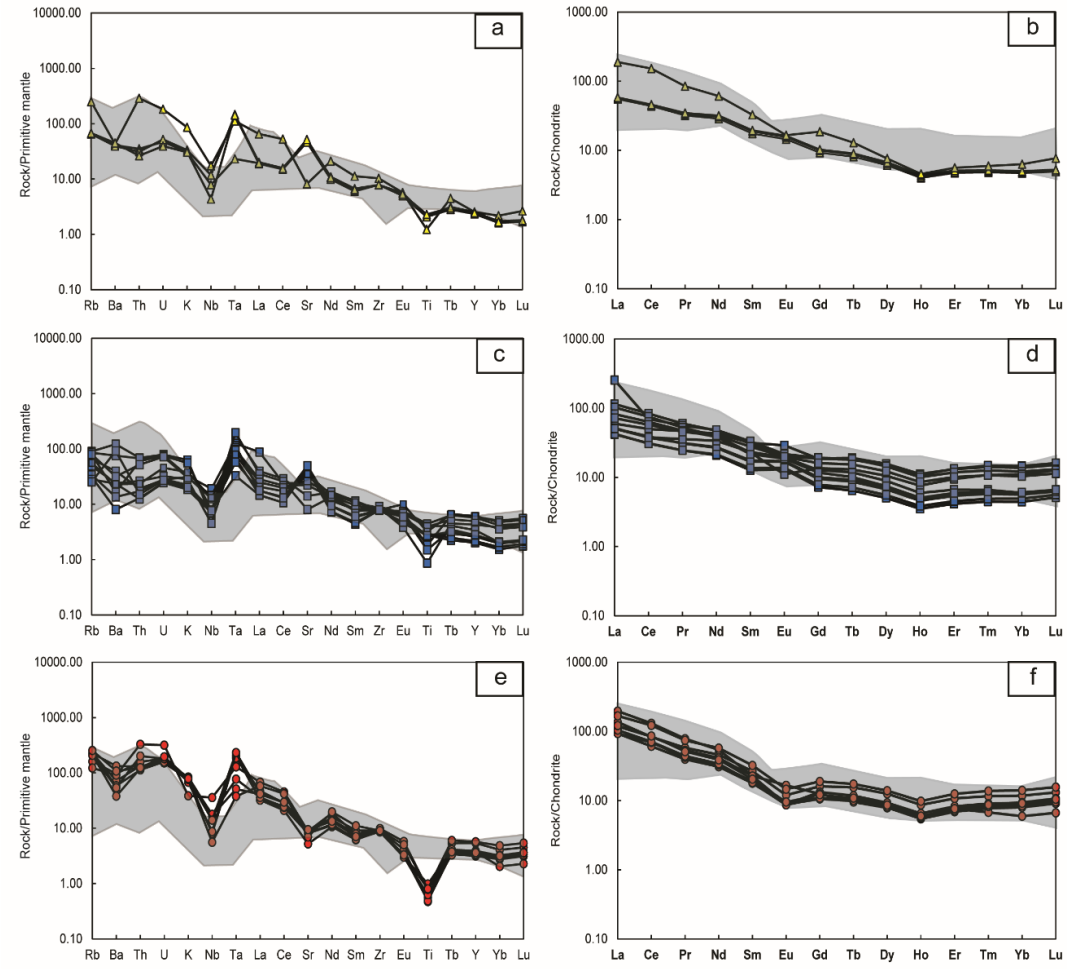

Figure 4.7 (a, c, e) Primitive mantle-normalized spider diagrams (primitive mantle values from Sun and McDonough (1989)) and (b, d, f) chondrite-normalized REE patterns (chondrite values from Sun and McDonough (1989)) of biotite granite, hornblende granite and biotite-hornblende granite, respectively, from the Wang Nam Khiao area, Nakhon Ratchasima, Thailand in comparison with typical arc setting (shade pattern data from Blein et al. (2001)).

4.5 Geothermobarometry

The pressure and temperature (P-T) crystallization conditions of granitic rocks have been carried out by the several geothermobarometers (Blundy and Holland, 1990; Schmidt, 1992; Holland and Blundy, 1994; Anderson and Smith, 1995; Anderson, 1996; Ague, 1997; Stein and Dietl, 2001).

According to plagioclase and hornblende assemblages, the hornblende granite and biotite-hornblende granites were also calculated the P-T condition, using the Al-in hornblende geobarometer and hornblende-plagioclase geothermometer.

The Al-in-hornblende geobarometers have been widely used to calculate pressure of magma crystallization (Hammarstrom and Zen, 1986; Hollister et al., 1987; Johnson and Rutherford, 1989; Rutter et al., 1989; Schmidt, 1992; Anderson and Smith, 1995; Hossain et al., 2009; Fanka et al., 2016). In this study, the calibration equation, P ($\pm$0.6 kbar) = -0.31 + 4.76 Al^{tot} which is experimental calibrated by the total Al in hornblende from H_2O-satrated tonalite of Schmidt (1992) was used to calculate the crystallization of the hornblende granite and biotite-hornblende granite (Table 4.5). The results indicate that the pressures of the hornblende granite (3.0-5.8 kbar) is higher than that of the biotite-hornblende granite (2.0-3.2 kbar).

The coexistence of hornblende and plagioclase has been commonly used as the geothermometer to calculate the crystallization temperature (Blundy and Holland, 1990; Holland and Blundy, 1994). The suggested geothermometer of Holland and Blundy (1994) based on the edenite-tremolite reaction (edenite + 4 quartz = tremolite + albite), which is suitable for quartz-bearing igneous rocks, with reported uncertain calibration of $\pm$ 40 ^{o}C was chosen to estimate the temperature of these granitic rocks (Table 4.5). The calculated temperatures of the hornblende granite range from 700 to 820 ^{o}C while those of the biotite-hornblende granite range from 600 to 750 ^{o}C.

Table 4.5 Geothermobarometry of the granitic rocks in the Wang Nam Khiao area, Nakhon Ratchasima.

Rock type	Hornblende granite						Biotite-hornblende granite					
Sample No.	2WK1-5	2WK1-9	2WK1-12	2WK2-13	2WK2-16	2WK4-35	2WK11-51	2WK11-58	2WK11-59	2WK11-66	2WK15-95	2WK15-96
Mineral Name	Hb	Hb	Hb	Hb	Hb	Hb	Hb	Hb	Hb	Hb	Hb	Hb
No. oxygen	23	23	23	23	23	23	23	23	23	23	23	23
SiO_2	44.90	46.43	44.24	44.22	43.40	47.03	47.02	48.83	47.27	48.46	47.36	47.73
Al_2O_3	9.59	8.31	10.20	9.24	10.24	7.41	7.11	6.80	7.46	6.65	7.46	7.17
TiO_2	1.80	1.29	1.82	1.30	1.14	1.61	0.86	0.72	0.90	0.76	0.94	0.84
Cr_2O_3	0.02	0.04	0.00	0.00	0.00	0.00	0.06	0.02	0.09	0.08	0.07	0.04
FeO_t	14.09	14.23	14.63	17.91	18.77	13.91	13.39	11.77	13.32	12.97	13.38	13.00
MnO	0.34	0.38	0.31	0.96	0.89	0.55	0.41	0.45	0.43	0.47	0.41	0.45
MgO	12.50	12.99	12.06	10.00	9.36	13.30	13.84	15.02	13.84	14.57	13.79	14.11
CaO	11.91	11.80	11.92	11.71	11.66	11.36	11.61	11.49	11.65	11.77	11.25	11.51
Na_2O	1.26	1.18	1.44	1.04	1.01	1.29	1.38	1.43	1.37	1.22	1.54	1.46
K_2O	0.68	0.45	0.73	1.09	1.19	0.55	0.55	0.25	0.44	0.25	0.39	0.34
Total	97.09	97.10	97.35	97.47	97.66	97.01	96.23	96.78	96.77	97.20	96.59	96.65
Formula 23(O)												
Si	6.615	6.806	6.529	6.627	6.510	6.897	6.939	7.071	6.925	7.024	6.941	6.981
Al	1.665	1.435	1.774	1.632	1.810	1.280	1.236	1.160	1.288	1.136	1.288	1.236
Ti	0.199	0.142	0.202	0.146	0.129	0.177	0.095	0.078	0.099	0.083	0.104	0.092
Cr	0.002	0.005	0.000	0.000	0.000	0.000	0.007	0.002	0.010	0.009	0.008	0.005
Fe_{3+}	0.452	0.508	0.445	0.547	0.635	0.466	0.472	0.462	0.473	0.543	0.492	0.464
Fe_{2+}	1.284	1.235	1.361	1.697	1.719	1.239	1.180	0.963	1.159	1.029	1.147	1.125
Mn	0.042	0.047	0.039	0.122	0.113	0.068	0.051	0.055	0.053	0.058	0.051	0.056
Mg	2.743	2.836	2.651	2.232	2.091	2.905	3.042	3.240	3.020	3.146	3.010	3.074
Ca	1.879	1.852	1.884	1.879	1.873	1.784	1.835	1.782	1.828	1.827	1.766	1.803
Na	0.360	0.335	0.412	0.302	0.294	0.367	0.395	0.401	0.389	0.343	0.437	0.414
K	0.128	0.084	0.137	0.208	0.228	0.103	0.104	0.046	0.082	0.046	0.073	0.063
Total	15.370	15.287	15.434	15.393	15.400	15.287	15.357	15.262	15.326	15.244	15.317	15.313
Geobarometer (Schmidt, 1992)												
P(kbar)(±0.6 kbar)	**4.99**	**3.90**	**5.52**	**4.85**	**5.73**	**3.15**	**2.94**	**2.57**	**3.18**	**2.46**	**3.19**	**2.93**
Depth (km)	**18.16**	**14.18**	**20.06**	**17.64**	**20.82**	**11.44**	**10.68**	**9.34**	**11.58**	**8.95**	**11.59**	**10.66**
Geothermometer (Holland & Blundy, 1994)												
cum	0.0006	0.0109	0.0006	0.0029	0.0059	0.0335	0.0168	0.0300	0.0167	0.0183	0.0329	0.0283
XTSi	0.6538	0.7015	0.6324	0.6567	0.6274	0.7242	0.7348	0.7678	0.7312	0.7561	0.7351	0.7452
XTAl	0.3462	0.2985	0.3676	0.3433	0.3726	0.2758	0.2652	0.2322	0.2688	0.2439	0.2649	0.2548
XMAl	0.1400	0.1207	0.1517	0.1292	0.1597	0.0886	0.0878	0.1158	0.1064	0.0801	0.1144	0.1083
XK	0.1278	0.0841	0.1374	0.2083	0.2276	0.1028	0.1035	0.0462	0.0822	0.0462	0.0729	0.0634
XBlk	0.6327	0.7173	0.5660	0.6074	0.6000	0.7129	0.6501	0.7406	0.6843	0.7656	0.6913	0.6916
XNa	0.2396	0.1985	0.2966	0.1843	0.1724	0.1842	0.2464	0.2133	0.2335	0.1881	0.2359	0.2450
XMNa	0.0601	0.0683	0.0576	0.0589	0.0606	0.0912	0.0741	0.0940	0.0777	0.0773	0.1007	0.0844
XMCa	0.9396	0.9262	0.9421	0.9397	0.9365	0.8921	0.9175	0.8910	0.9139	0.9136	0.8828	0.9015
XPlAb (0.1-0.9)	**0.42**	**0.63**	**0.44**	**0.53**	**0.58**	**0.53**	**0.62**	**0.83**	**0.83**	**0.65**	**0.78**	**0.86**
XPlAn	0.58	0.37	0.56	0.47	0.42	0.47	0.38	0.17	0.17	0.35	0.22	0.14
Y1	1.0368	0.0000	0.7632	0.0000	0.0000	0.0000	0.0000	0.0000	0.0000	0.0000	0.0000	0.0000
Y2	1.0800	3.0000	1.5600	3.0000	3.0000	3.0000	3.0000	3.0000	3.0000	3.0000	3.0000	3.0000
KD1	0.2209	0.5641	0.1523	0.3525	0.3584	0.5680	0.4780	1.0052	0.6981	0.8648	0.6692	0.7490
KD2	0.0703	0.0429	0.0565	0.0448	0.0333	0.1004	0.0579	0.0301	0.0200	0.0596	0.0377	0.0188
T1(° C) (±40 °C)	**792**	**731**	**805**	**750**	**728**	**756**	**741**	**673**	**694**	**727**	**697**	**685**

4.6 Zircon U-Pb geochronology

The representative granitic rocks (biotite granite, hornblende granite, and biotite-hornblende granite) were geochronologically studied to determine the ages of rock formation (Faure, 1986; Rollinson, 1993; Schoene, 2014) by the separated zircons as described below.

Thirty zircons from the biotite granite (Sample no. WKG1), 18 zircons from the hornblende granite (Sample no. 2WK4) and 25 zircons from the biotite-hornblende granite (Sample no. 2WK15) were LA-ICP-MS analyzed to examine the magmatic ages. All 33 analyses of the biotite granite (Table 4.6), 26 analyses of the hornblende granite (Table 4.7), and 28 analyses of the biotite-hornblende granite (Table 4.8), were plotted on the Concordia diagrams in Figs. 4.9, 4.11 and 4.13, respectively. The cathodoluminescence (CL) images and analytical spots with U-Pb dating results are presented in Figs. 4.8, 4.10 and 4.12 for the biotite granite, hornblende granite, and biotite-hornblende granite, respectively. The oscillatory zoning, medium-grained (100-400 μm), subhedral to euhedral shape, are obviously present in all zircon grains, which indicate crystallization from magma.

Based on the Tera-Wasserburg Concordia diagram (Figs. 4.9a, 4.11a, 4.13a) and weight histogram with density curve (Figs. 4.9b, 4.11b, 4.13b), the U-Pb zircon data show different ages of each rock unit. The biotite granite is divided into 2 distinctive groups (Figs. 4.9a, 4.9b) such as the dominant older ages defining a weighted mean ^{238}U-^{206}Pb age of 314.6 $\pm$ 4.4 Ma (Fig. 4.9b) and younger ages defining a weighted mean ^{238}U-^{206}Pb age of 284.9 $\pm$ 4.2 Ma. These defined ^{238}U-^{206}Pb ages should indicate the age of magmatic crystallization of granite during Late Carboniferous to Early Permian. The hornblende granite shows a weighted mean ^{238}U-^{206}Pb age of 253.4 $\pm$ 4.3 Ma (Figs. 4.11a, 4.11b) which reflect the crystallization of granites during Late Permian. For the biotite-hornblende granites, 3 groups were separated (Figs. 4.13a, 4.13b); they are the most younger weighted mean ^{238}U-^{206}Pb age of 237.8 $\pm$ 3.8 Ma, the older age of 308.5 $\pm$ 5.7 Ma, and the oldest ages yielded 429.0 $\pm$ 24 Ma. The concordant zircon ^{238}U-^{206}Pb age of 237.8 $\pm$ 3.8 Ma should indicate the Triassic magmatism. On the other hand, the older zircon ^{238}U-^{206}Pb ages of 308.5 $\pm$ 5.7 Ma and 429 $\pm$ 24 Ma may indicate the inherited zircons.

Therefore, these granitic rocks may occur in 3 main magmatic events that are Late Carboniferous to Early Permian, Late Permian, and Triassic magmatisms for the biotite granite, hornblende granite, and biotite-hornblende granite, respectively.

Table 4.6 Zircon LA-ICP-MS U-Pb data and calculated ages of zircons in the biotite granite (sample no. WKG1).

Anallytical spot number	$^{206}Pb_c$(1)(%)	U (ppm)	Th (ppm)	Th/U	$^{238}U/^{206}Pb^*$ (1)	$^{207}Pb^*/^{206}Pb^*$ (1)	$^{238}U/^{206}Pb^*$ age (1)(Ma)	$^{238}U/^{206}Pb^*$ age (2)(Ma)	Conc
WKG1_025	0.00	215	72	0.34	23.40 ± 0.46	0.0480 ± 0.0032	269.8 ± 5.2	269.8 ± 5.2	Conc
WKG1_004	0.80	473	172	0.37	22.68 ± 0.53	0.0456 ± 0.0032	278.2 ± 6.3	280.3 ± 6.4	Conc
WKG1_029	0.13	596	264	0.45	22.47 ± 0.42	0.0495 ± 0.0032	280.6 ± 5.1	281.0 ± 5.0	Conc
WKG1_026	0.42	257	80	0.32	22.43 ± 0.47	0.0472 ± 0.0046	281.2 ± 5.8	282.4 ± 5.7	Conc
WKG1_028	0.00	429	162	0.39	22.16 ± 0.41	0.0536 ± 0.0020	284.5 ± 5.1	283.9 ± 5.1	Conc
WKG1_006	0.91	347	150	0.44	22.32 ± 0.58	0.0470 ± 0.0039	282.5 ± 7.2	284.2 ± 7.2	Conc
WKG1_032	0.45	399	189	0.48	22.23 ± 0.42	0.0476 ± 0.0037	283.7 ± 5.2	284.9 ± 5.2	Conc
WKG1_030	0.00	237	87	0.37	22.03 ± 0.47	0.0552 ± 0.0033	286.1 ± 6.0	285.0 ± 6.1	Conc
WKG1_052	0.18	546	272	0.51	21.77 ± 0.35	0.0568 ± 0.0037	289.5 ± 4.5	287.8 ± 4.4	Conc
WKG1_027	7.24	432	259	0.61	21.80 ± 0.42	0.0464 ± 0.0092	289.2 ± 5.4	291.4 ± 5.2	Conc
WKG1_042	0.00	1009	761	0.77	21.56 ± 0.33	0.0539 ± 0.0014	292.2 ± 4.4	291.6 ± 4.4	Conc
WKG1_050	0.00	720	445	0.63	21.53 ± 0.35	0.0507 ± 0.0016	292.6 ± 4.7	292.6 ± 4.7	Conc
WKG1_003	0.58	212	74	0.36	20.96 ± 0.57	0.0540 ± 0.0043	300.5 ± 8.0	299.9 ± 8.0	Conc
WKG1_040	0.00	266	102	0.39	20.68 ± 0.44	0.0553 ± 0.0028	304.5 ± 6.3	303.4 ± 6.3	Conc
WKG1_008	0.05	289	96	0.34	20.66 ± 0.43	0.0511 ± 0.0035	304.7 ± 6.2	304.9 ± 6.2	Conc
WKG1_046	0.00	395	178	0.46	20.53 ± 0.41	0.0566 ± 0.0024	306.5 ± 5.9	305.0 ± 6.0	Conc
WKG1_047	0.00	606	256	0.43	20.46 ± 0.31	0.0560 ± 0.0019	307.6 ± 4.6	306.3 ± 4.6	Conc
WKG1_051	0.49	613	253	0.42	20.46 ± 0.35	0.0553 ± 0.0033	307.7 ± 5.1	306.7 ± 5.1	Conc
WKG1_034	0.00	408	197	0.50	20.47 ± 0.35	0.0526 ± 0.0020	307.5 ± 5.1	307.4 ± 5.1	Conc
WKG1_037	0.46	403	146	0.37	20.51 ± 0.37	0.0503 ± 0.0037	306.9 ± 5.4	307.7 ± 5.4	Conc
WKG1_038	1.04	405	191	0.48	20.36 ± 0.37	0.0536 ± 0.0044	309.1 ± 5.5	308.7 ± 5.4	Conc
WKG1_035	0.00	493	308	0.64	20.19 ± 0.37	0.0498 ± 0.0017	311.6 ± 5.6	311.6 ± 5.6	Conc
WKG1_001	2.80	271	107	0.41	20.27 ± 0.50	0.0479 ± 0.0041	310.5 ± 7.5	312.3 ± 7.6	Conc
WKG1_009	0.00	708	317	0.46	19.85 ± 0.36	0.0500 ± 0.0015	316.9 ± 5.6	316.9 ± 5.6	Conc
WKG1_010	0.30	317	125	0.41	19.85 ± 0.36	0.0483 ± 0.0035	316.8 ± 5.6	317.7 ± 5.5	Conc
WKG1_039	0.00	439	204	0.48	19.69 ± 0.36	0.0536 ± 0.0024	319.4 ± 5.7	319.1 ± 5.7	Conc
WKG1_048	0.75	309	135	0.45	19.56 ± 0.40	0.0557 ± 0.0041	321.4 ± 6.4	320.3 ± 6.4	Conc
WKG1_045	0.00	571	284	0.51	19.60 ± 0.33	0.0537 ± 0.0019	320.8 ± 5.3	320.4 ± 5.4	Conc
WKG1_014	0.00	507	226	0.46	19.36 ± 0.31	0.0536 ± 0.0020	324.6 ± 5.1	324.4 ± 5.2	Conc
WKG1_033	0.66	208	86	0.42	19.29 ± 0.45	0.0535 ± 0.0049	325.8 ± 7.3	325.6 ± 7.3	Conc
WKG1_015	0.00	649	270	0.43	19.27 ± 0.31	0.0506 ± 0.0017	326.1 ± 5.1	326.1 ± 5.1	Conc
WKG1_016	0.00	393	232	0.61	18.92 ± 0.31	0.0551 ± 0.0021	332.0 ± 5.2	331.1 ± 5.3	Conc
WKG1_011	0.00	327	172	0.54	18.76 ± 0.32	0.0535 ± 0.0021	334.9 ± 5.5	334.7 ± 5.6	Conc

Errors are 1-sigma; Pb_c and Pb^* indicate the common and radiogenic portions, respectively.
(1) Common Pb corrected by assuming $^{206}Pb/^{238}U$-$^{208}Pb/^{232}Th$ age-concordance
(2) Common Pb corrected by assuming $^{206}Pb/^{238}U$-$^{207}Pb/^{235}U$ age-concordance

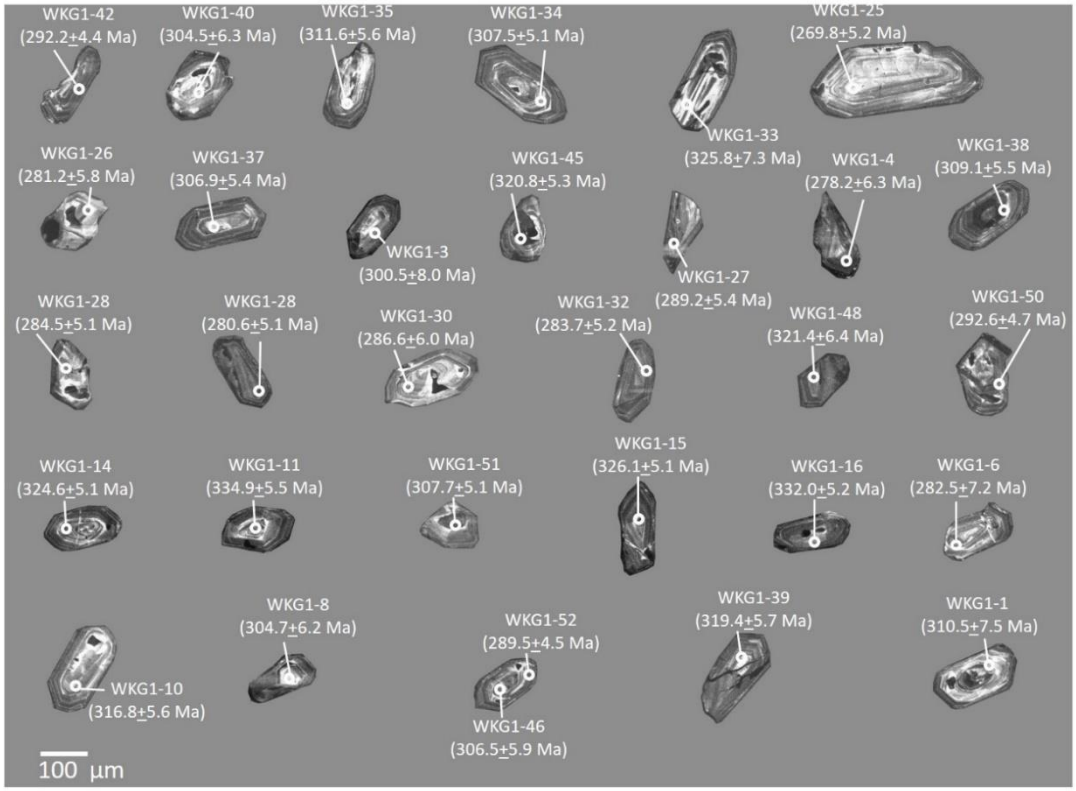

Figure 4.8 CL images of zircons showing $^{206}Pb/^{238}U$ ages from the biotite granite (sample no. WKG1). The analytical spot numbers in Table 4.6 are presented by circles.

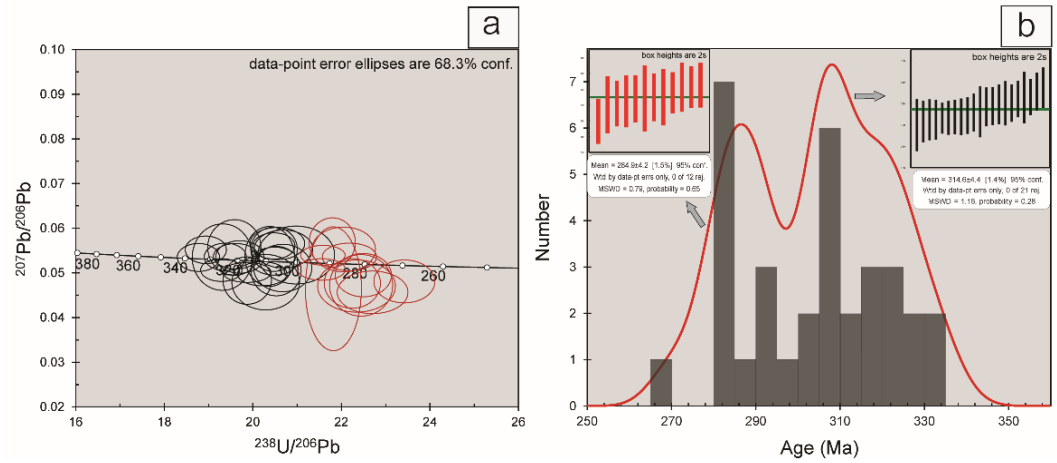

Figure 4.9 (a) The Tera-Wasserburg concordia diagram showing $^{238}U/^{206}Pb$ and $^{207}Pb/^{206}Pb$ ratio, and (b) Histogram displays ^{238}U - ^{206}Pb ages with a probability

curve and weighted average ^{238}U-^{206}Pb ages of zircons in the biotite granite (sample no. WKG1).

Table 4. 7 Zircon LA- ICP- MS U- Pb data and calculated ages of zircons in the hornblende granite (sample no. 2WK4).

Analytical spot number	$^{206}Pb_c$(1)(%)	U (ppm)	Th (ppm)	Th/U	$^{238}U/^{206}Pb^*$ (1)		$^{207}Pb^*/^{206}Pb^*$ (1)		$^{238}U/^{206}Pb^*$ age (1)(Ma)		$^{238}U/^{206}Pb^*$ age (2)(Ma)		Conc
2WK4_049	0.08	36	14	0.39	26.92	± 1.09	0.0747	± 0.0156	235.1	± 9.3	228.2	± 8.9	Conc
2WK4_050	0.48	41	17	0.42	24.90	± 0.89	0.0481	± 0.0120	253.9	± 8.9	254.8	± 8.8	Conc
2WK4_051	0.00	46	23	0.53	25.19	± 0.95	0.0640	± 0.0081	250.9	± 9.2	247.0	± 9.4	Conc
2WK4_052	0.00	39	17	0.44	23.10	± 0.82	0.0578	± 0.0079	273.2	± 9.6	271.2	± 9.8	Conc
2WK4_053	0.00	78	43	0.57	26.09	± 0.82	0.0614	± 0.0059	242.4	± 7.5	239.3	± 7.6	Conc
2WK4_055	0.00	45	18	0.42	24.33	± 0.81	0.0511	± 0.0068	259.6	± 8.5	259.6	± 8.5	Conc
2WK4_059	0.97	60	35	0.60	25.48	± 0.76	0.0365	± 0.0090	248.2	± 7.2	250.6	± 7.0	Conc
2WK4_061	0.00	62	39	0.64	25.19	± 0.93	0.0469	± 0.0053	250.9	± 9.1	250.9	± 9.1	Conc
2WK4_062	1.06	66	42	0.66	25.86	± 0.76	0.0477	± 0.0105	244.6	± 7.0	245.6	± 6.9	Conc
2WK4_063	0.00	46	26	0.58	24.89	± 0.87	0.0566	± 0.0086	254.0	± 8.7	252.3	± 9.1	Conc
2WK4_064	0.00	67	27	0.42	25.06	± 0.75	0.0590	± 0.0058	252.3	± 7.4	249.9	± 7.5	Conc
2WK4_065	0.00	55	33	0.62	23.36	± 0.80	0.0435	± 0.0061	270.2	± 9.1	270.2	± 9.1	Conc
2WK4_066	0.94	50	18	0.38	24.42	± 0.89	0.0554	± 0.0102	258.7	± 9.3	257.5	± 9.2	Conc
2WK4_071	0.12	46	25	0.55	24.03	± 1.01	0.0367	± 0.0110	262.8	± 10.8	263.1	± 10.5	Conc
2WK4_072	0.44	56	35	0.64	24.33	± 0.75	0.0507	± 0.0113	259.6	± 7.9	259.8	± 7.6	Conc
2WK4_073	0.98	50	21	0.44	23.81	± 0.88	0.0443	± 0.0097	265.2	± 9.6	267.5	± 9.6	Conc
2WK4_074	36.92	77	68	0.91	24.55	± 1.59	0.0709	± 0.0763	257.4	± 16.4	252.3	± 15.7	Conc
2WK4_075	2.21	63	24	0.40	25.32	± 0.83	0.0499	± 0.0108	249.7	± 8.0	250.1	± 7.9	Conc
2WK4_077	0.00	57	34	0.62	24.44	± 0.89	0.0532	± 0.0056	258.5	± 9.2	258.0	± 9.3	Conc
2WK4_081	0.96	46	18	0.40	26.10	± 0.84	0.0470	± 0.0109	242.4	± 7.6	243.6	± 7.6	Conc
2WK4_082	0.00	57	35	0.63	24.32	± 0.73	0.0420	± 0.0056	259.7	± 7.6	259.7	± 7.6	Conc
2WK4_083	0.00	52	26	0.51	24.80	± 0.92	0.0566	± 0.0063	254.8	± 9.3	253.2	± 9.4	Conc
2WK4_084	0.00	50	22	0.45	25.79	± 0.91	0.0491	± 0.0064	245.2	± 8.5	245.2	± 8.5	Conc
2WK4_085	0.00	55	28	0.52	23.36	± 0.76	0.0503	± 0.0070	270.2	± 8.6	270.2	± 8.6	Conc
2WK4_086	0.52	42	17	0.42	23.67	± 0.92	0.0397	± 0.0123	266.7	± 10.1	268.1	± 9.8	Conc
2WK4_088	0.00	54	33	0.62	23.10	± 0.86	0.0569	± 0.0061	273.2	± 9.9	271.5	± 10.1	Conc

Errors are 1-sigma; Pb_c and Pb^* indicate the common and radiogenic portions, respectively.
(1) Common Pb corrected by assuming $^{206}Pb/^{238}U$-$^{208}Pb/^{232}Th$ age-concordance
(2) Common Pb corrected by assuming $^{206}Pb/^{238}U$-$^{207}Pb/^{235}U$ age-concordance

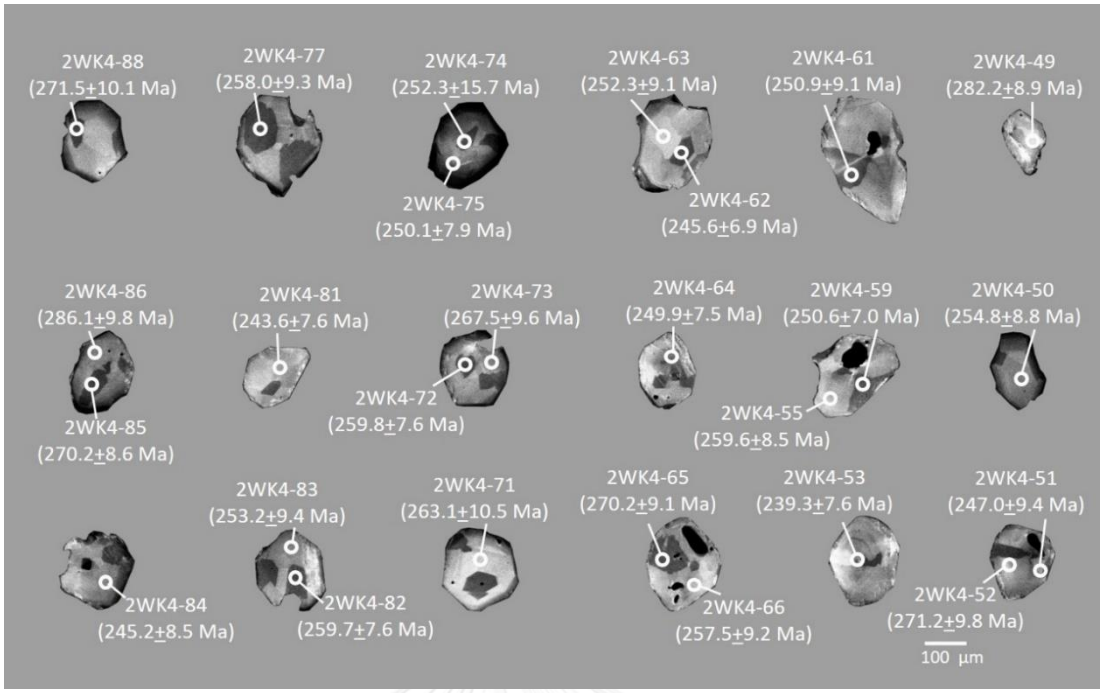

Figure 4.10 CL images of zircons showing $^{206}Pb/^{238}U$ ages from the hornblende granite (sample no. 2WK4). The analytical spot numbers in Table 4.7 are presented by circles.

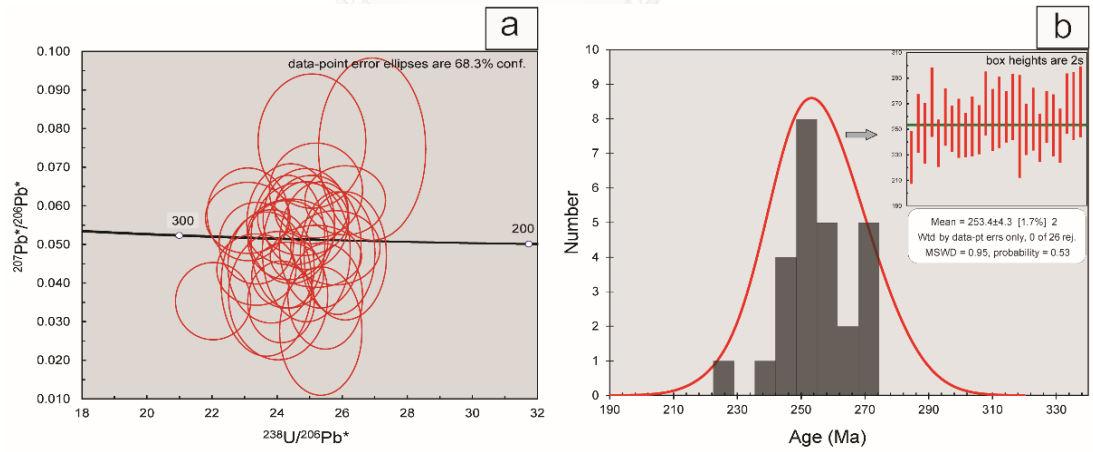

Figure 4.11 (a) The Tera-Wasserburg concordia diagram showing $^{238}U/^{206}Pb$ and $^{207}Pb/^{206}Pb$ ratio, and (b) Histogram display ^{238}U - ^{206}Pb ages with a probability curve and weighted average ^{238}U-^{206}Pb ages of zircons in the hornblende granite (sample no. 2WK4).

Table 4.8 Zircon LA-ICP-MS U-Pb data and calculated ages of zircons in the biotite-hornblende granite (sample no. 2WK15).

Analytical spot number	$^{206}Pb_c$(1)(%)	U (ppm)	Th (%)	Th/U	$^{238}U/^{206}Pb^*$(1)	$^{207}Pb^*/^{206}Pb^*$(1)	$^{238}U/^{206}Pb^*$ age (1)(%)	$^{238}U/^{206}Pb^*$ age (2)(%)	Conc
2WK15_001	0.00	195	80	0.42	27.37 ± 0.60	0.0473 ± 0.0033	231.3 ± 5.0	231.3 ± 5.0	Conc
2WK15_002	0.00	179	63	0.36	25.65 ± 0.61	0.0454 ± 0.0030	246.5 ± 5.7	246.5 ± 5.7	Conc
2WK15_003	0.00	214	106	0.51	20.40 ± 0.38	0.0543 ± 0.0022	308.5 ± 5.7	307.9 ± 5.7	Conc
2WK15_004	0.74	175	61	0.36	25.57 ± 0.56	0.0467 ± 0.0049	247.3 ± 5.3	248.7 ± 5.3	Conc
2WK15_005	0.00	154	52	0.34	26.58 ± 0.60	0.0543 ± 0.0039	238.0 ± 5.3	237.1 ± 5.4	Conc
2WK15_006	0.01	181	76	0.43	27.05 ± 0.58	0.0512 ± 0.0055	234.0 ± 5.0	233.9 ± 4.9	Conc
2WK15_007	0.00	250	145	0.59	25.98 ± 0.52	0.0513 ± 0.0034	243.5 ± 4.8	243.4 ± 4.9	Conc
2WK15_008	0.00	140	58	0.43	25.00 ± 0.65	0.0471 ± 0.0028	252.8 ± 6.5	252.8 ± 6.5	Conc
2WK15_009	0.00	157	60	0.39	24.72 ± 0.55	0.0490 ± 0.0036	255.6 ± 5.5	255.6 ± 5.5	Conc
2WK15_010	1.61	77	25	0.34	25.06 ± 0.75	0.0473 ± 0.0103	252.2 ± 7.4	253.5 ± 7.5	Conc
2WK15_011	0.00	486	320	0.68	14.30 ± 0.25	0.0545 ± 0.0018	435.7 ± 7.4	435.7 ± 7.4	Conc
2WK15_012	0.53	117	53	0.46	24.69 ± 0.79	0.0505 ± 0.0080	255.9 ± 8.0	256.2 ± 7.9	Conc
2WK15_013	0.00	126	57	0.46	26.25 ± 0.63	0.0556 ± 0.0052	241.0 ± 5.7	239.7 ± 5.8	Conc
2WK15_014	0.00	112	39	0.36	23.87 ± 0.80	0.0541 ± 0.0051	264.5 ± 8.7	263.7 ± 8.9	Conc
2WK15_015	0.00	224	141	0.64	24.88 ± 0.62	0.0584 ± 0.0041	254.1 ± 6.2	251.9 ± 6.3	Conc
2WK15_016	0.43	114	45	0.40	27.81 ± 0.70	0.0516 ± 0.0059	227.8 ± 5.6	227.5 ± 5.6	Conc
2WK15_017	0.00	84	22	0.27	27.87 ± 0.80	0.0593 ± 0.0051	227.3 ± 6.4	224.9 ± 6.5	Conc
2WK15_018	0.26	205	102	0.51	27.60 ± 0.50	0.0493 ± 0.0045	229.4 ± 4.1	229.8 ± 4.1	Conc
2WK15_019	0.79	141	44	0.32	26.83 ± 0.73	0.0433 ± 0.0055	235.9 ± 6.3	237.8 ± 6.2	Conc
2WK15_020	0.00	143	48	0.34	26.06 ± 0.69	0.0495 ± 0.0035	242.7 ± 6.3	242.7 ± 6.3	Conc
2WK15_021	0.48	197	94	0.49	26.82 ± 0.59	0.0499 ± 0.0056	236.0 ± 5.1	236.3 ± 5.1	Conc
2WK15_022	1.59	94	32	0.35	28.31 ± 0.89	0.0362 ± 0.0086	223.8 ± 6.9	227.4 ± 6.8	Conc
2WK15_023	3.66	169	50	0.30	25.84 ± 0.62	0.0533 ± 0.0063	244.7 ± 5.8	244.1 ± 5.7	Conc
2WK15_025	0.00	470	289	0.63	27.28 ± 0.50	0.0508 ± 0.0021	232.1 ± 4.2	232.1 ± 4.2	Conc
2WK15_026	0.00	346	175	0.52	27.35 ± 0.50	0.0530 ± 0.0023	231.5 ± 4.1	230.9 ± 4.2	Conc
2WK15_027	0.00	405	304	0.77	27.38 ± 0.59	0.0516 ± 0.0025	231.3 ± 4.9	231.1 ± 5.0	Conc
2WK15_029	1.07	422	507	1.23	14.81 ± 0.32	0.0444 ± 0.0066	421.2 ± 8.8	425.6 ± 8.3	Conc
2WK15_030	0.03	116	36	0.32	26.98 ± 0.77	0.0503 ± 0.0071	234.6 ± 6.6	234.7 ± 6.4	Conc

Errors are 1-sigma; Pb_c and Pb^* indicate the common and radiogenic portions, respectively.
(1) Common Pb corrected by assuming $^{206}Pb/^{238}U$-$^{208}Pb/^{232}Th$ age-concordance
(2) Common Pb corrected by assuming $^{206}Pb/^{238}U$-$^{207}Pb/^{235}U$ age-concordance

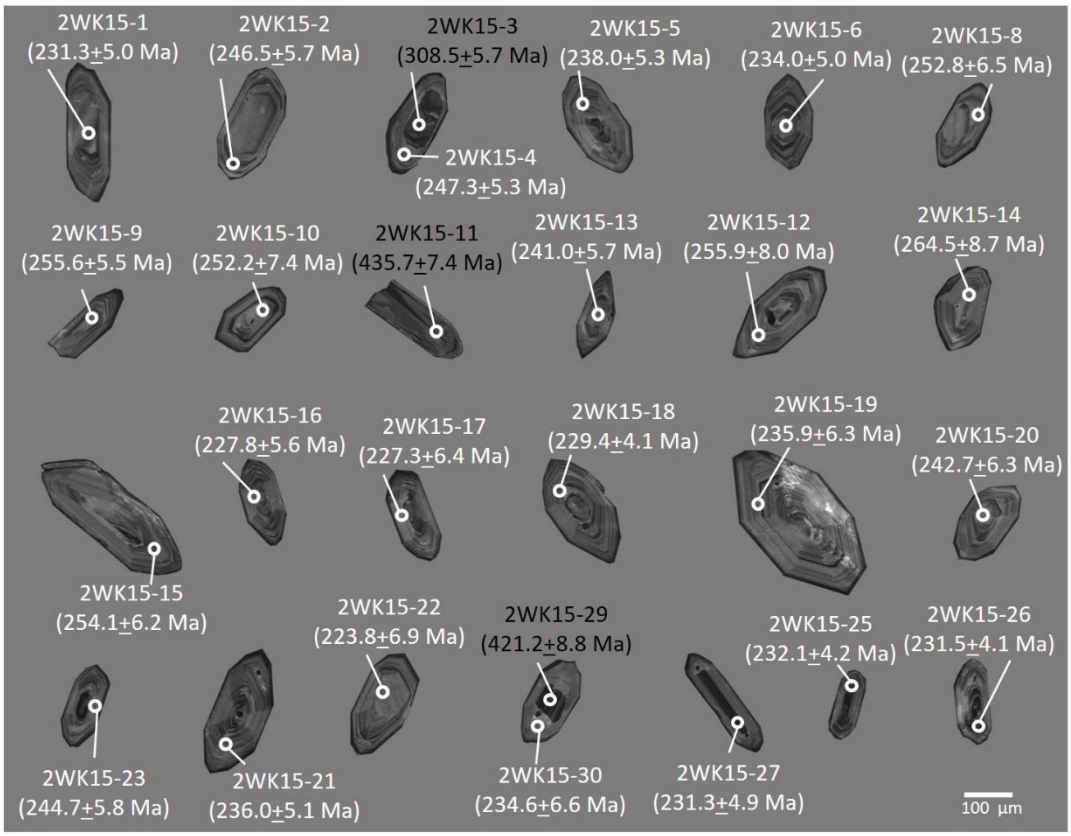

Figure 4. 12 CL images of zircons showing $^{206}Pb/^{238}U$ ages from the biotite-hornblende granite (sample no. 2WK15). The analytical spot numbers in Table 4.8 are presented by circles.

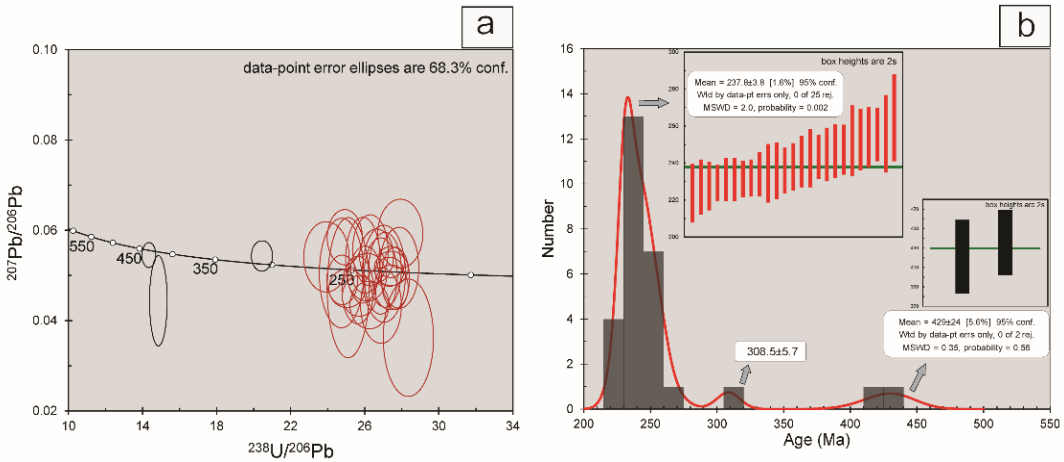

Figure 4. 13 (a) The Tera-Wasserburg concordia diagram showing $^{238}U/^{206}Pb$ and $^{207}Pb/^{206}Pb$ ratio, and (b) Histogram display ^{238}U - ^{206}Pb ages with a probability curve

and weighted average ^{238}U-^{206}Pb ages of zircons in the biotite-hornblende granite (sample no. 2WK15).

4.7 Discussions

Intrusion depths: Numerous previous studies have estimated crystallization depth of plutons using calculated pressure conditions of magmatic rocks (Schmidt, 1992; Stein and Dietl, 2001; Helmy et al., 2004; Hossain et al., 2009; Fanka et al., 2016). Calibration of Al component in hornblende has been regarded as a useful geobarometer for magmatic rocks as suggested by Hammarstrom and Zen (1986); Hollister et al. (1987); Vyhnal et al. (1991); Schmidt (1992). In this study, the intrusion depths of the hornblende granite and the biotite-hornblende granite were estimated based on the calculated pressures and the equation: $P = \rho gh$ (P = pressure (GPa), ρ = continental crust density (2.73 kg/m^3), g = specific gravity (10.0 m/s^2), h = depth (km)). The intrusion depths determined from calculated pressures using Al-in-hornblende geobarometry of both granite groups are reported in Table 4.1 and the mean depths of the plutons are estimated and shown in Fig. 4.14. These emplacement depths display 15 ± 3 km for the hornblende granite and 10±1 km for the biotite-hornblende granite, which correspond to the level of middle to upper crust (Petrini and Podladchikov, 2000; Ramo, 2005). These intrusion depths are also consistent with the calculated temperatures of the hornblende granite (700-820 ^oC) and the biotite-hornblende granites (600-750 ^oC) which are compatible with the temperature range of the middle to upper crust in the general continental crust (Wyllie et al., 1984; Peacock, 1993; Winter, 2001; Kelemen et al., 2003; Richards, 2003) with about 20-40 ^oC /km geothermal gradient (Rothstein and Manning, 2003; Annen et al., 2006).

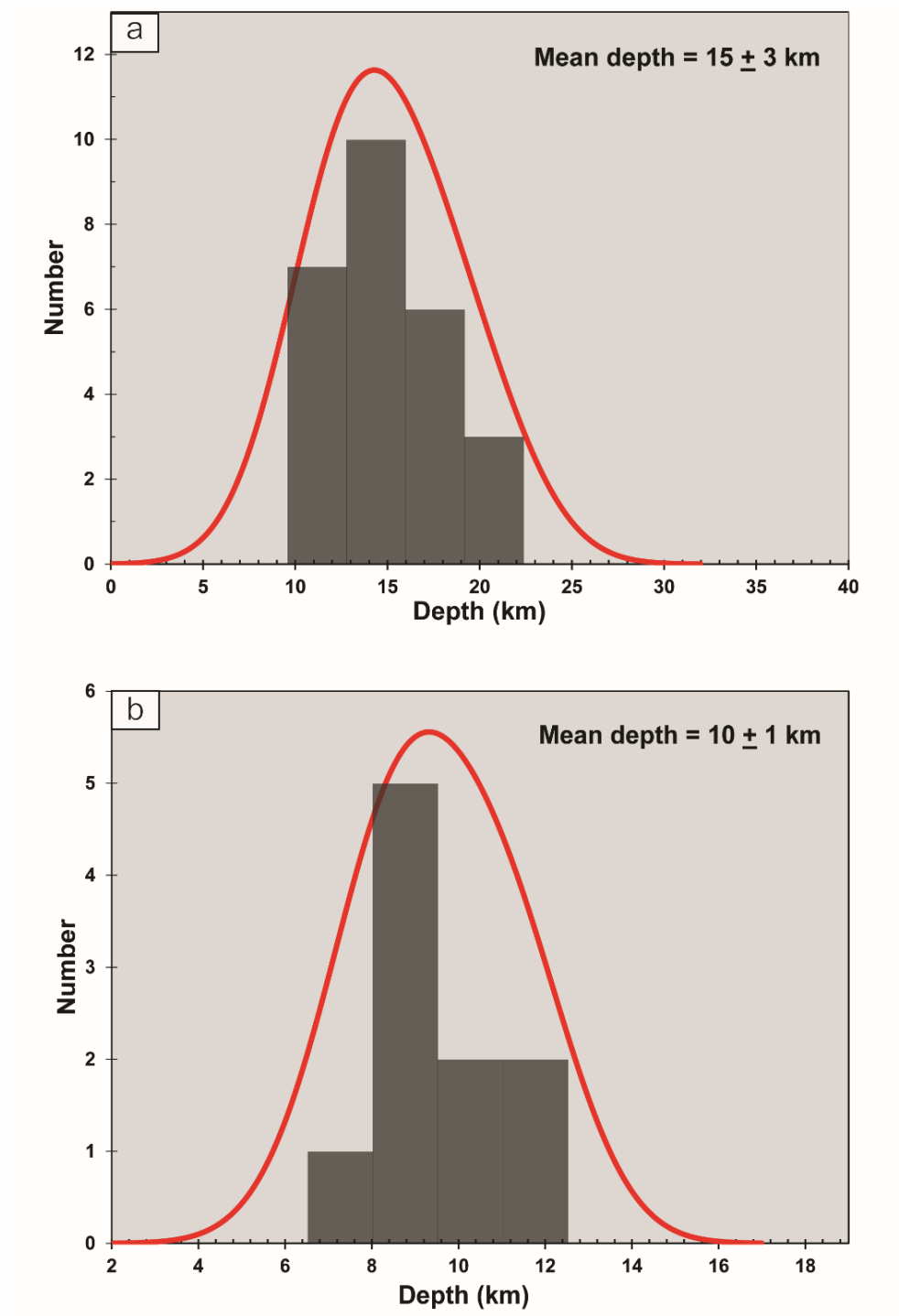

Figure 4.14 The histograms of calculated intrusion depth from (a) hornblende granite and (b) biotite-hornblende granite in the Wang Nam Khiao area, Nakhon Ratchasima, Thailand.

Magma genesis:

Based on field observations, these granitic rocks usually show mafic autholiths (Figs. 4.1c and 4.2e), which are typical feature of calc-alkaline granitoid magma (Barbarin, 1991; Barbarin and Didier, 1992; Barbarin, 2005). TAS diagram (Fig. 4.5) indicates that all the biotite granite, hornblende granite and biotite-hornblende granite samples are subalkali/tholeiitic composition. In addition, SiO_2 and K_2O plot (Fig. 4.15a) indicates that these granitic rocks correspond to calc-alkaline series to high K calc-alkaline series, which is consistent with those plots in alkaline-FeO_{total}-MgO (AFM) ternary diagram (Fig. 4.15b, after Irvine and Baragar (1971)) indicating the calc-alkaline magmatic series. Their mineral assemblages, particularly hornblende and biotite together with titanite, support the genetic model of hydrous magma (Best, 2003). Moreover, the whole-rock trace compositions reveal the enrichment of LILE (e.g. K, Sr, Th, U) and depletion of HFSE (e.g. Nb, Ti) in Figs. 4.7a, 4.7c and 4.7e, suggesting arc-derived magma in subduction-zone affinity (Pearce, 1983; Ryerson and Watson, 1987; Kelemen et al., 1990; Ringwood, 1990; Kelemen et al., 1993; Best, 2003). The REE patterns are clearly characterized by the steep LREE/HREE enrichment (Figs. 4.7b, 4.7d, 4.7f) which reflects low degree of partial melting (Rollinson, 1993).

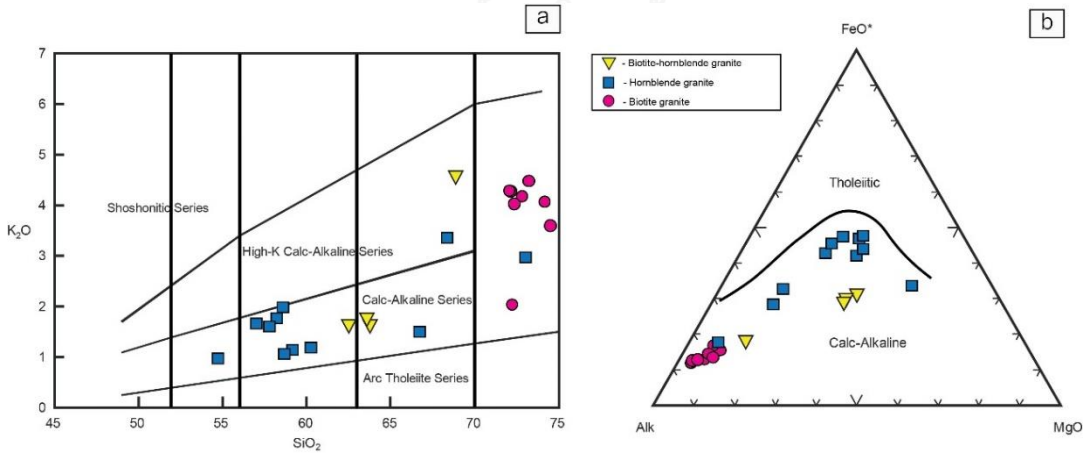

Figure 4.15 (a) SiO_2 vs. K_2O diagram plot (Peccerillo and Taylor, 1976; Rickwood, 1989) showing the calc-alkaline to high-K calc-alkaline series, and (b) the AFM diagram (Irvine and Baragar, 1971) showing the calc-alkaline series of granitic rocks in the Wang Nam Khiao area, Nakhon Ratchasima, Thailand.

The composition of parental magma can be inferred based on biotite chemistry (Burkhard, 1993; Lalonde and Bernard, 1993; Stussi and Cuney, 1996; Aydin et al., 2003; Shabani and Lalonde, 2003; Machev et al., 2004; Masoudi and Badr, 2008; Sarjoughian et al., 2015). Mg-rich biotites in the hornblende granite and the biotite-hornblende granite (Fig. 4.4d) coexist with hornblende whereas biotite is the only ferromagnesian mineral in the Carboniferous biotite granite (Fig. 4.16a). These properties indicate the characters of typical I-type granite (Sarjoughian et al., 2015) as defined by Chappell and White (1974) and Chappell and White (2001) or magnetite-series granite as defined by Ishihara (1977), reflecting a magmatic fractionation (Hecht, 1994). In addition, the granites probably have originated from mantle-crust mixed magmatic sources based on these biotite compositions (Fig. 4.16b), which are consistent with the interpreted mantle-crust mixed origin of calc-alkaline granitoids in the Peru, Chili, and California (Barbarin, 1999).

In summary, their magmatism may have originated under hydrous melting environment with low degree of partial melting.

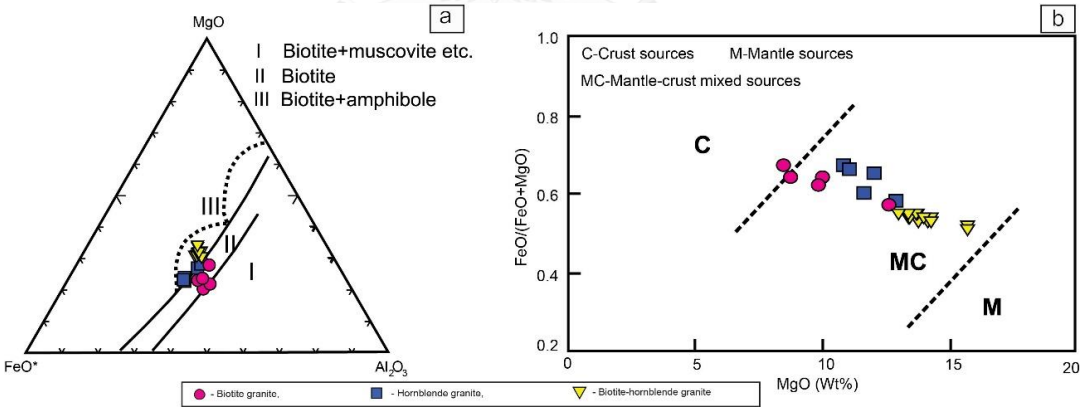

Figure 4.16 (a) Plots of biotite and coexisting minerals in the FeO*-MgO-Al_2O_3 ternary diagram (Nockolds, 1947). (b) Plots of MgO and FeO/(FeO+MgO) diagram (Zhou, 1986) of biotite from the studied granitic rocks showing most mantle-crust mixed source of all granitic rocks with more magma crust sources of the biotite granite.

Petrogenesis: The similar major assemblages of plagioclase, quartz, K-feldspar with significant hydrous minerals, particularly hornblende and biotite indicate the calc-alkaline magmatic series reflecting the hydrous magma derived from arc-related subduction. The biotite compositions plotted on the FeO-MgO-Al_2O_3 discrimination diagram (Abdel-Rahman, 1994) suggest the calc-alkaline magmas related to subduction (Fig. 4.17a). Moreover, the calcic-amphiboles plotted on the Si against Na+K diagram clearly indicate the arc accumulate affinity (Fig. 4.17b). Trace element plots, Y+Nb against Rb, tectonodiagram (Fig. 4.18a) indicate volcanic arc granite (VAG) affinity consistent with plots of Y against Nb (Fig. 4.19b) suggesting the volcanic arc granite with syn-collisional granite (VAG + syn-COLG) affinity. Moreover, depletion of Nb and Ti in the primitive mantle-normalized spider diagram (Figs. 4.7a, 4.7c and 4.7e) and the chondrite-normalized REE patterns (Figs. 4.7b, 4.7d and 4.7f) of these granite groups suggest a typical arc magmatic affinity (Blein et al., 2001).

Therefore, these granitic rocks appear to have crystallized convincingly from arc-related calc-alkaline magmas along subduction zone.

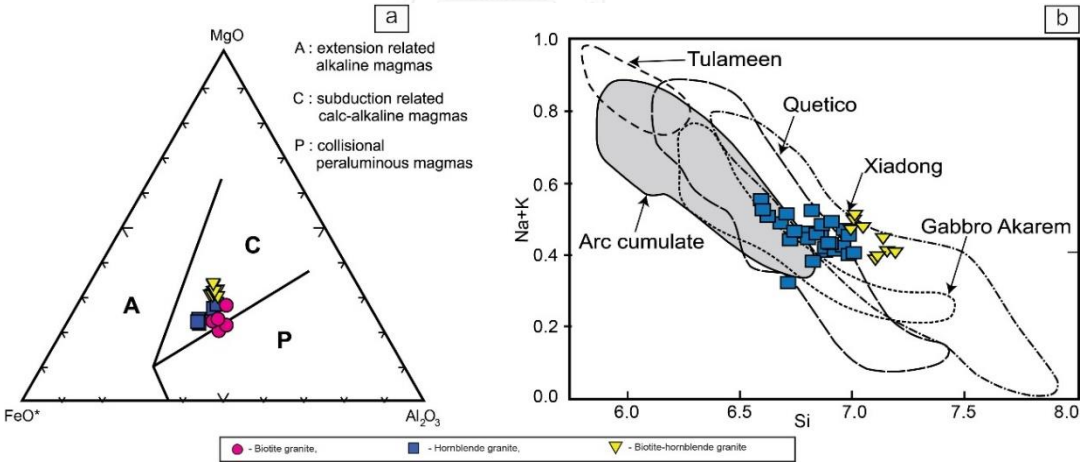

Figure 4.17 (a) Plots of biotite composition on the FeO*-MgO-Al_2O_3 ternary diagram (Abdel-Rahman, 1994) fall in subduction related calc-alkaline magma. (b) Plots of calcic amphibole composition on the Si vs. (Na+K) diagram (Beard and Barker, 1989) suggesting arc accumulate together with those of arc Alaskan-type intrusion of Tulameen Complex from Rublee (1994); Gabbro Akarem Complex from Helmy and El Mahallawi (2003); Quetico Intrusions from Pettigrew and Hattori (2006); Xiadong Complex from Su et al. (2012).

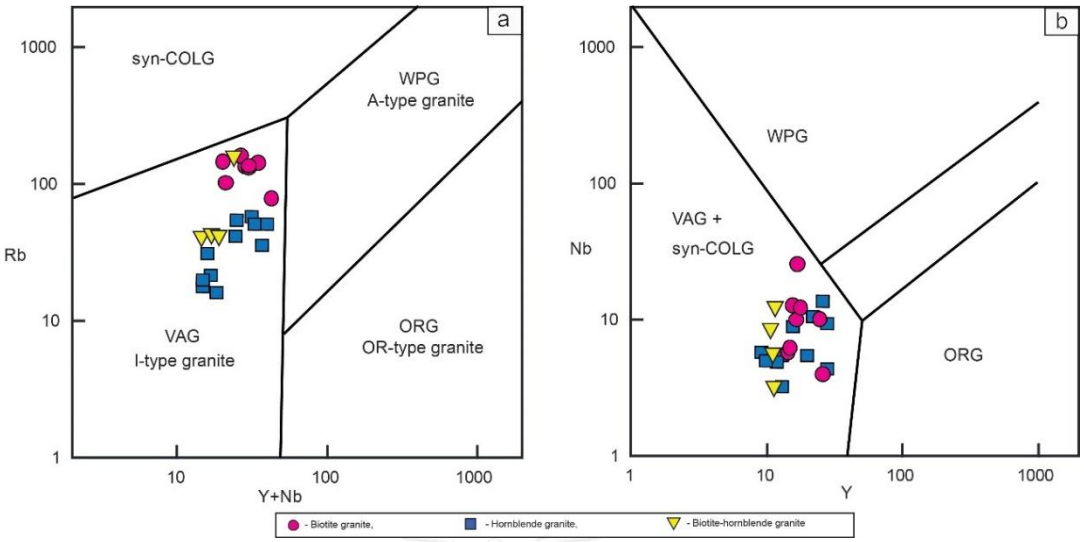

Figure 4.18 Plots of immobile elements of the granitic rocks in the Wang Nam Khiao area, Nakhon Ratchasima, Thailand. (a) (Nb+Y) vs. Rb discrimination diagram (Pearce et al., 1984) showing I-type granite related to volcanic arc. (b) Y vs. Nb discrimination diagram (Pearce et al., 1984) shows these granitic rocks falling within the volcanic arc granite (VAG) field. The abbreviations in the figures are syn-COLG (syn-collision granite), WPG (within plate granite), VAG (volcanic arc granite), ORG (ocean ridge granites).

Age of rocks formation: oscillatory zoning of zircon (Figs. 4.8, 4.10, 4.12) and zircon U-Pb age data (Fig. 4.9, 4.11, 4.13) indicate three events of crystallization which imply that these studied granites were probably crystallized from different magmas derived by discrete magmatic events. Moreover, zircon U-Pb geochronology of Loei Fold Belt have been reported by some researchers and interpreted for the emplacements age magmatic rocks (Zaw et al., 2007; Khositanont et al., 2008; Salam et al., 2014; Zaw et al., 2014; Qian et al., 2015) (Fig. 4.20). These ages are comparable to the new data gained from this study as reported below.

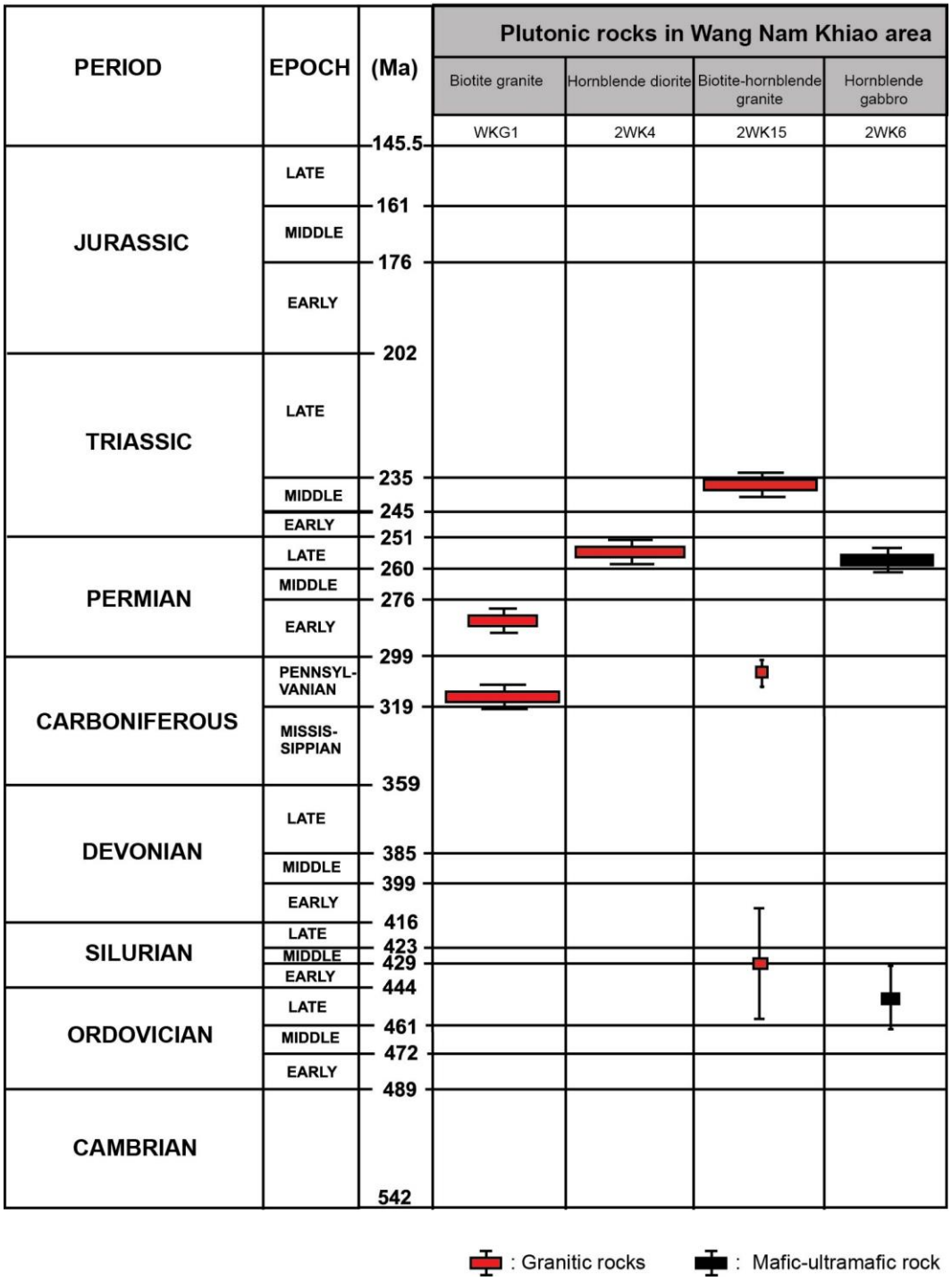

Figure 4.19 Summary of zircon U-Pb ages of magmatic rocks in the Wang Nam Khiao area, Nakhon Ratchasima, Thailand.

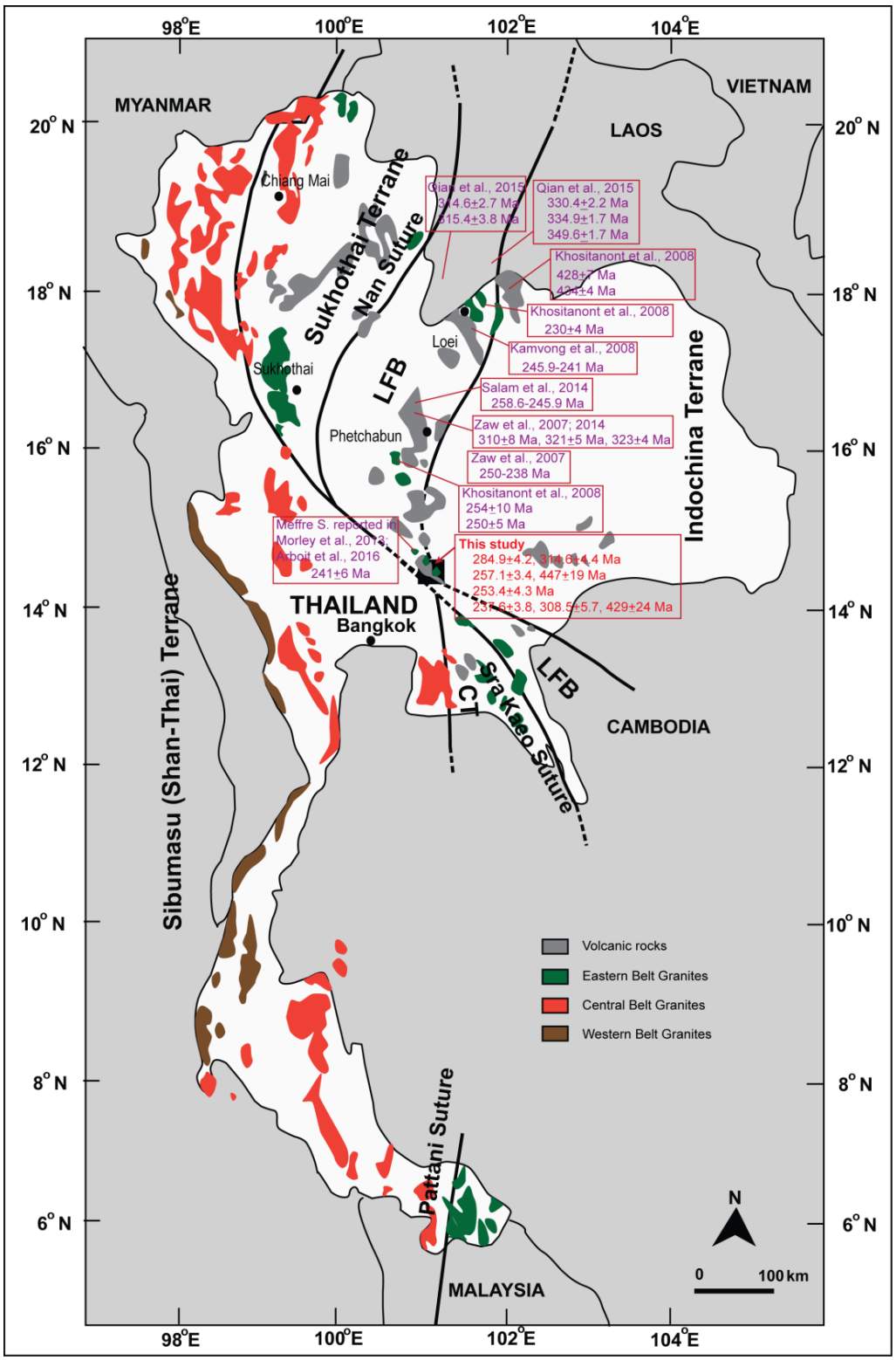

Figure 4.20 Map of Thailand showing distribution of main granite belts and locations of zircon U-Pb ages of magmatic rocks in the Loei Fold Belt including the Wang Nam Khiao area, Nakhon Ratchasima, Thailand.

The biotite granite with a weighted mean U-Pb age (Fig. 4.19) of 314.6 ± 4.4 Ma (Fig. 4.9b) and younger U-Pb ages of 284.9 ± 4.2 Ma were probably crystallized through magmatism related to subduction of Palaeo-Tethys under the Indochaina Terrane during Late Carboniferous to Early Permian (Charusiri et al., 2002; Sone and Metcalfe, 2008; Metcalfe, 2011b, 2013; Salam et al., 2014). These ages are comparable to previous reports of U-Pb zircon ages of Carboniferous granites (310-323 Ma, Zaw et al. (2007)) and volcanic rocks (314-315 Ma, Qian et al. (2015)) formed by arc-related magmatism within the Loei Fold Belt through subduction (Zaw et al., 2007; Salam et al., 2014; Zaw et al., 2014).

The hornblende granite with a weighted mean U-Pb age (Fig. 4.19) of 253.4 ± 4.3 Ma (Fig. 4.11b) probably indicate the magmatism related to Palaeo-Tethys subduction beneath the Indochina Terrane during Late Permian (Charusiri et al., 1993; Intasopa, 1993; Intasopa and Dunn, 1994; Charusiri et al., 2002; Shabani and Lalonde, 2003; Zaw et al., 2007; Sone and Metcalfe, 2008; Barr and Charusiri, 2011; Metcalfe, 2011b, a, 2013; Kamvong et al., 2014; Zaw et al., 2014; Fanka et al., 2016). This age is also consistent with available U-Pb zircon age of mafic-ultramafic plutonic rocks in the study area (257 Ma, Fig. 3.9), which is interpreted as the emplacement age of the mafic magma within the lower crustal level (Fanka et al., 2016). This event probably reflects arc magmatism in the Loei Fold Belt during Late Permian/Earliest Triassic (254-250 Ma, U-Pb zircon ages of granitic rocks and volcanic rocks reported by Khositanont et al. (2008); Salam et al. (2014); Zaw et al. (2014)) or Permian-Triassic arc magmatism related to Palaeo-Tethys subduction under Indochina (Sone and Metcalfe, 2008; Metcalfe, 2011b, a; Sone et al., 2012; Metcalfe, 2013).

The biotite-hornblende granite with the abundant weighted mean U-Pb age (Fig. 4.19) of 237.8 ± 3.8 Ma (Fig. 4.13b) is interpreted as a pluton formed by arc magmatism related to subduction during Middle Triassic (Charusiri et al., 2002; Zaw et al., 2007; Salam et al., 2014; Zaw et al., 2014), which is comparable to the published ages of Triassic granitic (238-249 Ma U-Pb zircon ages reported by Zaw et al. (2007); Kamvong et al. (2014); Salam et al. (2014)) and volcanic rocks (237-238 Ma Ar-Ar ages reported by Intasopa (1993)). The results of this study therefore indicate Triassic plutonic emplacement within the Loei Fold Belt (Bunopas, 1981; Zaw et al., 2007;

Salam et al., 2014; Zaw et al., 2014) with regarding to the major I-type granite in Eastern Granite Belt (Cobbing et al., 1986; Cobbing et al., 1992; Nakapadungrat and Putthapiban, 1992; Charusiri et al., 1993; Searle et al., 2012) of Thailand. In contrast, the older zircon U-Pb age of 308.5 ± 5.7 Ma in the biotite-hornblende granite which is similar to the dominant weighted mean U-Pb age of 314.6 ± 4.4 Ma (Fig. 4.13b) from the biotite granite and other magmatic rocks of the Loei Fold Belt (Zaw et al., 2007; Qian et al., 2015), may indicate the inherited age of Late Carboniferous magmatism in this area. The oldest mean weighted U-Pb age of 429.0 ± 24 Ma (Fig. 4.13b) might also be interpreted as the inherited zircon from the older arc-related magmatism of the Loei Fold Belt (428-434 Ma of U-Pb zircon ages by Khositanont et al. (2008) and 423 Ma of U-Pb zircon age reported by Zhao et al. (2016)).

CHAPTER 5
CONCLUSION AND RECOMMENDATION

5.1 Conlusions

Petrology, mineral chemistry, whole-rock geochemistry and zircon U-Pb geochronology of the studied mafic-ultramafic rocks and granitic rocks of the Wang Nam Khiao plutonic complex can be concluded below.

1) Plutonic rocks in the Wang Nam Khiao area, Nakhon Ratchasima can be classified into mafic-ultramafic plutonic rocks (i.e., hornblendite, hornblende gabbro and hornblende microgabbro) and granitic rocks (i.e., biotite granite, hornblende granite, and biotite-hornblende granite).

2) Mineral assemblages, mineral chemistry and whole-rock geochemistry indicate that both the mafic-ultramafic plutonic rocks and the granitic rocks appear to have evolved from the I-type affinity related to hydrous calc-alkaline magma.

3) Enrichment of LILE (e.g., Ba, K, Sr) and depletion of HFSE (e.g., Nb, Ta, Zr) together with compositions of clinopyroxene and hornblende in the mafic-ultramafic plutonic rocks indicate arc-related subduction within continental arc setting.

4) LILE enrichment (e.g., K, Sr, Th, U), HFSE depletion (e.g., Nb, Ti) and compositions of biotite and hornblende in all granitic rocks reflect arc-derived magma in subduction zone which the high steep LREE/HREE patterns introduce the low degree of partial melting.

5) P-T conditions of crystallization are estimated at 5.3-9.8 kbar with 670-1,000 ^{o}C, 7.6-9.0 kbar with 850-950 ^{o}C, and 7.6-8.8 kbar with 750-850 ^{o}C for hornblendite, hornblende gabbro and hornblende microgabbro, respectively. On the other hand, those of granitic rocks are calculated at 3.0-5.8 kbar with 700-820 ^{o}C, and 2.0-3.2 kbar with 600-750 ^{o}C for the hornblende granite and biotite-hornblende granite, respectively.

6) Based on equilibrated pressures of these plutonic rocks, their intrusion depths can be then estimated as following. Intrusion depths of mafic-ultramafic plutonic rocks are about 28-31 km equivalent to the lower crust. On the other hand, granitic

rocks appear to have crystallized at the depth of about 10-15 km in the middle to upper crust.

7) These mafic-ultramafic plutonic rocks and granitic rocks were emplaced at different periods in different depths of arc-related subduction environment which appears to have produced multi-stages of magmatism, accordingly.

8) According to zircon U-Pb geochronology, the sample of hornblende microgabbro intruded into hornblendite yields 257 Ma which corresponds to the minimum age of the mafic-ultramafic emplacement. These mafic-ultramafic magmas appear to have been generated by Late Permian arc magmatism resulted from subduction of Palaeo-Tethys beneath the Indochina Terrane. Representative samples of biotite granite, hornblende granite and biotite-hornblende granite, yield 314.6-284.9 Ma, 253.4 Ma, and 237.8 Ma, respectively, these results introduce the multiple arc-magmatism from Palaeo-Tethys subduction beneath Indochina Terrane during the Late Carboniferous/Early Permian, Late Permian, and Middle Triassic. The tectonic model of this study area can be reconstructed as shown in Figs. 5.1 to 5.4.

Several models of tectonic evolution in Thailand and Southeast Asia have been suggested by several researchers (Bunopas and Vella, 1983; Bunopas et al., 1989; Bunopas and Vella, 1992; Charusiri et al., 1993; Charusiri et al., 2002; Metcalfe, 2002; Zaw et al., 2007; Sone and Metcalfe, 2008; Barr and Charusiri, 2011; Metcalfe, 2011b, a; Searle et al., 2012; Metcalfe, 2013; Kamvong et al., 2014; Zaw et al., 2014; Ng et al., 2015a; Ng et al., 2015b). Based on petrology, mineral chemistry, geochemistry, and geochronology gained from this study as well as previously proposed regional tectonic models (Metcalfe, 2011b, 2013; Zaw et al., 2014), a new tectonic evolution model is suggested in Fig. 5.4.

Previous studies suggested that subduction of Palaeo-Tethys beneath the Indochina Terrane taken place during Carboniferous to Triassic (Bunopas, 1981; Sone and Metcalfe, 2008; Metcalfe, 2011b, 2013) and multiple arc magmatisms (Sone and Metcalfe, 2008; Metcalfe, 2011b, 2013; Salam et al., 2014) with formation of the Loei Fold Belt (Kamvong et al., 2014; Salam et al., 2014; Zaw et al., 2014) have given rise to the growth of the Sukhothai Arc and the generation of the Nan – Sra Keao arc/back-arc (Ueno and Hisada, 2001; Sone and Metcalfe, 2008; Metcalfe, 2011b, 2013).

During Late Carboniferous (Fig. 5.1), arc magmatism resulted from Palaeo-Tethys subduction under the Indochina Terrane might have started (Bunopas, 1981; Sone and Metcalfe, 2008; Metcalfe, 2011b, 2013) and continued through Early/Middle Permian (Sone and Metcalfe, 2008; Metcalfe, 2011b, 2013; Zaw et al., 2014). The Nan-Sra Kaeo Suture arc/back-arc basin had also formed during these periods (Ricou, 1994; Ueno and Hisada, 1997, 2001; Sone and Metcalfe, 2008).

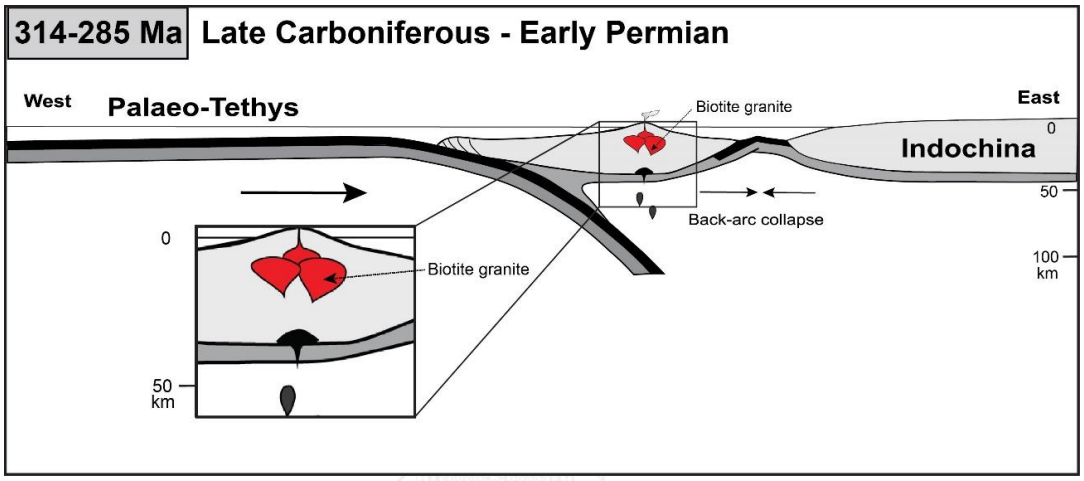

Figure 5.1 Schematic tectonic model of arc magmatism along Palaeo-Tethys subducted beneath Indochina and emplaced the biotite granite in the Wang Nam Khiao area, Nakhon Ratchasima, Thailand during Late Carboniferous to Early Permian (modified after Sone and Metcalfe (2008); Metcalfe (2011a, 2011b, 2013)).

The arc-related subduction continued during Late Permian (Sone and Metcalfe, 2008; Salam et al., 2014; Zaw et al., 2014; Fanka et al., 2016) with the emplacement of mafic-ultramafic plutonic rocks (Fanka et al., 2016) and the hornblende granite (Fig. 5.2), while Nan-Sra Kaeo Suture arc/back-arc collapsed (Sone and Metcalfe, 2008; Ridd, 2012; Salam et al., 2014; Zaw et al., 2014).

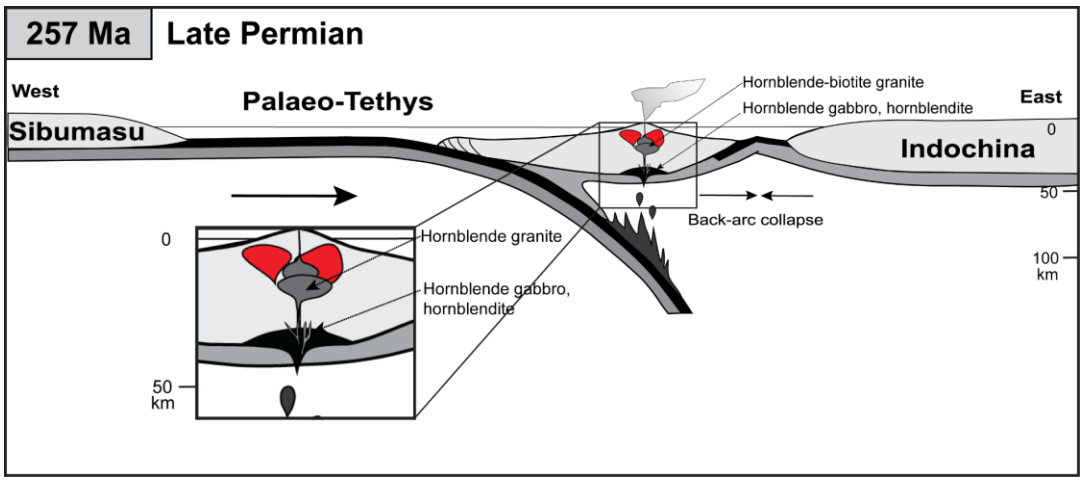

Figure 5.2 Schematic tectonic model of arc magmatism of Palaeo-Tethys subducted beneath Indochina and emplaced the mafic-ultramafic rocks and the hornblende granite in the Wang Nam Khiao area, Nakhon Ratchasima, Thailand during Late Permian (modified after Sone and Metcalfe (2008); Metcalfe (2011a, 2011b, 2013)).

During Middle Triassic (Fig. 5.3), the arc magmatism related to subduction of Palaeo-Tethys beneath progressive Indochina occurred and led to the formation of biotite-hornblende granite as a result of the collision between Sibumasu and Indochina, which probably had continued to Late Triassic (Sone and Metcalfe, 2008; Ridd, 2012; Salam *et al.*, 2014).

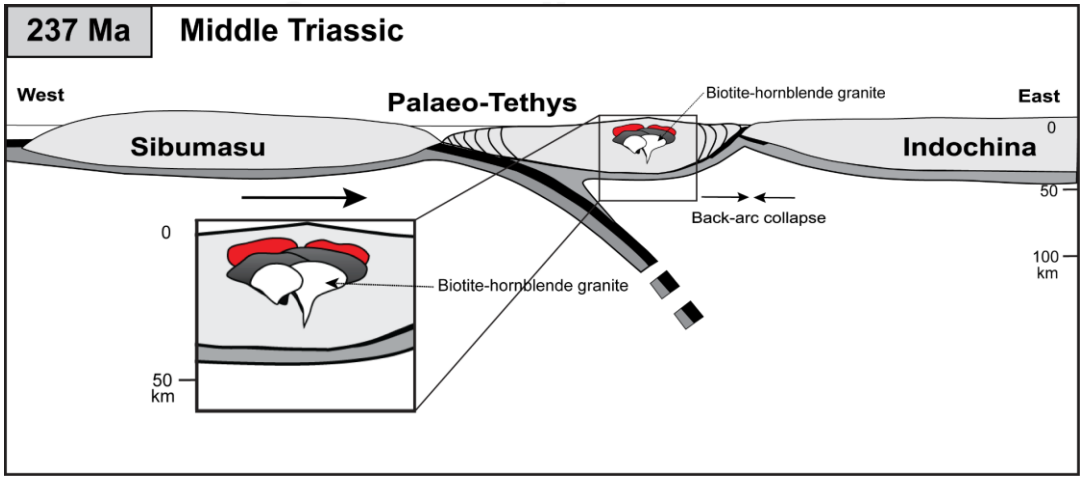

Figure 5.3 Schematic tectonic model of arc magmatism of Palaeo-Tethys subducted beneath Indochina and emplaced the biotite-hornblende granite in the Wang Nam

Khiao area, Nakhon Ratchasima, Thailand during Middle Triassic (Sone and Metcalfe, 2008; Metcalfe, 2011a, b, 2013).

In summary, the granitic rocks of this study appear to have originated by the calc-alkaline magmas related to subduction reflecting the magmatism of the LFB during Late Carboniferous to Middle Triassic (Fig. 5.4).

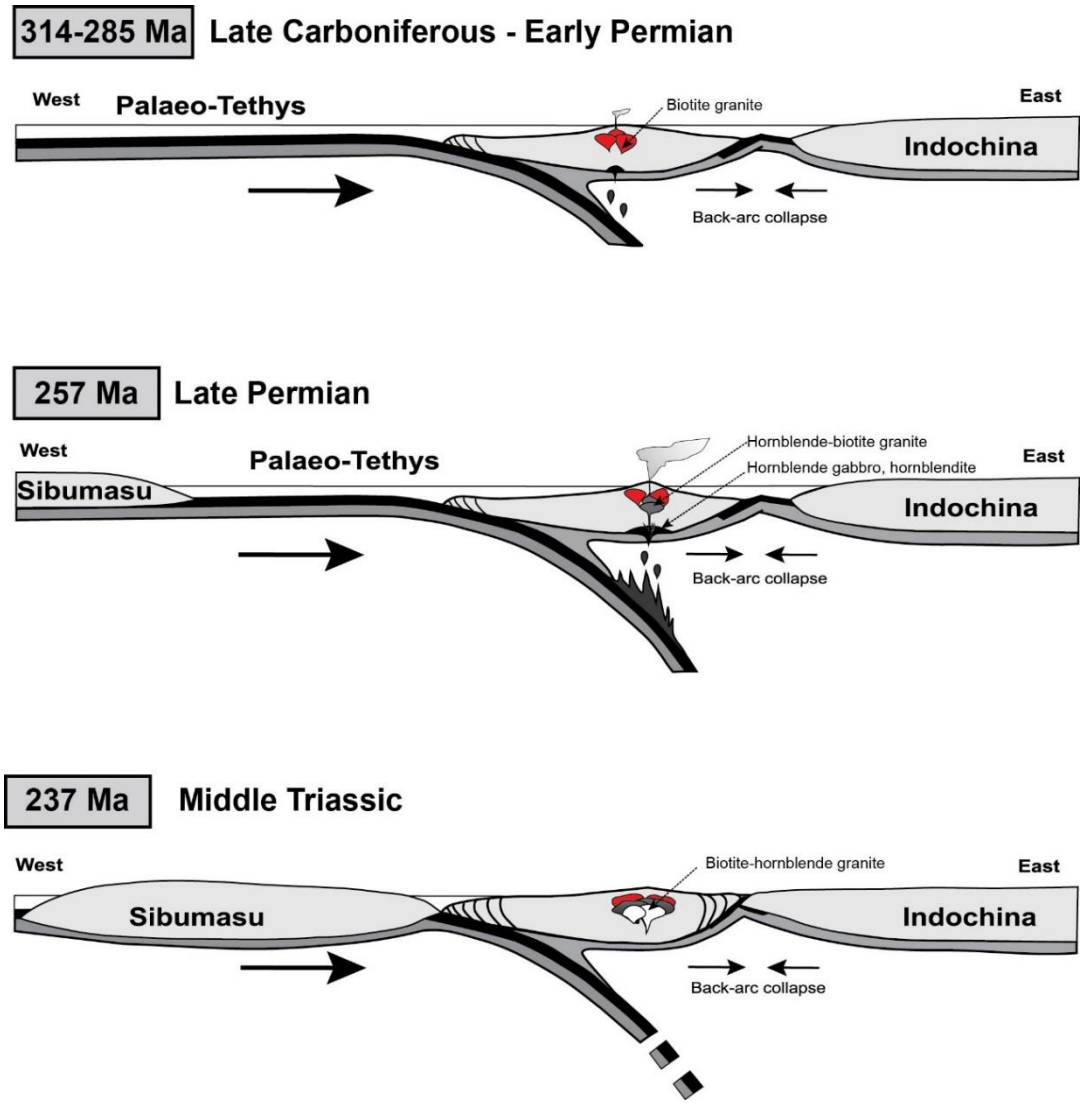

Figure 5.4 Schematic tectonic evolution model of the Wang Nam Khiao area, Nakhon Ratchasima, Thailand during Late Carboniferous to Middle Triassic (modified after Sone and Metcalfe (2008); Metcalfe (2011a, 2011b, 2013)).

5.2 Recommendation

Although, this thesis research was carefully designed and carried out, the author has found some points which should be suggested for further studies.

1. Fused bead samples may be prepared for whole-rock geochemical analyses using XRF for more accurate results.

2. Volcanic rocks exposed in the Wang Nam Khiao area, Changwat Nakhon Ratchasima should be studied to combine with the results of this study to understand and construct genesis model and magmatism within this region.

3. Because the evidence of Sukhothai Terrane (ST) disappears in the study area, detailed study on the igneous rocks in the other parts in the middle Thailand should be carried out to understand the missing of ST in this region.

REFERENCES

Abdel-Rahman, A.M., 1994. Nature of biotites from alkaline, calc-alkaline and peraluminous magmas. Journal of Petrology 35, 525-541.

Ague, J.J., 1997. Thermodynamic calculation of emplacement pressures for batholithic rocks, California; implications for the aluminium-in-hornblende barometer. Geology 25, 563-566.

Anderson, J.L., 1996. Status of thermobarometry in granitic batholiths. Transactions of Royal Society Edinburgh, Earth Sciences 87, 125-138.

Anderson, J.L., Smith, D.R., 1995. The effects of temperature and fO2 on the Al-in-hornblende barometer. American Mineralogist 80, 549-559.

Annen, C., Blundy, J.D., Sparks, R.S.J., 2006. The genesis of intermediate and silicic magmas in deep crustal hot zones. Journal of Petrology 47, 505-539.

Aydin, F., Karsli, O., Sadiklar, M.B., 2003. Mineralogy and chemistry of biotites from Eastern Pontide granitoid rocks, NE Turkey: Some petrological implications for granitiod magmas. Chemie der Erde - Geochemistry 63, 163-182.

Barbarin, B., 1991. Enclaves of the Mesozoic calc-alkaline granitoids of the Sierra Nevada batholith, California. In: Didier, J., Barbarin, B. (Eds.), Enclaves and Granite Petrology, Developments in Petrology, Elsevier, Amsterdam.

Barbarin, B., 1999. A review of the relationships between granitoid types, their origins and their geodynamic environments. Lithos 46, 605-626.

Barbarin, B., 2005. Mafic magmatic enclaves and mafic rocks associated with some granitoids of the central Sierra Nevada batholith, California: nature, origin, and relations with the hosts. Lithos 80, 155-177.

Barbarin, B., Didier, J., 1992. Genesis and evolution of mafic microgranular enclaves through various types of interaction between coexisting felsic and mafic magmas. Transactions of the Royal Society of Edinburgh: Earth Sciences 83, 145-153.

Barr, S.M., Charusiri, P., 2011. Volcanic rocks in Thailand. In: Ridd, M.F., Barber, A.J., Crow, M.J. (Eds.), The Geology of Thailand, Geological Society, London, 626 p.

Barr, S.M., Macdonald, A.S., Ounchanum, P., Hamilton, M.A., 2006. Age, tectonic setting and regional implications of the Chiang Khong volcanic suite, northern Thailand. Journal of the Geological Society 163, 1037-1046.

Barr, S.M., Tantisukrit, C., Yaowanoiyothin, W., Macdonald, A.S., 1990. Petrology and tectonic implications of upper Paleozoic volcanic rocks of the Chiang Mai belt, northern Thailand. Journal of Southeast Asian Earth Sciences 4, 37-47.

Batanova, V.G., Pertsev, A.N., Kamenetsky, V.S., Ariskin, A.A., Mochalov, A.G., Sobolev, A.V., 2005. Crustal evolution of island-arc ultramafic magma: Galmoenan pyroxenite-dunite plutonic complex, Koryak highland (Far East Russia). Journal of Petrology 46, 1345-1366.

Beard, J.S., Barker, F., 1989. Petrology and tectonic significance of gabbros, tonalities, hoshonites and anorthosites in a late Paleozoic arc-root complex in the Wrangellia terrane, southern Alaska. Journal of Geology 97, 667-683.

Best, M.G., 2003. Igneous and Metamorphic Petrology. In, Oxford Blackwell Science, 729 p.

Blein, O., Lapierre, H., Schweickert, R.A., 2001. A Permian island-arc with a continental basement: the Black Dyke Formation Nevada, North American Cordillera. Chemical Geology 175, 543-566.

Blundy, J.D., Holland, T.J.B., 1990. Calcic amphibole equilibria and a new amphibole-plagioclase geothermometer. Contributions to Mineralogy and Petrology 104, 208-224.

Booncharoen, P., 2011. Petrochemistry and geochemistry of granite from Ban Nong Mai Daeng, Tambon Wang Mee, Amphoe Wang Nam Keaw, Changwat Nakhon Ratchasima. B.Sc. Thesis, Department of Geology, Faculty of Science, Chulalongkorn University, 43 p.

Boonsoong, A., Panjasawatwong, Y., Metparsopsan, K., 2011. Petrochemistry and tectonic setting of mafic volcanic rocks in the Chon Daen-Wang Pong area, Phetchabun, Thailand. Island Arc 20, 107-124.

Booth, J.E., Sattayarak, N., 2011. Subsurface Carboniferous–Cretaceous Geology of NE Thailand. In: Ridd, M.F., Barber, A.J., Crow, M.J. (Eds.), The Geology of Thailand, Geological Society, London, 626 p.

Brophy, J.G., Marsh, B.D., 1986. On the origin of high-alumina arc basalts and the mechanism of melt extraction. Journal of Petrology 27, 763-789.

Brown, G.F., 1951. Geologic Reconnaissance of the Mineral Deposits of Thailand. US Government Printing Office 984.

Bunopas, S., 1981. Palaeogeographic History of Western Thailand and Adjacent Parts of Southeast Asia: A Plate Tectonic Interpretation. Ph.D. Thesis, Victoria University, Wellington, New Zealand, 810 p.

Bunopas, S., Marante, S., Vella, P., 1989. Palaeozoic and Early Mesozoic rotation and drifting of Shan-Thai from Gondwana-Australia. In, 4th International Symposium on Pre-Jurassic Evolution of East Asia, IGCP Project 224, pp. 63-64.

Bunopas, S., Vella, P., 1983. Tectonic and geologic evolution of Thailand. In, The Workshop on Stratigraphic Correlation of Thailand and Malaysia, Had Yai, Thailand, pp. 307-323.

Bunopas, S., Vella, P., 1992. Geotectonic and geologic evolution of Thailand. In: Piancharoen, C. (Ed.), National Conference on Geologic Resources of Thailand: Potential for Future Development. Department of Mineral Resource, Ministry of Industry, Bangkok, Thailand, pp. 209-228.

Burkhard, D.J.M., 1993. Biotite crystallization temperatures and redox states in granitic rocks as indicator for tectonic setting. Geologie en mijnbouw 71, 337-349.

Burrett, C., Zaw, K., Meffre, S., Lai, C.K., Khositanont, S., Chaodumrong, P., Udchachon, M., Ekins, S., Halpin, J., 2014. The configuration of Greater

Gondwana-evidence from LA ICPMS, U-Pb geochronology of detrital zircons from Southeast Asia and China. Gondwana Research 26, 31-51.

Carter, A., Clift, P.D., 2008. Was the Indosinian orogeny a Triassic mountain building or a thermotectonic reactivation event? Comptes Rendus Geoscience 340, 83-93.

Chappell, B.W., White, A.J.R., 1974. Two contrasting granite types. Pacific Geology 8, 173-174.

Chappell, B.W., White, A.J.R., 2001. Two contrasting granite types: 25 years later. Australian Journal of Earth Sciences 48, 489-499.

Charusiri, P., 1989. Lithophile metallogenetic epochs of Thailand: a geological and geochronological investigation. Ph.D. Thesis, Queen's University, Ontario, Canada, 819 p.

Charusiri, P., Clark, A.H., Farrar, E., Archibald, D., Charusiri, B., 1993. Granite belts in Thailand: evidence from the 40Ar/ 39Ar geochronological and geological syntheses. Journal of Southeast Asian Earth Sciences 8, 127-136.

Charusiri, P., Daorerk, V., Archibald, D., Hisada, K., Am-paiwan, T., 2002. Geotectonic evolution of Thailand, a new synthesis. Journal of Geological Society of Thailand 1, 1-20.

Cobbing, E.J., Mallick, D.I.J., Pitfield, P.E.J., Teoh, L.H., 1986. The granites of the Southeast Asian Tin Belt. Journal of Geological Society, London 143, 537-550.

Cobbing, E.J., Pitfield, P.E.J., Derbyshire, D.P.F., Mallick, D.I.J., 1992. The granites of the Southeast Asian Tin Belt. Overseas Memoirs of the British Geological Survey 10.

Cox, K.G., Bell, B.G., Pankhurst, R.J., 1979. The Interpretation of Igneous Rocks. In, Unwin Hyman, London, 450 p.

Crawford, A.J., Falloon, T.J., Eggins, S., 1987. The origin of island arc high-alumina basalts. Contributions to Mineralogy and Petrology 97, 417-430.

Droop, G.T.R., 1987. A general equation for estimating Fe3+ concentrations in ferromagnesian silicates and oxides from microprobe analyses, using stoichiometric criteria. Mineralogical Magazine 51, 431-435.

Eggins, S.M., Kinsley, L.P.J., Shelley, J.M.G., 1998. Deposition and element fractionation processes of occurring during atmospheric pressure sampling for analysis by ICP-MS. Applied Surface Science 129, 278-286.

Eyuboglu, Y., Dilek, Y., Bozkurt, E., Bektas, O., Rojay, B., Sen, C., 2010. Structure and geochemistry of an Alaskan-type ultramafic-mafic complex in the Eastern Pontides, NE Turkey. Gondwana Research 18, 230-252.

Fanka, A., Tsunogae, T., Daorerk, V., Tsutsumi, Y., Takamura, Y., Endo, T., Sutthirat, C., 2016. Petrochemistry and mineral chemistry of Late Permian hornblendite and hornblende gabbro from the Wang Nam Khiao area, Nakhon Ratchasima, Thailand: Indication of Palaeo-Tethyan subduction. Journal of Asian Earth Sciences 130, 239-255.

Faure, G., 1986. Principles of Isotope Geology. In, 589 p.

Ferrari, O.M., Hochard, C., Stampfli, G.M., 2008. An alternative plate tectonic model for the Palaeozoic–Early Mesozoic Palaeotethyan evolution of Southeast Asia (Northern Thailand–Burma). Tectonophysics 451, 346-365.

Foster, M.D., 1960. Interpretation of the Composition of Triocta-hedral Micas. USGS Professional Paper 354B, 1-49.

Greene, A.R., Debari, S.M., Kelemen, P.B., Blusztajn, J., Clift, P.D., 2006. A detailed geochemical study of island arc crust: the Talkeetna Arc section, south-central Alaska. Journal of Petrology 47, 1051-1093.

Hammarstrom, J.M., Zen, E., 1986. Aluminum in hornblende; an empirical igneous geobarometer. American Mineralogist 71, 1297-1313.

Harker, A., 1909. The natural history of igneous rocks. In, Methuen, London.

Hecht, L., 1994. The chemical composition of biotite as an indicator of magmatic fractionation and metasomatism in Sn-specialised granites of the

Fichtelgebirge (NW Bohemian massif, Germany). Metallogeny of collisional orogens, Czech Geological Survey, Prague, 295-300.

Helmy, H.M., Ahmed, A.F., El Mahallawi, M.M., Ali, S.M., 2004. Pressure, temperature and oxygen fugacity conditions of calc-alkaline granitoids, Eastern Desert of Egypt, and tectonic implications. Journal of African Earth Sciences 38, 255-268.

Helmy, H.M., El Mahallawi, M.M., 2003. Gabbro Akarem mafic-ultramafic complex, Eastern Desert, Egypt: a Late Precambrian analogue of Alaskan-type complexes. Mineralogy and Petrology 77, 85-108.

Himmelberg, G.R., Loney, R.A., 1995. Characteristics and petrogenesis of Alaskan-type ultramafic-mafic intrusions, southeastern Alaska. In, US Government Printing Office.

Holland, T., Blundy, J., 1994. Non-ideal interactions in calcic amphiboles and their bearing on amphibole-plagioclase thermometry. Contributions to Mineralogy and Petrology 116, 433-447.

Hollister, L.S., Grissom, G.C., Peters, E.K., Stowell, H.H., Sisson, V.B., 1987. Confirmation of the empirical correlation of Al in hornblende with pressure of solidification of calc-alkaline plutons. American Mineralogist 72, 231-239.

Hossain, I., Tsunogae, T., Rajesh, H.M., 2009. Geothermobarometry and fluid inclusions of dioritic rocks in Bangladesh: Implications for emplacement depth and exhumation rate. Journal of Asian Earth Sciences 34, 731-739.

Hunyek, V., 2012. Petrogenesis of Amphibolites in Amphoe Wang Nam Khiao Area, Changwat Nakhon Ratchasima. M.Sc. Thesis, Department of Geology, Faculty of Science, Chulalongkorn University, 92 p.

Intasopa, S., 1993. Petrology and geochronology of the volcanic rocks of central Thailand volcanic belt. Ph.D. Thesis, University of New Brunswick, Canada, 242 p.

Intasopa, S., Dunn, T., 1994. Petrology and Sr-Nd isotopic systems of the basalts and rhyolites, Loei, Thailand. Journal of Southeast Asian Earth Sciences 9, 167-180.

Irvine, T.N., 1974. Petrology of the Duke Island ultramafic complex southeastern Alaska. Geological Society of America Memoirs 138, 1-244.

Irvine, T.N., Baragar, W.R.A., 1971. A guide to the chemical classification of the common volcanic rocks. Canadian Journal of Earth Sciences 8, 523-548.

Irving, A.J., Frey, F.A., 1984. Trace element abundances in megacrysts and their host basalts: constraints on partition coefficients and megacryst genesis. Geochimica et Cosmochimica Acta 48, 1201-1221.

Ishihara, S., 1977. The magnetite-series and ilmenite-series granitic rocks. Mining Geology 27, 293-305.

Ishiwatari, A., Ichiyama, Y., 2004. Alaskan-type plutons and ultramafic lavas in Far East Russia, Northeast China, and Japan. International Geology Review 46, 316-331.

Javanaphet, J.C., 1969. Geological map of Thailand, scale 1:1,000,000. In, Department of Mineral Resources, Bangkok, Thailand.

Jiratitipat, T., 2010. Amphibolite and relationship rocks from Amphoe Wang Nam Keaw, Changwat Nakhon Ratchasima. B.Sc. Thesis, Department of Geology, Faculty of Science, Chulalongkorn University, 36 p.

Johan, Z., 2006. Platinum-group minerals from placers related to the Nizhni Tagil (Middle Urals, Russia) Uralian-Alaskan-type ultramafic complex: ore-mineralogy and studyof silicate inclusions in (Pt, Fe) alloys. Mineralogy and Petrology 87, 1-30.

Johnson, M.C., Rutherford, M.J., 1989. Experimental calibration of the aluminum-inhornblende geobarometer with application to Long Valley caldera (California) volcanic rocks. Geology 17, 837-841.

Jungyusuk, N., Khositanont, S., 1992. Volcanic rocks and associated mineralization in Thailand. In, Proceedings of National Conference on Geologic Resources of Thailand: Potential for Future, Development, Bangkok, Thailand, pp. 522-538.

Kamvong, T., Zaw, K., Meffre, S., Maas, R., Stein, H., Lai, C.K., 2014. Adakites in the Truong Son and Loei fold belts, Thailand and Laos: genesis and implications for geodynamics and metallogeny. Gondwana Research 26, 165-184.

Kelemen, P.B., Johnson, K.T.M., Kinzler, R.J., Irving, A.J., 1990. High-field-strength element depletions in arc basalts due to mantle-magma interactions. Nature 345, 521-524.

Kelemen, P.B., Rilling, J.L., Parmentier, E.M., Mehl, L., Hacker, B.R., 2003. Thermal structure due to solid-state flow in the mantle wedge beneath arcs. Inside the Subduction Factory, AGU Monograph 138, 293-311.

Kelemen, P.B., Shimizu, N., Dunn, T., 1993. Relative depletion of niobium in some arc magmas and the continental crust: partitioning of K, Nb, La and Ce during melt/rock reaction in the upper mantle. Earth and Planetary Science Letters 120, 111-134.

Khositanont, S., Panjasawatwong, Y., Ounchanum, P., Thanasuthipitak, T., Zaw, K., Meffre, S., 2008. Petrochemistry and zircon age determination of Loei–Phetchabun volcanic rocks. In: Chutakositkanon, V., Sutthirat, C., Charoentitirat, T. (Eds.), International Symposia on Geoscience Resources and Environments of Asian Terranes (GREAT 2008), 4th IGCP 516 and 5th APSEG, Bangkok, Thailand, pp. 272-278.

Kieffer, B., Arndt, N., Lapierre, H., Bastien, F., Bosch, D., Pecher, A., Yirgu, G., Ayalew, D., Weise, D., Jerram, D.A., Keller, F., Meugniot, C., 2004. Flood and shield basalts from Ethiopia: magmas from the African superswell. Journal of Petrology 45, 793-834.

Kromkhun, K., Baines, G., Satarugsa, P., Foden, J., 2013. Petrochemistry of Volcanic and Plutonic Rocks in Loei Province, Loei-Petchabun Fold Belt, Thailand. In, 2nd International Conference on Geological and Environmental Sciences, ACSIT Press, Singapore, pp. 55-59.

Lalonde, A., Bernard, P., 1993. Composition and color of biotite from granites: Two useful properties in the characterization of plutonic suites from the Hepburn internal zone of Wopmay orogen, NW Territories. Canadian Mineralogist 31, 203-217.

Leake, B.E., Woolley, A.R., Arps, C.E.S., Birch, W.D., Gilbert, M.C., Grice, J.D., Hawthorne, F.C., Kato, A., Kisch, H.J., Krivovichev, V.G., Linthout, K., Laird, J., Mandarino, J.A., Maresch, W.V., Nickel, E.H., Rock, N.M.S., Schumacher, J.C., Smith, D.C., Stephenson, N.C.N., Ungaretti, L., Whittaker, E.J.W., Guo, Y., 1997. Nomenclature of amphiboles: report of the subcommittee on amphiboles of the International Mineralogical Association, Commission on New Minerals and Mineral Names. American Mineralogist 82, 1019-1037.

Lepvrier, C., Faure, M., Van, V.N., Vu, T.V., Lin, W., Trong, T.T., Hoa, P.T., 2011. Northdirected Triassic nappes in Northeastern Vietnam (East Bac Bo). Journal of Asian Earth Sciences 41, 56-68.

Lepvrier, C., Van Vuong, N.Y., Maluski, H., Thi, P.T., Vu, V.T., 2008. Indosinian tectonics in Vietnam. Tectonics 340, 94-111.

Leterrier, J., Maury, R.C., Thonon, P., Girard, D., Marchal, M., 1982. Clinopyroxene composition as a method of identification of the magmatic affinities of paleo-volcanic series. Earth and Planetary Science Letters 59, 139-154.

Loucrs, R.R., 1990. Discrimination of ophiolitic from nonophiolitic ultramafic-mafic allochthons in orogenic belts by the Al/Ti ratio in clinopyroxene. Geology 18, 346-349.

Ludwig, K.R., 2008. User's Manual for Isoplot 3.70. In, Berkeley Geochronology Center Special Publication, 70 p.

Machev, P., Klain, L., Hecht, L., 2004. Mineralogy and chemistry of biotites from the Belogradchik pluton - some petrological implications for granitoid magmatism in North-West Bulgaria. In, the Annual Science Conference "Geology 2004". Bulgarian Geological Society, pp. 48-50.

Masoudi, F., Badr, M.J., 2008. Biotite and hornblende composition used to investigate the nature and thermobarometry of Pichagchi Pluton, Northwest Sanandaj-Sirjan Metamorphic Belt, Iran. Journal of Sciences, Islamic Republic of Iran 19, 329-338.

Metcalfe, I., 2002. Permian tectonic framework and palaeogeography of SE Asia. Journal of Asian Earth Sciences 20, 551-566.

Metcalfe, I., 2011a. Palaeozoic-Mesozoic history of SE Asia. Geological Society, London, Special Plublications 355, 7-35.

Metcalfe, I., 2011b. Tectonic framework and Phanerozoic evolution of Sundaland. Gondwana Research 19, 3-21.

Metcalfe, I., 2013. Review Gondwana dispersion and Asian accretion: Tectonic and Paleogeographic evolution of eastern Tethys. Journal of Asian Earth Sciences 66, 1-33.

Morimoto, N., Fabries, J., Ferguson, A.K., Ginzburg, I.V., Ross, M., Seifert, F.A., Zussman, J., Aoki, K., Gottardi, G., 1988. Nomenclature of pyroxene. American Mineralogist 73, 1123-1133.

Morley, C.K., 2007. Variations in late Cenozoic-Recent strike-slip and obliqueextensional geometries, within Indochina: the influence of pre-existing fabrics. Journal of Structural Geology 29, 36-58.

Morley, C.K., Ampaiwan, P., Thanudamrong, S., Kuenphan, N., Warren, J., 2013. Development of the Khao Khwang Fold and Thrust Belt: Implications for the geodynamic setting of Thailand and Cambodia during the Indosinian Orogeny. Journal of Asian Earth Sciences 62, 705-719.

Morley, K., Charusiri, P., Watkinson, I.M., 2011. Structural geology of Thailand during the Cenozoic. In: Ridd, M.J., Barber, M.F., Crow, A.J. (Eds.), The Geology of Thailand, The Geological Society, London, 626 p.

Na Lampang, T., 2015. Structural geology in Amphoe Wang Nam Khiao area, Changwat Nakhon Ratchasima. M.Sc. Thesis, Department of Geology, Faculty of Science, Chulalongkorn University, 120 p.

Nakapadungrat, S., Putthapiban, P., 1992. Granites and associated mineralization in Thailand. In: Piancharoen, C. (Ed.), National conference on Geologic Resources of Thailand: Potential for Future Development, Departmaent of Mineral Resources, Bangkok, Thailand, pp. 153-171.

Ng, S.W.P., Chung, S.L., Robb, L.J., Searle, M.P., Ghani, A.A., Whitehouse, M.J., Oliver, G.J.H., Sone, M., Gardiner, N.J., Roselee, M.H., 2015a. Petrogenesis of Malaysian granitoids in the Southeast Asian Tin Belt: Part 1. Geochemical and Sr-Nd isotopic characteristics. Geological Society of America Bulletin.

Ng, S.W.P., Whitehouse, M.J., Searle, M.P., Robb, L.J., Ghani, A.A., Chung, S.L., Oliver, G.J.H., Sone, M., Gardiner, N.J., Roselee, M.H., 2015b. Petrogenesis of Malaysian granitoids in the Southeast Asian Tin Belt: Part 2. U-Pb zircon geochronology and tectonic model. Geological Society of America Bulletin.

Nockolds, S.R., 1947. The relation between chemical composition and paragenesis in the biotite micas of igneous rocks. American Journal of Science 245, 401-420.

Nonsung, J., 2010. Petrochemistry of granite at Ban km80, Amphoe Nadee, Changwat Prachinburi. B.Sc. Thesis, Department of Geology, Faculty of Science, Chulalongkorn University, 34 p.

Paces, J.B., Miller, J.D., 1993. Precise U-Pb ages of Duluth Complex and related mafic intrusions, northeastern Minnesota: geochronological insights to physical, petrogenetic, paleomagnetic and tectonomagmatic processes associated with the 1.1 Ga midcontinent rift system. Journal of Geophysical Research 98, 13997-14013.

Panjasawatwong, Y., Zaw, K., Chantaramee, S., Limtrakun, P., Pirarai, K., 2006. Geochemistry and tectonic setting of the Central Loei volcanic rocks, Pak Chom area, Loei, northeastern Thailand. Journal of Asian Earth Sciences 26, 77-90.

Peacock, S.M., 1993. Large-scale hydration of the lithosphere above subducting slabs. Chemical Geology 108, 49-59.

Pearce, J.A., 1982. Trace element characteristics of lavas from destructive plate boundaries. In: Thorp, R.S. (Ed.), Andesites: Orogenic Andesites and Related Rocks, John Wiley and Sons, New York, 724 p.

Pearce, J.A., 1983. Role of sub-continental lithosphere in magma genesis at active continental margins. In: Hawkesworth, C.J., Norry, M.J. (Eds.), Continental basalts and mantle xenoliths, Shiva, Nantwich.

Pearce, J.A., 2008. Geochemical fingerprinting of oceanic basalts with applications to ophiolite classification and the search for Archean oceanic crust. Lithos 100, 14-48.

Pearce, J.A., Cann, J.R., 1973. Tectonic setting of basic volcanic rocks determined using trace element analyses. Earth and Planetary Science Letters 19, 290-300.

Pearce, J.A., Harris, N.B.W., Tindle, A.J., 1984. Trace element discrimination diagrams for the tectonic interpretation of granitic rocks. Journal of Petrology 25, 956-983.

Peccerillo, A., Taylor, S.R., 1976. Geochemistry of eocene calc-alkaline volcanic rocks from the Kastamonu area, northern Turkey. Contributions to Mineralogy and Petrology 58, 63-81.

Petrini, K., Podladchikov, Y., 2000. Lithospheric pressure-depth relationship in compressive regions of thickened crust. Journal of Metamorphic Geology 18, 67-77.

Pettigrew, N., Hattori, K., 2006. The Quetico intrusions of Western Superior Province: neo-archean examples of Alaskan/Ural-type mafic-ultramafic intrusions. Precambrian Research 149, 21-42.

Piyasin, S., 1985. Problems of stratigraphic classification and environments of Khorat Group. In, Conference on geology and mineral resources in Northeastern Thailand, Khon Kaen, Thailand, pp. 85-97.

Putthaphiban, P., Vichidchalerpong, A., Boonprasert, T., 1981a. Geologic Map of Thailand 1:50000 Ban Sap Bon (5337I). In, Department of Mineral Resources.

Putthaphiban, P., Vichidchalerpong, A., Boonprasert, T., 1981b. Geologic Map of Thailand 1:50000 Ban Tha I Som (5337IV). In, Department of Mineral Resources.

Putthaphiban, P., Vichidchalerpong, A., Boonprasert, T., 1989a. Geologic Map of Thailand 1:50000 Ban Sap Bon (5337I). In, Department of Mineral Resources.

Putthaphiban, P., Vichidchalerpong, A., Boonprasert, T., 1989b. Geologic Map of Thailand 1:50000 Ban Tha I Som (5337IV). In, Department of Mineral Resources.

Qian, X., Feng, Q., Yang, W., Wang, Y., Chonglakmani, C., Monjai, D., 2015. Arc-like volcanic rocks in NW Laos: Geochronological and geochemical constraints and their tectonic implications. Journal of Asian Earth Sciences 98, 342-357.

Racey, A., Goodall, J.G.S., Love, M.A., Jones, P.D., 1994. New age data on the Khorat Group of Northeast Thailand. In: Angsuwathana, P., Wongwanich, T., Tansathien, W., Wongsomsak, S., Tulyatid, J. (Eds.), International Symposium on Stratigraphic Correlation of Southeast Asia. Department of Mineral Resources, Bangkok, Thailand, pp. 245-252.

Raksaskulwong, L., Wongwanich, T., 1994. Stratigraphy of Kaeng Krachan Group in Peninsular and Western Thailand. In, Annual Technical Meeting of Geological Survey Division, pp. 106-115.

Ramo, O.T., 2005. Granitic systems a special issue in honor of Ilmari Haapala. Lithos 80, xi-xix.

Richards, J.P., 2003. Tectono-magmatic precursors for porphyry Cu-(Mo-Au) deposit formation. Economic Geology 98, 1515-1533.

Rickwood, P.C., 1989. Boundary lines within petrologic diagrams which use oxides of major and minor elements. Lithos 22, 247-263.

Ricou, L.E., 1994. Tethys reconstructed: plates, continental fragments and their boundaries since 260 Ma from Central America to South-eastern Asia. Geodinamica Acta 7, 169-218.

Ridd, M.F., 2012. The role of strike-slip faults in the displacement of the Palaeotethys suture zone in Southeast Thailand. Journal of Asian Earth Sciences 51, 63-84.

Ridd, M.F., Morley, C.K., 2011. The Khao Yai Fault on the southern margin of the Khorat Plateau, and the pattern of faulting in southeast Thailand. Proceedings of the Geologists, Association 122, 143-156.

Ringwood, A.E., 1990. Slab-mantle interactions, 3: petrogenesis of intraplate magmas and structure of the upper mantle. Chemical Geology 82, 187-207.

Rollinson, H.R., 1993. Using geochemical data: evaluation, presentation and interpretation. In, Longman Scientific and Technical Ltd., Harlow, UK, 352 p.

Rothstein, D.A., Manning, C.E., 2003. Geothermal gradients in continental magmatic arcs: Constraints from the eastern Peninsular Ranges batholith, Baja California, México. Geological Society of America Special Paper 374, 337-354.

Rublee, V.J., 1994. Chemical petrology, mineralogy and structure of the Tulameen Complex, Princeton area, British Colombia. M.Sc. Thesis, University of Ottawa, Canada, 179 p.

Rutter, M.J., Van der Laan, S.R., Wyllie, P.J., 1989. Experimental data for a proposed empirical igneous geobarometer: aluminium-in-hornblende at 10 kbar pressure. Geology 17, 897-900.

Ryerson, F.J., Watson, E.B., 1987. Rutile saturation in magmas: implications for Ti-Nb-Ta depletion in orogenic rock series. Earth and Planetary Science Letters 86, 225-239.

Salam, A., Zaw, K., Meffre, S., McPhie, J., Lai, C.K., 2014. Geochemistry and geochronology of epithermal Au-hosted Chatree volcanic sequence: implication for tectonic setting of the Loei Fold Belt in central Thailand. Gondwana Research 26, 198-217.

Sarjoughian, F., Kananian, A., Ahmadian, J., M., M., 2015. Chemical composition of biotite from the Kuh-e Dom pluton, Central Iran: implication for granitoid

magmatism and related Cu–Au mineralization. Arabian Journal of Geosciences 8.

Schmidt, M.W., 1992. Amphibole composition in tonalite as a function of pressure: an experimental calibration of the Al-in-hornblende barometer. Contributions to Mineralogy and Petrology 110, 304-310.

Schnetzler, C.C., Philpotts, J.A., 1970. Partition coefficients of rare-earth elements between igneous matrix material and rock-forming mineral phenocrysts-II. Geochimica et Cosmochimica Acta 34, 331-340.

Schoene, B., 2014. U-Th-Pb geochronology. In, Princeton University, Princeton, NJ, USA.

Searle, M.P., Whitehouse, M.J., Robb, L.J., Ghani, A.A., Hutchison, C.S., Sone, M., NG, S.W.P., Roselee, M.H., Chung, S.L., Oliver, G.J.H., 2012. Tectonic evolution of the Sibumasu-Indochina terrane collision zone in Thailand and Malaysia: constains from new U-Pb zircon chronology of SE Asian tin granitoids. Journal of the Geological Society 169, 489-500.

Shabani, A.A.T., Lalonde, A.E., 2003. Composition of biotite from granitic rocks of the Canadian Appalachian Orogen: A potential tectonomagmatic indicator? The Canadian Mineralogist 41, 1381-1396.

Shapiro, L., 1975. Rapid Analysis of Silicate, Carbonate, and Phosphate Rocks-Revised Edition. In, Geological Survey Bulletin, 76 p.

Singharajwarapan, S., Berry, R., 2000. Tectonic implications of Nan Suture Zone and its relationship to the Sukhothai Fold Belt, Northern Thailand. Journal of Asian Earth Sciences 18, 663-673.

Sisson, T.W., Grove, T.L., Coleman, D.S., 1996. Hornblende gabbro sill complex at Onion Valley, California, and a mixing origin for the the Sierra Nevada batholith. Contributions to Mineralogy and Petrology 126, 81-108.

Sisson, T.W., Layne, G.D., 1993. H2O in basalt and basaltic andesite glass inclusions from four subduction-related volcanoes. Earth and Planetary Science Letters 117, 619-635.

Smith, J.V., Brown, W.L., 1974. Feldspar minerals. Germany: Springer-Verlag, 1-690.

Snoke, A.W., Quick, J.E., Bowman, H.R., 1981. Bear Mountain igneous complex, Klamath Mountains, California: an ultrabasic to silicic calc-alkaline suite. Journal of Petrology 22, 501-552.

Sone, M., Metcalfe, I., 2008. Parallel Tethyan sutures in mainland Southeast Asia: New insights for Palaeo-Tethys closure and implications for the Indosinian orogeny. Tectonics 340, 166-179.

Sone, M., Metcalfe, I., Chaodumrong, P., 2012. The Chanthaburi terrane of southeastern Thailand: Stratigraphic confirmation as a disrupted segment of the Sukhothai Arc. Journal of Asian Earth Sciences 61, 16-32.

Srichan, W., A.J., C., Berry, R.F., 2009. Geochemistry and geochronology of Late Triassic volcanic rocks in the Chiang Khong region, northern Thailand. Island Arc 18, 32-51.

Stacey, J.S., Kramers, J.D., 1975. Approximation of terrestrial lead isotope evolution by a two-stage model. Earth and Planetary Science Letters 26, 207-221.

Stein, E., Dietl, C., 2001. Hornblende thermobarometry of granitoids from the Central Odenwald (Germany) and their implications for the geotectonic development of the Odenwald. Mineralogy and Petrology 72, 185-207.

Stussi, J.M., Cuney, M., 1996. Nature of biotites from alkaline, calc-alkaline and peraluminous magmas by Abdel-Fattah M. Abdel-Rahman: A Comment. Journal of Petrology 37, 1025-1029.

Su, B., Qin, K., Sakyi, P.A., Malaviarachchid, S.P.K., Liu, P., Tang, D., Xiao, Q., Sun, H., Ma, Y., Mao, Q., 2012. Occurrence of an Alaskan-type complex in the Middle Tianshan Massif, Central Asian Orogenic Belt: inferences from petrological and mineralogical studies. International Geology Review 54, 249-269.

Sun, S.S., McDonough, W.F., 1989. Chemical and isotopic systematics of oceanic basalts: implications for mantle composition and processes. In: Saunders,

A.D., Norry, M.J. (Eds.), Magmatism in the Ocean Basins, Geological Society of London Special Publication.

Tapponnier, P., Peltzer, G., Armijo, R., 1986. On the mechanics of the collision between India and Asia. In Ramsey, J.G., Coward, M.P., and Ries, A. (Eds.), Collision Tectonics. Geological Society, London, Special Plublications 19, 115-157.

Taylor, H.P., 1967. The zoned ultramafic complexes of southeastern Alaska. In: Wyllie, P.J. (Ed.), Ultramafic and related rocks, New York, Wiley.

Togashi, S., Tanaka, T., Yoshida, T., Ishikawa, K., Fujinawa, A., Kurasawa, H., 1992. Trace elements and Nd-Sr isotopes of island arc tholeiites from frontal arc of northeast Japan. Geochemical Journal 26, 261-277.

Tsutsumi, Y., Horie, K., Sano, T., Miyawaki, R., Momma, K., Matsubara, S., Shigeoka, M., Yokoyama, K., 2012. LA-ICP-MS and SHRIMP ages of zircons in chevkinite and monazite tuffs from the Boso Peninsula, Central Japan. Bulletin of that National Museum of Nature and Science Series C, Geology/Paleontology 38, 15-32.

Ueno, K., Charoentitirat, T., 2011. Carboniferous and Permian. In: Ridd, M.F., Barber, A.J., Crow, M.J. (Eds.), The Geology of Thailand, The Geological Society of London, 626 p.

Ueno, K., Hisada, K., 1997. The Nan-Uttaradit-Sa Kaeo Sutures as a main Paleo-Tethyan suture in Thailand: Is it real? Gondwana Research 4, 804-805.

Ueno, K., Hisada, K., 2001. The Nan-Uttaradit-Sa Kaeo Sutures as a main Paleo-Tethyan suture in Thailand: Is it real? Gondwana Research 4, 804-805.

Vivatpinyo, J., Charusiri, P., Sutthirat, C., 2014. Volcanic Rocks from Q-Prospect, Chatree Gold Deposit, Phichit Province, North Central Thailand: Indicators of Ancient Subduction. Arabian Journal for Science and Engineering 39, 325-338.

Vyhnal, C., McSween, H.Y.J., Speer, J.A., 1991. Hornblende chemistry in southern appalachian granitoids-implications for aluminum hornblende

thermobarometry and magmatic epidote stability. American Mineralogist 76, 176-188.

Williams, I.S., 1998. U-Th-Pb geochronology by ion microprobe. In: McKibben, M.A., Shanks, W.C. (Eds.), Applications of Microanalytical Techniques to Understanding Mineralizing Processes. Reviews in Economic Geology 7, 1-35.

Winter, J.D., 2001. An introduction to igneous and metamorphic petrology. In, Upper Saddle River, New Jersey, Prentice-Hall, 697 p.

Wood, D.A., 1980. The application of a Th-Hf-Ta diagram to problems of tectonomagmatic classification and to establishing the nature of crustal contamination of basaltic lavas of the British Tertiary volcanic province. Earth and Planetary Science Letters 50, 11-30.

Woodhead, J.D., Eggins, S.M., Johnson, R.W., 1998. Magma Genesis in the New Britain Island Arc: Further Insights into Melting and Mass Transfer Processes. Journal of Petrology 39, 1641-1668.

Wyllie, P.J., Osmaston, M.F., Morrison, M.A., 1984. Constraints imposed by experimental petrology on possible and impossible magma sources and products. Philosophical Transactions of the Royal Society of London. Series A Mathematical and Physical Sciences 310, 439-456.

Zaw, K., Meffre, S., Lai, C.K., Santosh, M., Burrett, C., Graham, I.T., Manaka, T., Salam, A., Kamvong, T., Cromie, P.W., 2014. Tectonics and metallogeny of mainland Southeast Asia-a review and contribution. Gondwana Research 26, 5-30.

Zaw, K., Rodmanee, T., Khositanont, S., Thanasuthipitak, T., Ruamkid, S., 2007. Geology and genesis of Phu Thap Fah gold skarn deposit, northeastern Thailand: implications for reduced gold skarn formation and mineral exploration. In: Tantiwanit, W. (Ed.), GEOTHAI'07 International Conference on Geology of Thailand, Bangkok, Thailand, pp. 93-95.

Zhao, T., Qian, X., Feng, Q., 2016. Geochemistry, Zircon U-Pb Age and Hf Isotopic Constraints on the Petrogenesis of the Silurian Rhyolites in the Loei Fold Belt and Their Tectonic Implications. Journal of Earth Science 27, 391-402.

Zhou, Z.X., 1986. The origin of intrusive mass in Fengshandong, Hubei province. Acta Petrologica Sinica 2, 59-70.

APPENDIX
GEOTHERMOBAROMERTY CALCULATION

The several mineral equilibriums such as amphibole and plagioclase (e. g. Blundy and Holland, 1990; Holland and Blundy, 1994; Schmidt, 1992; Anderson and Smith, 1995; Anderson, 1996; Ague, 1997; Stein and Dietl, 2001), will be engaged for P-T calculation. For instance, the P-T calculation can be carried out by hornblende-plagioclase geothermometer and Al in hornblende geobarometer for the main geothermobarometry of this study.

1. Geothermometer

1.1 Amphibole – plagioclase geothermometer: The amphibole – plagioclase geothermometer has been commonly used for temperature calculation (Blundy and Holland, 1990; Holland and Blundy, 1994). Based on the experimental data of coexisting amphibole and plagioclase, Holland and Blundy (1994) suggested two geothermometers based on the edenite-tremolite reaction (Reaction A) and edenite-richterite reaction (Reaction B) below.

$NaCa_2Mg_5Si_4(AlSi_3)O_{22}(OH)_2 + 4\,SiO_2 = Ca_2Mg_5Si_8O_{22}(OH)_2 + NaAlSi_3O_8$ .....***(Reaction A)***

(edenite) + (quartz) = (tremolite) + (albite)

$NaCa_2Mg_5Si_4(AlSi_3)O_{22}(OH)_2 + NaAlSi_3O_8 = Na(NaCa)Mg_5Si_8O_{22}(OH)_2 + CaAl_2Si_2O_8$ ...***(Reaction B)***

(edenite) + (albite) = (richterite) + (anorthite)

According to two reaction above, the edenite-tremolite geothermometer and edenite-richterite geothermometer were suggested for quartz-bearing rocks (eq. 1) and quartz-free rocks (eq. 2), respectively, with reported uncertain calibration of $\pm$ 40 ^{o}C. The detailed equations to calculate temperature of both geothermometers are explained by the following equations with R=0.0083144 kJ K^{-1} mol^{-1}.

$$T_A = \frac{-76.95+0.79P+Y_{ab}+39.4\,X_{Na}^{A}+22.4X_{K}^{A}+(41.5-2.89P).X_{Al}^{M2}}{-0.0650-R\cdot\ln\left(\frac{27\cdot X_{\square}^{A}\cdot X_{Si}^{T1}\cdot x_{ab}^{plag}}{256\cdot X_{Na}^{A}\cdot X_{Al}^{T1}}\right)} \quad \text{.....(eq. 1)}$$

Where Y_{ab} term is given by: for X_{ab} > 0.5 then $Y_{ab} = 0$

Otherwise $Y_{ab} = 12.0(1 - X_{ab})^2 - 3.0\ kJ$

$$T_B = \frac{78.44 + Y_{ab-an} - 33.6\,X_{Na}^{M4} - (66.8 - 2.92P).X_{Al}^{M2} + 78.5X_{Al}^{T1} + 9.4X_{Na}^{A}}{0.0721 - R\cdot\ln\left(\frac{27\cdot X_{Na}^{M4}\cdot X_{Si}^{T1}\cdot X_{an}^{plag}}{64\cdot X_{Ca}^{M4}\cdot X_{Al}^{T1}\cdot X_{ab}^{plag}}\right)} \quad \text{.....(eq. 2)}$$

Where Y_{ab-an} term is given by: for X_{ab} > 0.5 then $Y_{ab-an} = 3.0\ kJ$

Otherwise $Y_{ab-an} = 12.0(2X_{ab} - 1) + 3.0\ kJ$

T is the temperature in Kelvins, *P* is the pressure in kbar and the $X_i^{\emptyset}$ term denotes the molar fraction of species (or component) *i* in phase (or crystallographic site) ϕ

The required site term of amphibole for these calculation equations are defined as follows:

cm = Si+Al+Ti+Fe^{3+} +Fe^{2+} +Mg+Mn-13.0

X_{Si}^{T1} = (Si-4)/4

X_{Al}^{T1} = (8-Si)/4

X_{Al}^{M2} = (Al+Si-8)/2

X_{K}^{A} = K

$X_{\blacksquare}^{A}$ = 3-Ca-Na-K-cm

X_{Na}^{A} = Ca+Na+cm-2

X_{Na}^{M4} = (2-Ca-cm)/2

X_{Ca}^{M4} = Ca/2

The calculation terms of plagioclase are required as follows:

X_{an}^{plag} = Ca/(Ca+Na)

X_{ab}^{plag} = Na/(Ca+Na)

These thermometers can be applied to calculate the temperature of the rocks, both igneous rocks and metamorphic rocks, which contain plagioclase and amphibole assemblages.

1.2 Biotite geothermometer: the temperature of crystallization can be also carried out by the other geothermometers such as biotite geothermometer in eq. 3 (Henry et al., 2005) with the precision of ±24 ºC.

$$T = \{\frac{\ln(Ti) - a - c(X_{Mg})^3}{b}\}^{0.333} \quad \textbf{(eq. 3)}$$

Where *T* is temperature in ºC, *Ti* is the atoms per formula unit based on 22 of oxygen, X_{Mg} is Mg/(Mg+Fe) and *a, b, c* are parameters ($a = -2.3594$, $b = 4.6482x10^{-9}$, $c = -1.7283$).

2. Geobarometer

2.1 Hornblende geobarometer: The Al in hornblende has been widely used to calculate the crystallization pressure of magmatic rocks (Hammarstrom and Zen, 1986; Hollister et al., 1987; Schmidt, 1992). The total Al content of calcic amphibole has correlation with the pressure which was confirmed by experimental studies (Hollister et al., 1987; Johnson and Rutherford, 1989; Schmidt, 1992; Anderson and Smith, 1995). The calibration equation of Schmidt (1992) (eq. 4) has been chosen to estimate the crystallization.

$$P\ (\pm\ 0.6\ kbar) = -3.01 + 4.76\ Al^{tot} \quad \textbf{(eq. 4)}$$

Where *P* is the pressure in kbar, Al^{tot} is the total aluminum content of hornblende in atoms per formula unit.

2.2 Biotite geobarometer: The biotite geobarometer suggested by Etsuo et al. (2007) can be employed to calculate the solidification pressure (P) of the host granitic rocks by using the total Al content in biotite. The good positive correlation can be seen between the total Al content in biotite and the solidification pressure by eq. 5.

$$P\ (\pm\ 0.33\ kbar) = 3.0\ {}^{T}Al - 6.53 \quad \textbf{(eq. 5)}$$

Where P is the pressure in kbar, ${}^{T}Al$ is the total aluminum content of biotite (based on oxygen = 22)

VITA

Mr. Alongkot Fanka was born on March 9, 1986 in Wiangsa, Nan, Thailand. He completed high school from Sa School, Nan in 2004. He then graduated Bachelor's Degree (B.Sc) in geology in 2008 from Department of Geology, Faculty of Science, Chulalongkorn University focused on petrography and geochemistry of igneous rocks. After graduated his bachelor degree, he got the scholarship from the Human Resources Development in Science Project (Science Achievement Scholarship of Thailand, SAST) for his Master's and Ph.D.'s Degrees. He started the Master's Degree in Geology Program at Department of Geology, Faculty of Science, Chulalongkorn University and his research focused on the petrochemistry of corundum-bearing rocks of Montepuez Deposits, Mozambique and published in the Journal of The Gemmological Association of Hong Kong (ISSN2076-7412) Volume XXXIV in 2013. For his Ph.D.'s Degree, he study have focused on the petrology, geochemistry, mineral chemistry, geothermobarometry, and geochronology of plutonic rocks. His research is published in the Journal of Asian Earth Sciences, Volume 130 in 2016.